

Mémoire présenté le 16/07/2025

**pour l'obtention du diplôme de la filière ESSEC-ISUP Risque & Actuariat
et l'admission à l'Institut des Actuaire en vue du titre d'Actuaire**

par

YIXUAN CHEN

**Titre: "An Enhanced Internal Model for Pandemic Risk: Hybrid LN-E-GPD Distribution
and Combined Algorithmic Optimization"**

Confidentialité ☒ NON ☐ OUI (durée : ☐ 1 an ☐ 2 ans)

Les signataires s'engagent à respecter la confidentialité indiquée ci-dessus.

Membres présents du jury de la filière :

Marie KRATZ



*Membres présents du jury de l'Institut des
Actuaire*

Grégory BOUTIER (Président du Jury)



Ali GOUMAR



Gabriel FAUCHET



Signature du candidat :




Signature du responsable entreprise :

Entreprise : AXA GIE

*Directeur du mémoire en entreprise :
Auréliе VIOSSAT*

GIE AXA DRH
Siège social : 23, avenue Matignon
75008 Paris
333 491 066 RCS Paris

Signature: 

Invité :

Signature :

*Autorisation de publication et de mise en
ligne sur sites de diffusion de documents
actuariels (après expiration de l'éventuel délai de
confidentialité)*

Signature du responsable entreprise :





An Enhanced Internal Model for Pandemic Risk: Hybrid LN-E-GPD Distribution and Combined Algorithmic Optimization

Actuarial Mémoire presented by

Yixuan CHEN

for the obtention of the French Actuarial Qualification

Company: AXA GIE

supervised by:

Prof. Marie KRATZ - ESSEC Business School

Aurélie Viossat - AXA GIE

June. 15, 2025

Abstract

The COVID-19 pandemic has highlighted significant challenges in accurately assessing pandemic mortality risk for insurers like AXA, which have broad international exposure. The Solvency II Directive mandates a standard mortality shock of 0.15% under the Solvency Capital Requirement (SCR), but this uniform approach fails to consider variations in age structure, gender distribution, healthcare systems, and government response effectiveness across countries. Consequently, insurers need sophisticated internal models that adapt to these diverse factors for more accurate risk assessments. Developing such models is challenging due to the infrequency of pandemics, with each event presenting unique characteristics, such as high transmission rates and varying mitigation actions.

This study aims to create an internal pandemic model tailored to insurers' demographic and geographic profiles, contributing in three significant ways. First, it builds on the Swiss Re pandemic model by integrating epidemiological modeling with statistical methods to capture pandemic dynamics, including mitigation measures. Second, the model's parameters are calibrated using extensive research, incorporating age, gender, and regional factors on lethality, while adjusting quarantine effects based on COVID-19 data. Third, a novel optimization approach combining Genetic Algorithms with the Levenberg-Marquardt method is introduced to streamline the CAT Pandemic model and improve parameter fitting in multidimensional contexts. The model's reliability is demonstrated through comparisons with the standard SCR formula and historical pandemic data, confirming its robustness for mortality risk assessment in extreme scenarios.

Keywords: COVID-19, epidemiological model, extreme value theory, genetic algorithm, Levenberg-Marquardt method, pandemic mortality risk

Résumé

La pandémie de COVID-19 a mis en évidence d'importants défis pour évaluer avec précision le risque de mortalité pandémique pour les assureurs tels qu'AXA, qui ont une large exposition internationale. La directive Solvabilité II impose un choc de mortalité standard de 0,15% dans le cadre de l'exigence de capital de solvabilité (SCR), mais cette approche uniforme ne prend pas en compte les variations dans la structure d'âge, la répartition par sexe, les systèmes de santé et l'efficacité des réponses gouvernementales entre les pays. Par conséquent, les assureurs ont besoin de modèles internes sophistiqués qui s'adaptent à ces divers facteurs pour des évaluations de risque plus précises. Le développement de tels modèles est compliqué en raison de l'infrequency des pandémies, chaque événement présentant des caractéristiques uniques, telles que des taux de transmission élevés et des actions d'atténuation variées.

Cette étude vise à créer un modèle pandémique interne adapté aux profils démographiques et géographiques des assureurs, en contribuant de trois manières significatives. Premièrement, elle s'appuie sur le modèle pandémique de Swiss Re en intégrant la modélisation épidémiologique avec des méthodes statistiques pour capturer la dynamique des pandémies, y compris les mesures d'atténuation. Deuxièmement, les paramètres du modèle sont calibrés en utilisant des recherches approfondies, en tenant compte des facteurs d'âge, de sexe et régionaux sur la létalité, tout en ajustant les effets de quarantaine en fonction des données de COVID-19. Enfin, une approche d'optimisation novatrice combinant des algorithmes génétiques avec la méthode de Levenberg-Marquardt est introduite pour rationaliser le modèle de pandémie CAT et améliorer l'ajustement des paramètres dans des contextes multidimensionnels. La fiabilité du modèle est démontrée par des comparaisons avec la formule standard du SCR et les données historiques des pandémies, confirmant sa robustesse pour l'évaluation du risque de mortalité dans des scénarios extrêmes.

Mots-clés : algorithme génétique, COVID-19, méthode de Levenberg-Marquardt, modèle épidémiologique, risques de mortalité en pandémie, théorie des valeurs extrêmes

Synthèse

La pandémie de COVID-19 a considérablement perturbé les méthodologies traditionnelles d'évaluation des risques dans le secteur de l'assurance, mettant particulièrement en évidence les limitations rencontrées par des assureurs mondiaux comme AXA. Elle souligne l'insuffisance du choc de mortalité standardisé de 0,15% imposé par la directive Solvabilité II, qui ne tient pas compte des impacts divers de la pandémie à travers différents pays et populations. Reconnaisant la nécessité de modèles internes plus sophistiqués, cette étude vise à développer un modèle pandémique sur mesure qui intègre des facteurs épidémiologiques et socio-économiques affectant la mortalité, s'appuyant sur le cadre du modèle pandémique de Swiss Re. De plus, l'étude introduit une approche d'optimisation novatrice combinant algorithmiques génétiques et de Levenberg-Marquardt pour améliorer l'ajustement des paramètres dans des modèles complexes. En fin de compte, le but ultime est d'améliorer la compréhension des risques de mortalité pandémique, faciliter la conformité avec les réglementations de l'exigence de capital de solvabilité (SCR), et fournir des connaissances stratégiques pour une gestion efficace des risques dans les portefeuilles d'assurance mondiaux.

Aperçu du Modèle Pandémique

Le modèle pandémique de cette étude adopte une structure **Fréquence** × **Gravité** :

- **Fréquence** : Modélisée en utilisant $I \sim \text{Bernoulli}(p)$ avec $p = 4\%$. Le paramètre est estimé à partir des pandémies respiratoires historiques.
- **Gravité** : Calculée via le modèle épidémiologique SIID (Susceptible–Infecté–Immunisé–Décédé) avec des dynamiques d'atténuation.

La partie Gravité du modèle pandémique contient 3 composants différents : Transmissibilité, Létalité et Atténuation. Ces trois composants interagissent à travers le modèle épidémiologique SIID, comme illustré en Figure 1.

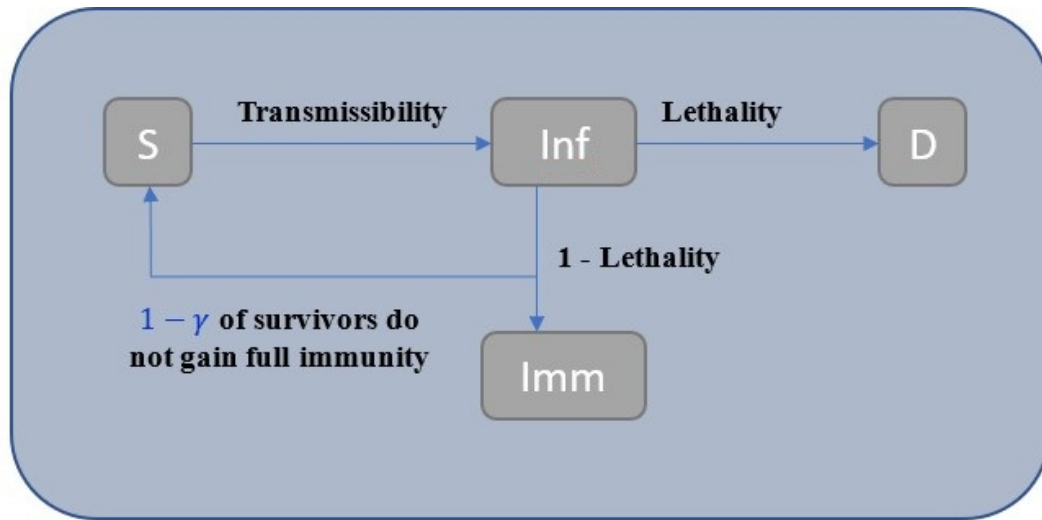


Figure 1: Structure du modèle épidémiologique

Structure du Modèle Épidémiologique

Ce modèle épidémiologique simule des scénarios pandémiques sur une période de 3 ans (1095 jours) en utilisant des étapes de temps discrets et quotidiens. Le modèle suit les transitions de la population entre quatre statuts de santé : **Susceptible (S)**, **Infecté (Inf)**, **Immunisé (Imm)** et **Décès (D)**; cf. Figure 1.

Paramètres Clés

Paramètres Stochastiques (générés aléatoirement par scénario) :

- **Taux de Reproduction de Base (R_0)** : Nombre moyen d'infections causées par une personne infectée dans une population entièrement susceptible.
- **Taux de Létalité de Base (\bar{L})** : Taux de décès moyen par infection dans la population totale.
- **Profil de Durée de Contagiosité (f)** : Fonction de densité de probabilité décrivant la contagiosité dans le temps selon le type de virus.

- **Facteur Spécifique à l'Âge (α)** : Ajuste la létalité en fonction du profil d'âge selon le type de virus.

Paramètres Prédéterminés :

- **Facteur Spécifique au Genre (δ)** : Ajuste la létalité selon la composition par sexe.
- **Facteur Spécifique à la Zone (β)** : Ajuste la létalité selon les caractéristiques du pays ou de la région.

Composant d'Atténuation

Les composants d'atténuation sont principalement calibrés en utilisant des connaissances de la récente expérience COVID-19, qui sont plus pertinents pour les réponses gouvernementales contemporaines aux pandémies.

- **Quarantaine** : Réduit la transmissibilité par la réduction des contacts. Elle définit la dynamique du nombre de reproduction au cours des différentes phases de quarantaine (c'est-à-dire, épidémie initiale, quarantaine, réouverture et transition).
- **Vaccination** : Réduit à la fois la transmissibilité et la létalité. Elle définit l'efficacité de la vaccination, le moment de distribution et la couverture maximale de la population.

Dynamique du Modèle Épidémiologique avec Atténuation

Avec la structure du modèle épidémiologique SIID, les dynamiques pandémiques sont capturées par les formules de transition. Nous présentons ici les deux formules de transition centrales définissant le nombre de nouvelles infections et le nombre de nouveaux décès.

Nouvelles Infections Quotidiennes

Le nombre de nouvelles personnes infectées le jour $t + 1$ est donné par :

$$\text{Inf}_r(t + 1, 1) \leftarrow R_t \cdot \frac{S_r(t)}{N_r(t)} \cdot \sum_{d=1}^{d_{\max}} \text{Inf}_r(t, d) \cdot f(d),$$

où R_t est le paramètre principal pour la Transmissibilité, qui est le nombre de reproduction (nombre moyen de personnes qui seraient ensuite infectées par une personne actuellement infectée) d'un virus au jour t , en fonction des phases de quarantaine; $f(d)$ est une fonction de densité de probabilité discrète pour une pandémie donnée (grippe ou coronavirus) décrivant la contagiosité au fil du temps après l'infection; $\frac{S_r(t)}{N_r(t)}$ est la proportion de la population susceptible ; d_{max} est le nombre maximum de jours d'infection.

Nouveaux Décès Quotidiens

Le nombre de nouveaux décès le jour $t + 1$ est :

$$\begin{aligned} newD_r(t+1) &\leftarrow Inf_r(t, d_{max}) * effective_Lethality \\ &= Inf_r(t, d_{max}) * \bar{L} * \alpha_{entity, shape} * \delta_{entity} * \beta_r * \mu(t - d_{max}), \end{aligned}$$

où \bar{L} est le taux de létalité de base ; $\alpha_r, \delta_r, \beta_r$ sont respectivement les facteurs d'âge, de sexe et de zone pour la létalité dans le pays ou la région r ; μ est l'effet de réduction de la létalité dû à l'immunité partielle (lorsque les personnes ne bénéficient pas d'une immunité complète après infection ou vaccination et peuvent être réinfectées).

Calibration des Facteurs de Zone

En plus d'utiliser les données historiques des pandémies pour calibrer d'autres paramètres clés, l'étude présente également une nouvelle méthodologie pour calibrer les facteurs de létalité spécifiques à la zone, tenant compte des variations au niveau des pays dans la mortalité pandémique. L'approche utilise les données de COVID-19 pour établir des ajustements de létalité de base basés sur les caractéristiques des pays, avec une méthode d'ajustement indirect par âge.

Étape 1 : Sélection de la Mesure de Mortalité

- **Mesure choisie** : Mortalité excédentaire par million d'habitants (janv. 2020 - janv. 2021)
- **Raisonnement** : Plus complet que les décès COVID-19 seuls ; capture les effets indirects de la pandémie ; évite les problèmes de sous-déclaration dus à des tests limités

- **Période temporelle** : Période pré-vaccination pour éviter les effets de confusion

Étape 2 : Ajustement de la Structure d'Âge

Nous utilisons une méthode d'ajustement indirect par âge avec la France comme référence :

$$Compare_exM^{country} = \sum_{age} exM_{age}^{France} \times Proportion_{age}^{country}, \quad (1)$$

où $Compare_exM^{country}$ est la mortalité excédentaire comparable lors de l'application des taux en France avec la structure d'âge du pays cible (ce qui aide à éliminer l'impact de l'âge) ; exM_{age}^{France} est la mortalité excédentaire en France pour une certaine tranche d'âge ; $Proportion_{age}^{country}$ est la structure d'âge pour le pays cible.

Ensuite, nous calculons un ratio ajusté par âge pour évaluer la performance du pays cible :

$$exM_Adj_Rate^{country} = \frac{exM^{country}}{Compare_exM^{country}} \quad (2)$$

Étape 3 : Normalisation du Taux d'Infection

Nous utilisons les estimations d'infection pour normaliser le taux d'infection (Indice de Létalité) entre différents pays :

$$Lethality_Index^{country} = \frac{exM_Adj_Rate^{country}}{Infected_Ratio^{country}} \quad (3)$$

L'étude applique ensuite des méthodes de régression (linéaire, log-linéaire et exponentielle) à l'Indice de Létalité calculé, en utilisant un éventail d'indicateurs au niveau des pays comme variables explicatives. Ceux-ci incluent l'espérance de vie, l'Indice de Vulnérabilité à la Santé (GHS), le coefficient de Gini, l'Indice de Préparation de l'OMS et le PIB par habitant.

Le modèle le mieux ajusté—régression linéaire—est sélectionné, donnant une valeur $R^2 = 45.5\%$. L'espérance de vie est utilisée comme seule variable prédictive, étant donné sa forte corrélation avec les autres indicateurs au niveau des pays, qui pourraient autrement introduire de la multicolinéarité.

$$Lethality_Index_r = -1.1929 \times LE_r + 105.36 \quad (4)$$

En utilisant la France comme référence, le facteur de zone est ensuite calculé comme :

$$\beta_r = \frac{Lethality_Index_r}{Lethality_Index_{France}} \quad (5)$$

Métriques de Sortie

Le modèle génère des taux de mortalité à travers différents scénarios avec une simulation de Quasi-Monte-Carlo pour déterminer le risque au 99,5e percentile, tenant compte de l'hypothèse de fréquence pandémique de 4%.

Innovation du Modèle

Tout d'abord, contrairement au Modèle Pandémique de Swiss Re—qui repose uniquement sur trois pandémies historiques—cette étude élargit l'ensemble de données pour inclure six grandes pandémies historiques, s'appuyant sur une littérature extensive pour soutenir un calibrage des paramètres plus robuste. Deuxièmement, l'étude introduit une approche novatrice pour calibrer le Facteur de Zone, conçue pour isoler l'impact des caractéristiques spécifiques aux pays sur la létalité en éliminant les influences démographiques. Troisièmement, en s'appuyant sur des insights empiriques de la pandémie de COVID-19, l'étude intègre un cadre de quarantaine en quatre phases pour modéliser les changements temporels dans le nombre de reproduction effectif (R_t), capturant les effets dynamiques des interventions de santé publique au cours d'une épidémie.

Nouvelle Méthode d'Initialisation Pour l'Ajustement de la Distribution Hybride LN-EGPD

Méthode actuelle via l'introduction d'une distribution hybride : Lognormale-Exponentielle-GPD (Ln-E-GPD)

Nous fournissons une analyse statistique des taux de mortalité pandémique simulés à travers la théorie des valeurs extrêmes (EVT), en mettant l'accent sur les défis posés par des données à queues lourdes et asymétriques dérivées de plus de 10 000 scénarios de simulation. Plutôt que d'utiliser les méthodes 'POT' Peak over threshold, méthodes classiques en EVT, nous empruntons la méthode algorithmique de [Dacorogna et al. \(2023\)](#) basée sur le modèle hybride LN-E-GPD, qui permet la détection automatique du seuil à partir duquel les observations sont considérées comme extrêmes. Le modèle LN-E-GPD combine trois composants : une distribution lognormale, une distribution exponentielle et une distribution de Pareto généralisée (GPD). Ce cadre hybride est spécifiquement conçu pour traiter les caractéristiques des données positives asymétriques, courantes dans les scénarios CAT. La fonction de densité de probabilité (pdf) du LN-E-GPD est exprimée comme suit :

$$h(x; \theta) = \gamma_1 f(x; \mu, \sigma) \mathbf{1}_{(x \leq u_1)} + \gamma_2 e(x; \lambda) \mathbf{1}_{(u_1 \leq x \leq u_2)} + \gamma_3 g(x - u_2; \xi, \beta) \mathbf{1}_{(x \geq u_2)},$$

où :

- $f(x; \mu, \sigma)$ est la pdf lognormale avec les paramètres μ (moyenne) et σ (écart type).
- $e(x; \lambda)$ est la pdf exponentielle caractérisée par l'intensité λ .
- $g(x - u_2; \xi, \beta)$ est la pdf de la GPD, définie avec un indice de queue ξ (indiquant un comportement à queues lourdes) et un paramètre d'échelle β .

Les poids γ_i (pour $i \in \{1, 2, 3\}$) garantissent que l'ensemble de la fonction est une pdf valide, satisfaisant la condition $\gamma_1 + \gamma_2 + \gamma_3 \geq 1$. Les points de jonction u_1 et u_2 définissent les transitions entre les différents composants de distribution.

L'ajustement de ce modèle repose sur un algorithme itératif basé sur la méthode de Levenberg-Marquardt (cf. [Debbabi et al. \(2016\)](#)), suite à une 1ère étape d'initialisation des paramètres, non automatique (qui souvent nécessite une analyse distincte des données). La convergence de l'algorithme est analysée tant sur le plan analytique que numérique. Initialement, les paramètres pour le corps de la distribution et le seuil u_2 sont fixés, permettant l'estimation de l'indice de queue lors de la première itération. L'indice de queue est ensuite maintenu constant tandis que d'autres paramètres sont estimés à travers un processus itératif qui alterne entre l'estimation du corps et de la queue, utilisant la technique de Levenberg-Marquardt (LM) pour minimiser deux métriques de distance : une pour l'ajustement global du modèle et une autre axée sur le comportement de la queue jusqu'à ce que la convergence soit atteinte.

Défis Principaux

Un défi majeur dans cette approche est la sélection des paramètres initiaux. Dans le cas du modèle G-E-GPD pour des données plus ou moins symétriques autour de la moyenne, où l'on applique le CLT pour approcher le comportement moyen par une Gaussienne, prendre un estimateur de moments pour l'initialisation des paramètres de la Gaussienne conduit à la convergence. Pour la Lognormale, cette phase d'initialisation est plus manuelle. De plus, la susceptibilité de la technique LM aux minima locaux souligne la nécessité d'une initialisation soignée pour garantir une optimisation robuste.

Introduction de l'Algorithme Génétique (GA) pour l'Initialisation

Pour surmonter les défis associés à l'initialisation des paramètres et, en conséquence, à l'optimisation dans le calibrage du modèle LN-E-GPD, cette étude introduit l'Algorithme Génétique (GA) comme une innovation clé pour cette étude. Le GA est une technique d'optimisation métaheuristique inspirée par les principes de la sélection naturelle et de l'évolution génétique. Il est particulièrement efficace pour explorer des espaces de paramètres plus larges, ce qui le rend bien adapté aux fonctions complexes caractéristiques du modèle LN-E-GPD.

Le GA fonctionne à travers quatre composants majeurs :

- **Initialisation** : Génère une population initiale diversifiée de solutions potentielles, aidant à élargir l'exploration et réduisant le risque d'optimisation locale.

- **Sélection** : Choisit des individus en fonction de leur aptitude pour créer la prochaine génération, guidant l'algorithme vers de meilleures solutions.
- **Crossover** : Combine le matériel génétique d'individus sélectionnés pour produire des descendants, promouvant la diversité et l'exploration de nouvelles solutions.
- **Mutation** : Introduit des changements aléatoires pour maintenir la diversité de la population, empêchant la convergence prématurée.

Utiliser le GA pour l'optimisation des paramètres initiaux permet d'éviter la convergence de l'algorithme vers un min local et améliore ainsi le processus de calibrage du modèle LN-E-GPD. Après avoir établi un ensemble robuste de valeurs initiales de paramètres grâce au GA, le modèle peut ensuite être ajusté à l'aide de la méthode LM pour une convergence vers un optimum global. Combiner ces 2 méthodes algorithmiques (GA et LM basé sur le modèle LN-E-GPD) améliore non seulement le processus d'optimisation, mais renforce également l'applicabilité du modèle à travers divers ensembles de données, en particulier dans le contexte de la modélisation de la mortalité pandémique.

Pour évaluer la robustesse des différents réglages de paramètres dans l'algorithme génétique (GA), une approche semblable à celle du jackknife a été mise en œuvre. Cette méthode évalue la stabilité et la cohérence des paramètres de sortie du modèle en excluant itérativement des sous-ensembles de données et en observant l'impact sur les estimations de paramètres. Des configurations de paramètres robustes produisent des résultats stables à travers différents sous-ensembles, indiquant une résilience face à des points de données spécifiques ou de petites variations.

L'analyse englobe 16 combinaisons différentes de réglages de paramètres GA, dérivées de 2 méthodes pour chaque composant :

- Deux méthodes d'initialisation : Échantillonnage par hypercube latin (LHS) et population d'échantillons aléatoires.
- Deux méthodes de sélection : classement linéaire (LR) et roulette (RW).
- Deux méthodes de crossover : mélange (BLX) et point unique (SP).
- Deux méthodes de mutation : arithmétique aléatoire (RA) et substitution aléatoire (RS).

Ces 8 méthodes ont été choisies en fonction du principe de réglage minimal afin d'assurer la robustesse et la facilité de mise en œuvre.

Les étapes suivantes ont été exécutées pour effectuer l'analyse jackknife :

- **Exclusion de Données :** 10% des données ont été aléatoirement exclues à chaque exécution, répétées sur dix itérations par configuration de paramètres.
- **Évaluation des Paramètres :** Les paramètres de sortie ont été enregistrés après chaque itération. L'écart type normalisé par la moyenne (c'est-à-dire le coefficient de variation) a été calculé pour indiquer la volatilité, des valeurs plus faibles indiquant une plus grande stabilité.
- **Classement de Robustesse :** Chaque configuration a été classée en fonction de la stabilité des paramètres de sortie, les coefficients de variation plus bas étant considérés comme plus robustes.

Une fois que le GA a identifié un ensemble optimal de paramètres initiaux, la méthode de Levenberg-Marquardt (LM) est utilisée pour obtenir les estimations de LN-E-GPD. Ce processus d'optimisation hybride GA et LM atteint à la fois une initialisation informée au niveau global et permet un traitement automatique de début à la fin pour estimer les paramètres du modèle LN-E-GPD, améliorant ainsi la robustesse et la précision de l'ajustement du modèle.

Résultats d'Ajustement du Modèle Pandémique Final

La configuration du GA a été calculée en utilisant le package GA dans R, avec les paramètres définis sur des valeurs par défaut pour la comparabilité.

La configuration la plus stable est **Pop:LHS, Sel:RW, Mut:RS, Cross:SP** avec les plus faibles rapports d'écart type global à la moyenne. Cette configuration démontre l'efficacité de l'échantillonnage par hypercube latin, de la sélection par roulette, de la mutation par remplacement aléatoire et du crossover à un point unique.

Les paramètres finaux estimés ont été obtenus en combinant l'Algorithme Génétique (GA) et l'optimiseur de Levenberg-Marquardt (LM). La performance de cette méthode combinée a été évaluée à l'aide de données simulées, démontrant sa stabilité et sa supériorité par rapport à la méthode LM pure, i.e. sans recherche préalable des paramètres initiaux. Pour l'analyse des sorties du modèle CAT Pandemic,

l'indice de queue a été examiné, et l'approche hybride a été comparée aux distributions traditionnelles (Normale, Lognormale et Exponentielle) ainsi qu'à la méthode LM pure appliquée à la LN-E-GPD. La performance a été évaluée à l'aide de l'erreur quadratique moyenne (RMSE) pour l'ajustement global et pour la région de la queue (valeurs au-dessus du seuil u_2).

L'optimisation GA+LM a abouti aux estimations finales des paramètres sur le résultat du modèle pandémique, résumées dans le tableau 1.

Modèle	μ	σ	γ_1	u_1	λ	γ_2	ξ	u_2	β	γ_3
LN-E-GPD	-6.662	1.883	1.4	0.11%	894.1	0.815	0.559	0.312%	0.00174	0.0780

Table 1: Valeurs des paramètres pour le modèle LN-E-GPD

L'indice de queue ξ est crucial pour caractériser le comportement extrême ; une valeur positive indique une distribution à queues lourdes. La GPD ajustée au-dessus de u_2 montre un paramètre de forme $\alpha = 1/\xi = 1.80$, indiquant une queue lourde avec un premier moment fini mais variance infinie.

Les valeurs RMSE pour chaque méthode sont résumées dans le tableau 2.

Modèle	RMSE Global (%)	RMSE de la Queue (%) (au-dessus de u_2)
Distribution Normale	11.8	2.0
Distribution Lognormale	3.1	2.9
Méthode LM Pure	0.364	0.718
Optimiseur GA+LM	0.357	0.628

Table 2: Comparaison des RMSE pour les régions globale et de queue

L'optimiseur GA+LM démontre des valeurs RMSE significativement plus basses dans les régions globale et de queue par rapport aux distributions traditionnelles et surpasse légèrement la méthode LM pure. Bien que les distributions traditionnelles comme la Lognormale présentent un ajustement global raisonnable (RMSE de 3.1%), l'optimiseur GA+LM réalise une amélioration de 2% du RMSE global et de 14% du RMSE de la queue par rapport à la méthode LM pure, indiquant une meilleure solution optimale.

Analyse des Résultats et Validation

La sortie de mortalité pandémique du modèle Hybrid GPD ajusté à l'aide de l'optimiseur GA+LM est comparée au composant de choc de mortalité dans la formule SCR standard de 0.15%, à travers divers pays et régions où AXA opère, ainsi que différents groupes d'âge.

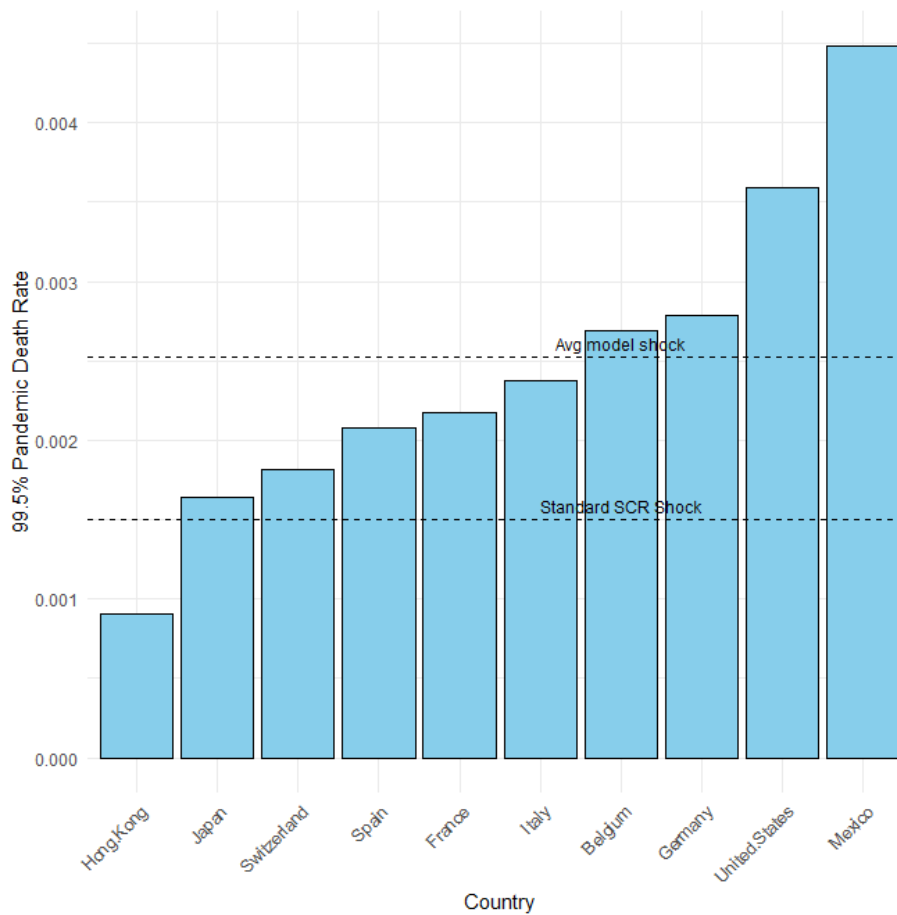


Figure 2: Comparaison avec le choc standard de la SCR

La formule SCR sert de référence pour l'adéquation du capital en réponse aux risques de mortalité. Elle dicte les buffers de capital nécessaires pour résister à des événements de mortalité extrêmes, garantissant la solvabilité et la gestion des risques. En revanche, le modèle interne offre une approche sur mesure et empiriquement calibrée qui capture les facteurs géographiques et démographiques sous-représentés dans la formule SCR standard.

Les données présentées dans la Figure 2 indiquent que la majorité des chocs de mortalité dépassent le choc standard de la SCR, avec un choc moyen du modèle de 0.253% par rapport au choc standard de la SCR de 0.15%. Il est important de noter que le choc moyen du modèle est calculé sans tenir compte de la taille de la population de chaque pays, et le profil d'âge peut différer entre le portefeuille d'assurance et la population générale. Pour d'autres études, les données du portefeuille d'assurance peuvent être analysées en utilisant le modèle CAT Pandemic introduit dans cette étude.

Conclusion

Cette thèse fait progresser significativement le domaine dans trois domaines clés :

1. Elle améliore le modèle pandémique de Swiss Re en intégrant des facteurs géographiques et en le calibrant sur de vastes ensembles de données, en s'appuyant sur les enseignements tirés de la COVID-19 pour une plus grande pertinence dans le monde réel.
2. Elle développe un nouvel algorithme d'optimisation hybride qui combine des algorithmes génétiques pour la phase d'initialisation des paramètres du modèle hybride LN-E-GPD estimés via un algorithme itératif basé sur la méthode de Levenberg-Marquardt, améliorant ainsi le calibrage du modèle LN-E-GPD pour les pandémies et élargissant son applicabilité à d'autres défis d'optimisation.
3. Elle valide le modèle par rapport aux données historiques des pandémies, démontrant son utilité pratique pour les compagnies d'assurance dans la gestion des risques et fournissant une base quantitative pour que les décideurs évaluent les stratégies d'intervention.

Synthesis

COVID-19 pandemic has significantly disrupted traditional risk assessment methodologies in the insurance sector, particularly highlighting the limitations faced by global insurers like AXA. It emphasizes the inadequacy of the standardized mortality shock of 0.15% mandated by the Solvency II Directive, which fails to account for the diverse impacts of the pandemic across various countries and populations. Recognizing the need for more sophisticated internal models, the study aims to develop a tailored pandemic model that integrates epidemiological and socio-economic factors affecting mortality, building on the Swiss Re pandemic model framework. Additionally, the study introduces a novel optimization approach combining Genetic Algorithms with the Levenberg-Marquardt method to enhance parameter fitting in complex models. Ultimately, the aim is to improve understanding of pandemic mortality risks, facilitate compliance with Solvency Capital Requirement (SCR) regulations, and provide strategic insights for effective risk management in global insurance portfolios.

Pandemic Model Overview

The pandemic model in this study adopts a **Frequency** \times **Severity** structure:

- **Frequency**: Modeled using $I \sim \text{Bernoulli}(p)$ with $p = 4\%$. The parameter is estimated from historical respiratory pandemics.
- **Severity**: Computed via the SIID (Susceptible–Infected–Immune–Deceased) epidemiological model with mitigation dynamics.

The Severity part of the pandemic model contains 3 different components: Transmissibility, Lethality, and Mitigation. The three components interact through the SIID epidemiological model, as shown in 3.

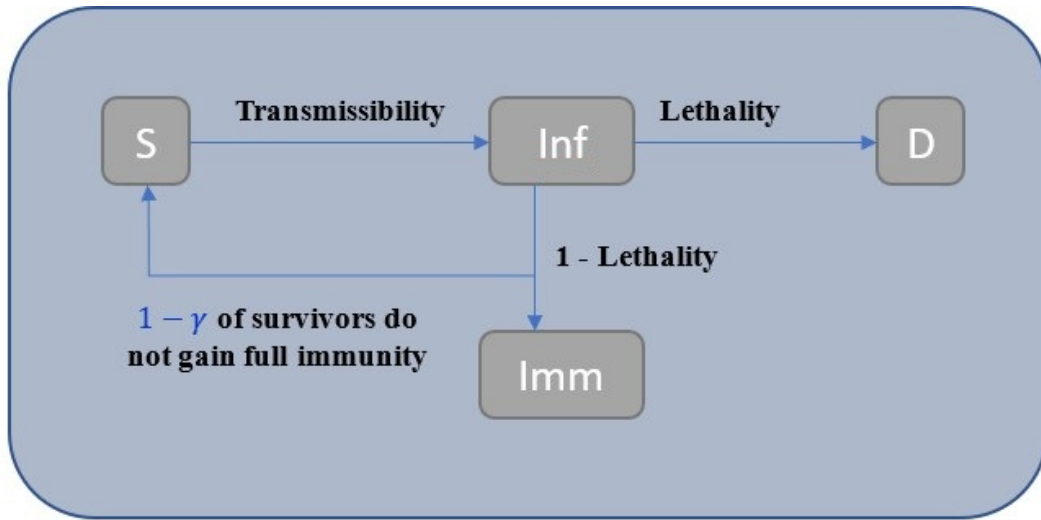


Figure 3: Epidemiological model structure

Epidemiological Model Structure

This epidemiological model simulates pandemic scenarios over a 3-year period (1095 days) using discrete daily time steps. The model tracks population transitions between four health statuses: **Susceptible** (*S*), **Infected** (*Inf*), **Immune** (*Imm*), and **Death** (*D*); see in Figure 3.

Core Parameters

Stochastic Parameters (randomly generated per scenario):

- **Basic Reproduction Number (R_0)**: Average infections caused by one infected person in a fully susceptible population.
- **Baseline Lethality Rate (\bar{L})**: Average death rate per infection in total population.
- **Duration Profile of Infectiousness (f)**: Probability density function describing infectiousness over time depending on virus type.
- **Age-specific Factor (α)**: Adjusts lethality by age profile depending on virus type.

Pre-determined Parameters:

- **Gender-specific Factor (δ)**: Adjusts lethality by gender composition.
- **Area-specific Factor (β)**: Adjusts lethality by country or region characteristics.

Mitigation Component

The mitigation components are mainly calibrated using insights from the latest COVID-19 experience, which is more relevant to contemporary government responses to pandemics.

- **Quarantine:** Reduces transmissibility through contact reduction. It defines the reproduction number dynamic over different quarantine phases (i.e., outbreak, quarantine, reopening, and transition).
- **Vaccination:** Reduces both transmissibility and lethality. It defines the vaccination effectiveness, the distribution timing, and the maximum coverage over a population.

Epidemiological Model Dynamics with Mitigation

With the SIID epidemiological model structure, the pandemic dynamics are captured by the transition formulas. Here we show the two core transition formulas defining the new infection number and new death numbers.

New Daily Infections

The number of newly infected individuals on day $t + 1$ is given by:

$$\text{Inf}_r(t + 1, 1) \leftarrow R_t \cdot \frac{S_r(t)}{N_r(t)} \cdot \sum_{d=1}^{d_{\max}} \text{Inf}_r(t, d) \cdot f(d),$$

where R_t is the major parameter for Transmissibility, which is the reproduction number (average number of people who would subsequently be infected by one currently infected person) of a virus on day t , depending on quarantine phases; $f(d)$ is a discrete probability density function for a given pandemic (Influenza or Coronavirus) describing the infectiousness over time after infection; $\frac{S_r(t)}{N_r(t)}$ is the proportion of susceptible population; d_{\max} is the maximum number of days being infected.

New Daily Deaths

The number of new deaths on day $t + 1$ is:

$$\begin{aligned} newD_r(t + 1) &\leftarrow Inf_r(t, d_{max}) * effective_Lethality \\ &= Inf_r(t, d_{max}) * \bar{L} * \alpha_{entity, shape} * \delta_{entity} * \beta_r * \mu(t - d_{max}), \end{aligned}$$

where \bar{L} is the baseline lethality rate; $\alpha_r, \delta_r, \beta_r$ are the age, gender, area factors for lethality in country or region r , respectively; μ is the lethality reduction effect from partial immunity (when people do not get full immunity after infection or vaccination and can be infected again).

Area Factor Calibration

Apart from using historical pandemic data to calibrate other core parameters, the study also presents a new methodology for calibrating area-specific lethality factors that account for country-level variations in pandemic mortality. The approach uses COVID-19 data to establish baseline lethality adjustments based on country characteristics, with an indirect age-adjustment method.

Step 1: Mortality Measure Selection

- **Chosen measure:** Excess mortality per million people (Jan 2020 - Jan 2021)
- **Rationale:** More comprehensive than COVID-19 deaths alone; captures indirect pandemic effects; avoids under reporting issues from limited testing
- **Time period:** Pre-vaccination period to avoid confounding effects

Step 2: Age Structure Adjustment

We use indirect age-adjustment method with France as benchmark:

$$Compare_exM^{country} = \sum_{age} exM_{age}^{France} \times Proportion_{age}^{country}, \quad (6)$$

where $Compare_exM^{country}$ is the comparable excess mortality when applying the rates in France with

the target country's age structure (this helps remove the age impact); exM_{age}^{France} is the excess mortality in France for certain age band; $Proportion_{age}^{country}$ is the age structure for the target country.

Then we compute an Age-adjusted ratio to assess the target country's performance:

$$exM_Adj_Rate^{country} = \frac{exM^{country}}{Compare_exM^{country}} \quad (7)$$

Step 3: Infection Rate Normalization

We use IHME infection estimates to normalize the infection rate (Lethality Index) between different countries:

$$Lethality_Index^{country} = \frac{exM_Adj_Rate^{country}}{Infected_Ratio^{country}} \quad (8)$$

The study then applies regression methods (linear, log-linear and exponential) to the computed Lethality Index, using a range of country-level indicators as explanatory variables. These include life expectancy, the Global Health Security (GHS) Health Vulnerability Index, the Gini coefficient, the WHO Preparedness Index, and GDP per capita.

The best-fitting model—linear regression—is selected, yielding a value of $R^2 = 45.5\%$. Life expectancy is used as the sole predictor variable, given its strong correlation with the other country-level indicators, which could otherwise introduce multicollinearity.

$$Lethality_Index_r = -1.1929 \times LE_r + 105.36 \quad (9)$$

Using France as reference the area factor is then computed as:

$$\beta_r = \frac{Lethality_Index_r}{Lethality_Index_{France}} \quad (10)$$

Output Metrics

The model generates mortality rates across different scenarios with Quasi-Monte-Carlo simulation to determine the 99.5th percentile risk, accounting for the 4% pandemic frequency assumption.

Model Innovation

First, in contrast to the Swiss Re’s Pandemic Model—which relies on only three historical pandemics—this study expands the dataset to include six major historical pandemics, drawing from extensive literature to support more robust parameter calibration. Second, the study introduces a novel approach to calibrating the Area Factor, designed to isolate the impact of country-specific characteristics on lethality by removing demographic influences. Third, leveraging empirical insights from the COVID-19 pandemic, the study incorporates a four-phase quarantine framework to model time-varying changes in the effective reproduction number (R_t), capturing the dynamic effects of public health interventions over the course of an outbreak.

New Initialization Method For Hybrid LN-E-GPD Fitting

Current Method Via The Introduction Of A Hybrid Distribution: Lognormal-Exponential-GPD (Ln-E-GPD)

We provide statistical analysis of simulated pandemic mortality rates through Extreme Value Theory (EVT), emphasizing the challenges posed by heavy-tailed and asymmetric data derived from over 10,000 simulation scenarios. Rather than using the classic Peak over threshold ‘POT’ methods in EVT, we use the algorithmic method of [Dacorogna et al. \(2023\)](#) based on the hybrid LN-E-GPD model, which allows the automatic detection of the threshold from which observations are considered extreme.

The LN-E-GPD model combines three components: a lognormal distribution, an exponential distribution, and a generalized Pareto distribution (GPD). This hybrid framework is specifically designed to address the characteristics of asymmetric positive data, which is common in CAT scenarios. The probability density function (pdf) of the LN-E-GPD is expressed as:

$$h(x; \theta) = \gamma_1 f(x; \mu, \sigma) \mathbf{1}_{(x \leq u_1)} + \gamma_2 e(x; \lambda) \mathbf{1}_{(u_1 \leq x \leq u_2)} + \gamma_3 g(x - u_2; \xi, \beta) \mathbf{1}_{(x \geq u_2)},$$

where:

- $f(x; \mu, \sigma)$ is the lognormal pdf with parameters μ (mean) and σ (standard deviation).

- $e(x; \lambda)$ is the exponential pdf characterized by intensity λ .
- $g(x - u_2; \xi, \beta)$ is the pdf of the GPD, defined with tail index ξ (indicating heavy-tailed behavior) and scale parameter β .

The weights γ_i (for $i \in \{1, 2, 3\}$) ensure that the entire function is a valid pdf, satisfying the condition $\gamma_1 + \gamma_2 + \gamma_3 \geq 1$. The junction points u_1 and u_2 define the transitions between the different distribution components.

The adjustment of this model is based on an iterative algorithm based on the Levenberg-Marquardt method (see [Debbabi et al. \(2016\)](#)), following a first step of initialization of the parameters, which is not automatic (which often requires a separate analysis of the data). The convergence of the algorithm is analyzed both analytically and numerically. Initially, parameters for the body of the distribution and the threshold u_2 are set, allowing for the estimation of the tail index in the first iteration. The tail index is subsequently held constant while other parameters are estimated through an iterative process that alternates between body and tail estimation, utilizing the Levenberg-Marquardt (LM) technique to minimize two distance metrics: one for the overall model fit and another focused on the tail behavior until convergence is achieved.

Core Challenges

A significant challenge in this approach is the selection of initial parameters. In the case of the G-E-GPD model for data more or less symmetrical around the mean, where we apply the CLT to approximate the mean behavior by a Gaussian, taking a moment estimator for the initialization of the parameters of the Gaussian leads to convergence. For the Lognormal, this initialization phase is more manual. Furthermore, the LM technique's susceptibility to local minima underscores the need for careful initialization to ensure robust optimization.

Introduction of Genetic Algorithm (GA) for Initialization

To overcome the challenges associated with parameter initialization and, consequently, to optimization in calibrating the LN-E-GPD model, this study introduces the Genetic Algorithm (GA) as a key innovation for this study. GA is a metaheuristic optimization technique inspired by the principles of natural selection

and genetic evolution. It is particularly effective in exploring broader parameter spaces, making it well suited for the complex functions characteristic of the LN-E-GPD model.

The GA functions through four major components:

- **Initialization:** Generates a diverse initial population of potential solutions, helping to broaden exploration and reducing the risk of local optimization.
- **Selection:** Chooses individuals based on fitness to create the next generation, guiding the algorithm toward better solutions.
- **Crossover:** Combines genetic material from selected individuals to produce offspring, promoting diversity and the exploration of new solutions.
- **Mutation:** Introduces random changes to maintain population diversity, preventing premature convergence.

Employ the GA for the initial parameter optimization allows to avoid the convergence of the algorithm towards a local min and thus improves the calibration process of the LN-E-GPD model. After establishing a robust set of initial parameter values through GA, the model can then be fine-tuned using the LM method for a convergence towards a global optimum. Combine these 2 algorithmic methods (GA and LM based on the LN-E-GPD model) not only improves the optimization process but also enhances the model's applicability across various datasets, particularly in the context of pandemic mortality modeling.

To assess the robustness of various parameter settings in the genetic algorithm (GA), a jackknife-like approach was implemented. This method evaluates the stability and consistency of model output parameters by iteratively excluding subsets of data and observing the impact on parameter estimates. Robust parameter configurations produce stable results across different subsets, indicating resilience to specific data points or small variations.

The analysis encompasses 16 different combinations of GA parameter settings, derived from 2 methods for each component:

- Two initialization methods: Latin Hypercube Sampling (LHS) and random sample population.
- Two selection methods: linear rank (LR) and roulette wheel (RW).

- Two crossover methods: blend (BLX) and single point (SP).
- Two mutation methods: random arithmetic (RA) and random substitute (RS).

These 8 methods are chosen based on the principle of minimal fine-tuning to ensure robustness and ease of implementation.

The following steps were executed to perform the jackknife analysis:

- **Data Exclusion:** 10% of the data was randomly excluded in each run, repeated across ten iterations per parameter configuration.
- **Parameter Evaluation:** Output parameters were recorded after each iteration. The standard deviation normalized by the mean (i.e., the coefficient of variation) was calculated to indicate volatility, with lower values indicating greater stability.
- **Robustness Ranking:** Each configuration was ranked based on the stability of output parameters, with lower coefficients of variation considered more robust.

Once the GA identifies an optimal set of initial parameters, the Levenberg-Marquardt (LM) method is employed to obtain LN-E-GPD estimates. This hybrid GA and LM optimization process achieves both globally informed initialization and allows automatic processing to estimate the parameters of the LN-E-GPD model, enhancing the overall robustness and accuracy of the model fitting.

Final Pandemic Model Output Fitting Results

The GA configuration was computed using the GA package in R, with the parameters set to default values for comparability.

The most stable configuration is **Pop:LHS, Sel:RW, Mut:RS, Cross:SP** with the lowest overall standard deviation to mean ratios. This configuration demonstrates the effectiveness of Latin Hypercube Sampling, roulette wheel selection, random replace mutation, and single point crossover.

The final estimated parameters were obtained by combining the Genetic Algorithm (GA) and the Levenberg-Marquardt (LM) optimizer. The performance of this combined method was evaluated using simulated data, demonstrating its stability and superiority compared to the pure LM method, i.e., without

prior search of the initial parameters. For the analysis of the CAT Pandemic model outputs, the tail index was examined, and the hybrid approach was compared against traditional distributions (Normal, Lognormal, and Exponential) and the pure LM method applied to LN-E-GPD. Performance was assessed using the Root Mean Square Error (RMSE) for both the overall fit and the tail region (values above threshold u_2).

The GA+LM optimization yielded the final parameter estimates on the pandemic model result, summarized in Table 3.

Model	μ	σ	γ_1	u_1	λ	γ_2	ξ	u_2	β	γ_3
LN-E-GPD	-6.662	1.883	1.4	0.11%	894.1	0.815	0.559	0.312%	0.00174	0.0780

Table 3: Parameter values for the LN-E-GPD model

The tail index ξ is crucial for characterizing extremal behavior; a positive value indicates a heavy-tailed distribution. The fitted GPD above u_2 shows a shape parameter $\alpha = 1/\xi = 1.80$, indicating a heavy tail with a finite first moment but infinite variance.

The RMSE values for each method are summarized in Table 4.

Model	Overall RMSE (%)	Tail RMSE (%) (above u_2)
Normal Distribution	11.8	2.0
Lognormal Distribution	3.1	2.9
Pure LM Method	0.364	0.718
GA+LM Optimizer	0.357	0.628

Table 4: RMSE comparison for overall and tail regions

The GA+LM optimizer demonstrates significantly lower RMSE values in both overall and tail regions compared to traditional distributions and slightly outperforms the pure LM method. While traditional distributions like the Lognormal exhibit reasonable overall fit (3.1% RMSE), the GA+LM optimizer achieves a 2% improvement in overall RMSE and a 14% improvement in tail RMSE compared to the pure LM method, indicating a better optimal solution.

Results Analysis and Validation

The pandemic mortality output from the Hybrid GPD model fitted using the GA+LM optimizer is compared against the mortality shock component in the standard SCR formula of 0.15%, across various countries and regions where AXA operates, and different age groups.

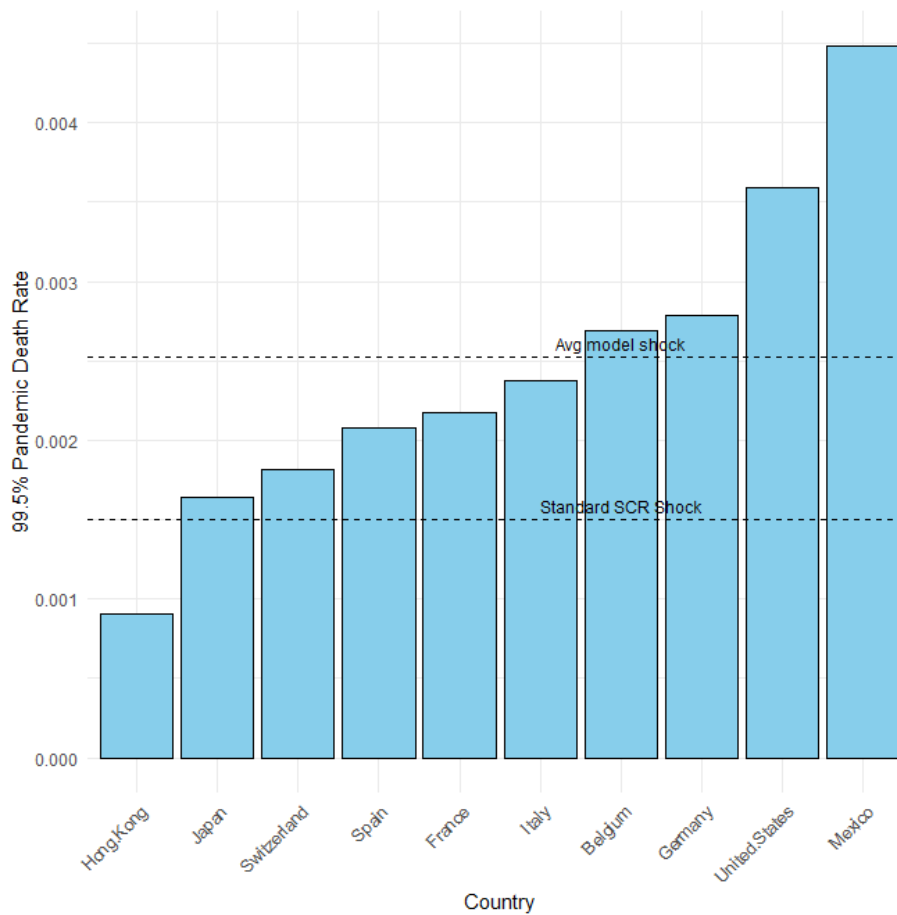


Figure 4: Comparison with Standard SCR shock

The SCR formula serves as a benchmark for capital adequacy in response to mortality risks. It dictates the capital buffers necessary to withstand extreme mortality events, ensuring solvency and risk management. In contrast, the internal model offers a tailored and empirically calibrated approach that captures geographic and demographic factors underrepresented in the standard SCR formula.

The data presented in Figure 4 indicates that the majority of death shocks surpass the standard SCR shock, with an average model shock of 0.253% compared to the standard SCR shock of 0.15%. It is important to note that the average model shock is calculated without accounting for the population size of each country, and the age profile may vary between the insurance portfolio and the general population. For further studies, the insurance portfolio data can be analyzed using the CAT Pandemic model introduced in this study.

Conclusion

This thesis significantly advances the field in three key areas:

1. It enhances the Swiss Re pandemic model by incorporating geographical factors and calibrating it against extensive datasets, drawing on insights from COVID-19 for greater real-world relevance.
2. It develops a new hybrid optimization algorithm that combines genetic algorithms for the initialization phase of the parameters of the hybrid LN-E-GPD model improved via an iterative algorithm based on the method of Levenberg-Marquardt methods, thereby improving the calibration of the LN-E-GPD model for pandemics and expanding its applicability to other optimization challenges.
3. It validates the model against historical pandemic data, demonstrating its practical utility for insurance companies in risk management and providing a quantitative foundation for policymakers to assess intervention strategies.

Acknowledgments

First of all, I would like to express my great gratitude to Professor Marie Kratz for her invaluable guidance throughout the writing of this thesis. Her ability to clarify complex ideas and offer thoughtful feedback whenever I found myself stuck was instrumental in moving my research forward. I am especially inspired by her professionalism and meticulous attention to detail, which continuously encouraged me to refine and elevate the quality of my work. Her unwavering support and intellectual generosity made this journey both intellectually enriching and personally rewarding.

I am also deeply thankful to my managers at work, Pierre-Henri Brouard and Aurélie Viossat, for their mentorship and encouragement during my research on pandemic modeling. Their practical insights helped bridge the gap between academic theory and business application, bringing real-world clarity to abstract ideas. Many obstacles I faced were resolved thanks to their thoughtful questions and constructive discussions, which shaped my understanding of how to approach complex modeling problems in a pragmatic and structured way.

My sincere thanks go as well to the AXA GRM Life team. Working alongside them gave me a deeper appreciation of the challenges and responsibilities involved in insurance risk management. Their openness in sharing knowledge, willingness to answer my questions, and everyday collaboration created a supportive environment that contributed significantly to my learning.

I would also like to thank my peers, Shengyu Zheng and Tong Sun, for their consistent encouragement and generous support. Their patience during moments of doubt, and their willingness to help me think through problems, made a real difference in both the progress of my thesis and my personal morale. I'm truly grateful for their presence during this demanding but rewarding period.

Lastly, I am profoundly grateful to my family for their unwavering support, love, and understanding.

Their encouragement gave me strength during moments of fatigue and uncertainty, even when I doubted myself. This work would not have been possible without the solid foundation they have provided me throughout my life.

Contents

I	Introduction	1
II	Background	4
1	Business and Organizational Context	5
1.1	Pandemic and insurance	5
1.2	Solvency II Framework	7
1.3	AXA Group Structure	8
2	Technical Background	10
2.1	Pandemic Definition	10
2.2	Pandemics in the Past 150 Years	12
2.3	Focus On Respiratory Pandemics	13
2.4	Pandemic Models in the Market	16
2.5	Swiss Re's Pandemic Model	17
III	New Internal Model Methodology	22
3	Overview of the New Internal CAT Pandemic Model	23
3.1	Objective	23
3.2	Frequency and Severity Model	25

4	Model Dynamic: Generation of Pandemic Scenarios	29
4.1	Methodology	29
4.2	Input Parameters	31
4.3	Dynamics of the Model without Mitigation	34
4.4	Dynamics of the Model with Mitigation	40
IV	Model Calibration and Simulation	47
5	Parameter Calibration	48
5.1	Transmissibility	49
5.2	Lethality	56
5.3	Mitigation	77
6	Model Simulation	90
6.1	Quasi-Monte Carlo	91
6.2	Simulation Convergence	94
V	Model Output Analysis	96
7	Statistical Analysis of Simulated Pandemic Mortality Rates with Extreme Value Theory	97
7.1	An Unsupervised Modelling Method – Hybrid Generalized Pareto Distribution (LN-E-GPD)	98
7.2	A New Optimization Algorithm for Hybrid GPD	101
7.3	Results and Analysis	116
VI	Conclusion	129
VII	Appendices	131
Appendix A	Simulation Study of GA Algorithm and LM Optimizer	132

Appendix B	Convergence Study on Quasi Monte Carlo Simulation	136
Appendix C	National or Regional Input Age Structure	139
Appendix D	Solvency II Framework Details	141
Appendix E	A Brief Survey of Extreme Value Theory	145
References		156

Part I

Introduction

The COVID-19 pandemic has fundamentally altered the landscape of risk assessment for insurance companies, revealing significant gaps in the methodologies traditionally employed to evaluate mortality risk. In particular, for global insurers like AXA, the challenges have been exacerbated by the pandemic's diverse impacts across different countries and populations. The existing regulatory framework under the Solvency II Directive mandates a standardized approach to capital requirements, specifically through a uniform mortality shock of 0.15%. However, this one-size-fits-all model fails to account for the myriad factors that influence pandemic outcomes, such as variations in age demographics, gender distribution, healthcare infrastructure, and the effectiveness of government responses.

As the pandemic has illustrated, these factors can significantly alter the mortality risk landscape, necessitating a more nuanced approach to risk assessment. Insurers need sophisticated internal models that can adapt to the diverse and dynamic nature of global demographics and geographies. The infrequent occurrence of pandemics, coupled with the unique characteristics presented by each event—such as those seen during COVID-19—further complicates the development of such models. High transmission rates and the varying impacts of mitigation measures, including quarantine and vaccination strategies, underscore the urgent need for a robust, data-driven approach to pandemic risk modeling.

This study aims to address these challenges by developing a pandemic model tailored to diverse demographic and geographic profiles. Building on the framework established by the Swiss Re pandemic model, this research integrates epidemiological modeling with advanced statistical methods. The model captures the complexities of pandemic progression, taking into account not only the biological aspects but also the socio-economic variables that affect mortality. By calibrating the model parameters with extensive research and data, particularly focusing on age, gender, and regional lethality factors, this study seeks to create a more accurate representation of pandemic risks.

In addition, the research introduces a novel optimization approach that combines Genetic Algorithms with the Levenberg-Marquardt method, aiming to streamline the model while effectively analyzing its outputs. This hybrid methodology addresses the common challenges associated with parameter fitting in multidimensional models, particularly in the context of extreme value theory relevant to pandemic scenarios.

By providing a comprehensive framework that enhances the current understanding of pandemic mortality risks, this study not only aims to improve SCR compliance for insurers but also offers valuable

insights for strategic risk management across global insurance portfolios. Through this work, we bridge the gap between theoretical pandemic modeling and practical applications, equipping insurance companies and policymakers with the tools necessary to better navigate the complexities of future pandemic events.

Part II

Background

1

Business and Organizational Context

1.1 Pandemic and insurance

A pandemic is a global outbreak of an infectious disease that spreads rapidly across multiple countries or continents, affecting a large number of people. Unlike localized epidemics, pandemics are marked by their extensive reach and high transmissibility, often resulting in widespread illness, significant mortality, and substantial societal impact. Pandemics can disrupt healthcare systems, economies, and social structures on a global scale, with far-reaching consequences that persist long after the initial outbreak. Notable examples include the 1918 influenza pandemic, which caused millions of deaths worldwide, and the more recent COVID-19 pandemic, which highlighted both the transmission speed in the interconnected world.

For the insurance industry, pandemics pose unique challenges, as they generate a surge in claims across multiple lines. A pandemic can affect different activities in the insurance business (life insurance,

pensions, health insurance, non-life insurance and reinsurance). The risks that are linked to the pandemic event can be separated into two categories: the liabilities side and the assets side.

Assets	Liabilities
<ul style="list-style-type: none"> • Market risk • Credit risk • Operational risk 	<ul style="list-style-type: none"> • Mortality • Medical Expenses • Disability

Figure 1.1: Pandemic impact on asset and liability

On the Liability Side

Except through business interruption, Non-life business will generally be the less impacted. Life insurance on the other hand could be affected in different ways depending on the type of policies. In fact, an increase in mortality affects negatively death benefits that are paid as lump sums to beneficiaries in case the insured dies. Moderate influenza pandemic similar to 1957 and 1968 outbreaks could cost U.S. life insurers 15 billion dollars in additional claims (see [Weisbart \(2006\)](#)). But longevity benefits like savings would be affected positively because they are paid in case the insured is still alive at a certain age. Other than that, the impact will be different for each life insurance company because of differences in the location of insureds relative to outbreak zones.

For health insurance, an increase in morbidity implies more disability payments and medical expenses caused by illness as people will heavily seek medical services and buy more drugs.

On the Asset Side

The pandemic has introduced a substantial market risk for insurance companies, particularly impacting the asset side of their operations. This is evidenced by the potential decrease in revenues for businesses closely tied to public gatherings, such as events, concerts, public transportation, and shopping malls. Moreover, joined with a diminution of investors' confidence in the global economy, this could lead to a significative deterioration of assets. If a severe pandemic with multiple waves persists, it could significantly influence people's behaviors and attitudes, rendering market risk particularly acute in such circumstances.

For credit risk, if the pandemic leads to a decrease in revenues, this can lead to more businesses and individuals defaulting on loans, affecting the credit quality of insurers. Moreover, the financial strain experienced by re-insurers further exacerbates the counter-party risk, amplifying the challenges associated with credit risk management in the insurance sector.

The operational risk is significantly affected by the pandemic's impact on public gatherings and mobility. Employees may encounter challenges in accessing their workplaces, affecting customer service delivery. Additionally, the surge in digital activities also leads to potential cyber-security threats.

1.2 Solvency II Framework

As the study only focuses on Pandemic Mortality Risk, we here introduce simply the relative standard formula and more details on the Solvency II Framework can be found in Appendix D.

1.2.1 Pandemic Risk in the Solvency II Framework

The standard formula suggested by the Solvency II regulation for pandemic risk in the Life Catastrophe category is an increase of 0.15 points in the mortality rates used to calculate the technical provisions and reflecting the estimated mortality of policyholders over the next 12 months. In a simplified way, there is:

$$SCR_{pandemic} = 0.15\% \times CapitalAtRisk \quad (1.1)$$

The increase of 0.15 points in mortality rates is supported by a study carried out by Swiss Re (see [Swiss \(2007\)](#)) which suggests that the 1 in 200-year pandemic stress for most developed countries is between 1.0 and 1.5 per thousand within insured lives. This study was based on a sophisticated epidemiological model.

1.3 AXA Group Structure

1.3.1 AXA GIE

AXA, as a global insurance and financial services organization, operates through various entities across different regions, each with its own set of risks and exposures. The global headquarters of the AXA Group, the GIE AXA (Economic Interest Group) coordinates the entities and serves as the central element of the Group's governance and operates along three major axes:

- Sovereign missions: development of the Group's strategy, preparation and publication of financial statements, balance sheet management, portfolio management, brand protection and promotion, management of executives and Group values, as well as representation of the Group to external stakeholders.
- Risk management and control missions: management of the Group's material risks and regulatory exposures.
- Its position and role as a shareholder of the Group's operational entities.

This comprehensive oversight and coordination provided by GIE AXA are essential for ensuring the effective governance, risk management, and strategic alignment of the AXA Group's diverse entities and operations worldwide.

1.3.2 AXA Group Risk Management

The Group Risk Management (GRM) department plays a crucial role in the risk management and control missions of GIE AXA. Its primary responsibility is to oversee the management of the Group's material risks and regulatory exposures, particularly the pillar I and II in the Solvency II Framework. This involves identifying, assessing, and mitigating risks that could potentially impact the financial stability of the AXA Group.

The GRM team works closely with various entities within the AXA Group to ensure that risk management practices are effectively implemented and aligned with regulatory requirements. This includes

developing risk management frameworks, conducting risk assessments, and establishing risk mitigation strategies to safeguard the Group's interests.

Furthermore, the GRM team provides insights and recommendations to the top management team, enabling informed decision-making related to risk exposures and control measures. By actively monitoring and reporting on the Group's risk profile, the GRM team contributes to maintaining a robust risk management framework that aligns with the Group's strategic objectives and regulatory obligations.

2

Technical Background

2.1 Pandemic Definition

A pandemic, from ancient Greek: pãn (all) and deĩ mos (people), is the spread of a contagious disease (often caused by pathogenic microorganisms such as viruses or bacteria) affecting:

- Many people: the whole population of different countries
- In a very large geographical area: at least two continents
- In a short period: between a few months and a few years

A Pandemic should not be confused with an epidemic which is the development and propagation in a short period of a disease but among a given population or area. For instance, one of the most recent epidemics is the Ebola virus epidemic that happened in the Democratic Republic of Congo from 2018 to 2020. There were more than 3,400 cases and more than 2,300 deaths.

Also, Pandemics and Epidemics should not be confused with an endemic which is the presence of a disease in a population that remains at a steady state. For instance, chickenpox is an endemic that affects mainly young people. That's why endemic is less risky than epidemic since endemic diseases are often well-known (mostly in the way that efficient medical countermeasures exist) and the rate of infected people is predictable. Another reason is that the disease that starts an epidemic is a new one or an old enough that makes people vulnerable as they do not have matching antibodies.

An epidemic that spreads in a wide geographical area then becomes a pandemic.

To measure the impact of a pandemic, the following indicators can be analyzed:

- Incidence of a disease: the number of new cases of a disease occurring during a given period in a specified population.
- Attack rate (AR): the total number of infected people (either symptomatic or asymptomatic) amongst the whole population (once the pandemic is over). $AR = \frac{\text{Infected}}{\text{Population}}$
- Infection Fatality Rate (IFR): the proportion of all infected cases (including non-tested cases) that die. Counts all the persons that seemingly died from the disease (not only positively tested people) throughout the pandemic event. It represents the Lethality rate (L) in the model described in next chapter. $IFR = \frac{\text{Death by Infection}}{\text{Infected}}$
- Excess-mortality: mortality that is above what would be expected based on the non-crisis mortality rate in the population of interest (i.e. in "normal conditions"). Excess-mortality is thus attributable to the crisis conditions.

$$\text{Excess_Mortality} = \text{Observed_Mortality_in_Crisis} - \text{Expected_Mortality_in_Non_Crisis}$$

- Basic reproduction number (R_0): a measure of the average number of infections produced by one infected individual in the early stages of an epidemic.
- Effective reproduction number (R_t): the value of the R_0 index can be changed as a result of the introduction of preventive measures (i.e. physical distancing, use of masks, ...) or following a reduction in the number of susceptible people due to post-infection acquired immunity or to

vaccinations. This reproduction number is defined as R_t , that is the actual transmission rate of the virus at a given time t .

- Quarantine: separates and restricts the movement of apparently healthy people who were exposed to a contagious disease to see if they become sick. It can be applied at the individual, group, or community level.

These indicators will be used later in the document to describe past pandemics notably.

2.2 Pandemics in the Past 150 Years

When looking at the catastrophes (all causes except famine and other eradicated causes in developed countries) that happened since the 20th century, pandemics are, by far, the deadliest ones with up to tens of millions of deaths. Table 2.1 summarizes the different major pandemics that happened in the last 2 centuries.

Year(s)	Name	Deaths in million (% of world population)	Agent	Respiratory
1889-1890	Russian flu	1 (0.06%)	Influenza	YES
1918-1920	Spanish flu	17 to 100 (0.0691%-5.38%)	Influenza A (H1N1)	YES
1957-1958	Asian flu	1 to 4 (0.03%-0.14%)	Influenza A (H2N2)	YES
1960-present	HIV/AIDS	42	HIV	NO
1961-1975	7th cholera pandemic	Lack of reliable source	Cholera	NO
1968-1969	Hong Kong flu	1 to 4 (0.03%-0.11%)	Influenza A (H3N2)	YES
2009-2010	Swine flu	0.3 (0.004%)	Influenza A (H1N1)	YES
2020-2023	COVID-19	7 to 37 (0.09%-0.47%)	Coronavirus (SARS-CoV-2)	YES

Table 2.1: Pandemics in the past 150 years (using global population in the year of relative pandemic outbreak)

2.3 Focus On Respiratory Pandemics

2.3.1 Past Respiratory Pandemics

In the past 150 years duration, there were 6 severe airborne, respiratory pandemics reaching 1 million global deaths, which include four Influenza pandemics (1889, 1918, 1957, 1968, and 2009) and one Coronavirus pandemic (2020).

- **Russian flu (1889)**

The Russian Flu was a worldwide respiratory viral pandemic. It was the last great pandemic of the 19th century and is among the deadliest pandemics in history. The pandemic killed about 1 million people (0.06% of a world population of 1.65 billion people at that time). The most reported effects of the pandemic took place from October 1889 to December 1890, with recurrences in March to June 1891, November 1891 to June 1892, the northern winter of 1893–1894, and early 1895.

- **Spanish flu (1918)**

The Spanish Flu was the most severe pandemic in recent history. With avian origins, the virus was H1N1 type. It is hypothesized that the pandemic is outbreaked in Kansas in the US. First identified in the US in the spring 1918 within the military personnel, the soldiers spread the virus worldwide. As Spain was not implicated directly in the war, they were able to report and spread the news on the pandemic evolution. That is how this flu got the name of Spanish Flu. The pandemic ended more than a year after and infected at the end roughly 500 million people (around one-third of the world's population at that time). The estimate of the number of deaths was around 50 million people (2.69% of a world population of 1.86 billion people) with some studies raising the number to 100 million (5.38%), while the most recent puts it at around 15-20 million (0.81%-1.08%). Moreover, the mortality was different from the usual mortality linked to the flu. The youngest and oldest were highly affected as usual but people around 20 to 40 years old also presented high mortality rates.

- **Asian flu (1957)**

When the pandemic started, the virus was circulating throughout China and some regions nearby.

By midsummer it had reached the United States and few months later, the rest of the globe. The virus associated to this pandemic is the influenza A (H2N2) which has an avian origin. Compared to the Spanish flu, the Asian flu is considered to be moderate, with a death toll estimated at 1-4 million people (0.03%-0.14% of a world population of 2.92 billion people at that time).

- **Hong Kong flu (1968)**

The Hong Kong flu outbreak in Southeast Asia and killed around 1 to 4 million people worldwide (0.03%-0.11% of a world population of 3.54 billion people at that time). Soldiers returning from Vietnam introduced the virus in the United States and after few months it had spread throughout Europe. This pandemic was the first known outbreak of the H3N2 Influenza A virus. The death toll was relatively low, but the virus was highly contagious and spread rapidly. The mortality was higher in infants and the elderly, and the virus is still circulating today during seasonal influenza.

- **Swine Flu (2009)**

Detected firstly in the US during the spring of 2009, the H1N1 virus spread across the US and the world. The number of deaths linked to this pandemic is relatively low, around 100,000 and 400,000 deaths worldwide (0.0015%-0.006% of a world population of 6.84 billion people at that time), leading this pandemic to be labeled as a pandemic with low lethality. Some criticisms were also made on the fact that this epidemic was labeled as a pandemic by the World Health Organization (WHO).

- **COVID-19 (2020)**

The COVID-19 pandemic, also known as the coronavirus pandemic, is a global pandemic of coronavirus disease 2019 (COVID-19) caused by severe acute respiratory syndrome coronavirus 2 (SARS-CoV-2). This new virus was first identified from an outbreak in Wuhan, China, in December 2019. Attempts to contain it there failed, allowing the virus to spread worldwide. The WHO declared a Public Health Emergency of International Concern on 30 January 2020 and a pandemic on 11 March 2020. As of 29 August 2023, the pandemic had caused around 770 million cases and 7 million to 37 million deaths (0.09%-0.47% of a world population of 7.89 billion people), making it the second deadliest in the past 150 years.

2.3.2 Respiratory Disease Is The Most Likely Next Pandemic

As shown in the previous section, almost all the major pandemics in the last century were caused by respiratory viruses. Moreover, in 2018, the Center for Health Security of Johns Hopkins University published a report (see [Adalja et al. \(2019\)](#)) on the characteristics of microorganisms that could lead to a global catastrophic biological risk. They listed common characteristics of potential pandemic pathogens, some of which are described below:

- **Efficient human-to-human transmissibility:** Of the various modes of transmission, the respiratory route is the mechanism most likely to lead to pandemic spread. This is chiefly because interventions to interrupt this method of spread are more difficult to implement when the simple and universal act of breathing can spread a pathogen.
- **Timing of transmission:** Diseases that are contagious before symptom development, during the incubation period, or when only mild symptoms are present have greater opportunities for spread as infected individuals can conduct their activities of daily living with little or no interruption.
- **Absence of an effective or widely available medical countermeasure:** The lack of a broad-spectrum antiviral agent—like ones available for bacterial and even fungal organisms—also confers a special status on viruses.

Influenza and Coronavirus appear to comply with all the requirements for a perfect pandemic pathogen candidate.

Lastly, influenza and Coronavirus are present in our daily lives. Every year, the seasonal flu and common cold are present and can be a base for a pandemic strain if it mutates into a dangerous type of flu or Coronavirus.

All these reasons place the respiratory virus as the pathogen with the greatest combination of outbreak probability and material impact.

2.4 Pandemic Models in the Market

In the years preceding the COVID-19 pandemic, the insurance market had already been actively developing and refining models to assess the potential impact of pandemics. The emergence of infectious diseases for Influenza had prompted insurers to explore and implement various pandemic models to understand the potential financial and operational implications of widespread outbreaks. These pre-COVID-19 pandemic models were designed to evaluate the potential loss scenarios, estimate the economic impact, and develop strategies to manage the associated risks. Understanding the evolution of these models is crucial in comprehending the insurance industry's approach to pandemics and provides valuable insights into the development of future pandemic risk assessment frameworks.

Several pandemic models exist and are used by insurance or consultant companies are listed in Table 2.2:

Model	Risks
Milliman Disease model	Mortality
RMS Pandemic model	Mortality, disability and medical expenses
Swiss Re Pandemic model	Mortality
AIR	Mortality
Metabiota	Mortality

Table 2.2: Pandemic Models by different companies

- **Milliman disease model** is a frequency severity model based on past pandemics, the majority of which are influenza. It quantifies the risk of excess mortality.
- **RMS (Risk Management Solutions) pandemic model** is an epidemiological model that projects virus infectiousness and lethality as well as behavioral effects and containment plans. RMS uses epidemiologic modeling (known as SIR (see [Kermack & McKendrick \(1927\)](#)) modeling) to determine how a pandemic virus would impact the population. One specificity of the RMS model is the fact that the pandemic's severity is determined based on a mix of past pandemic features and potential pandemic scenarios. Another feature is that the model takes into account factors like vaccines, anti-viral drugs, public reaction, etc. that could potentially reduce the impact of the pandemic.

- **Swiss Re Pandemic model** is a combined actuarial and epidemiological model and considers the benefit of medical advancements (e.g. antibiotics, vaccines, antiviral medication). This is the model from which the QIS5 calibration of a 1.5% additional increase in mortality has been derived (see [Solvency II Calibration Paper \(2010\)](#)). The Insurance-Linked Securities issued on Life risks to date (mortality, longevity, medical expenses, etc.) have been based on either Milliman or RMS models.
- **AIR pandemic model** is a combined actuarial and epidemiological model for pandemics. It uses the SIR approach to model the intensity and the footprint of each event (catalog including 18,000 influenza pandemics), including the historical events that occurred during the 20th and 21st centuries. AIR's model is mostly known for being used for ILS (Insurance Linked Securities) transactions.
- **Metabiota pandemic model** is a firm specializing in pandemic modeling. The model encompassed a high biological expertise.

2.5 Swiss Re's Pandemic Model

2.5.1 Introduction and Objective of Swiss Re Model

Since the Swiss Re's pandemic model is cited in QIS5 as the basis of the SII standard formula, this study initiates an examination of this model and then apply it as a foundational framework for the development of a new Internal CAT Pandemic model. [Swiss \(2007\)](#) provides a comprehensive look at Swiss Re's pandemic model methodology.

The model is designed to generate two main outcomes:

- Creates a large set of randomly generated, synthetic pandemics by using information about viruses that have caused past pandemics, in particular their ability to cause disease and death, and their ability to spread. The outcomes of these hypothetical pandemics, modeled to simulate the effects of a range of modern interventions, provide an understanding of the range and likelihood of possible pandemic events based on historical precedents.

- It includes the effect of a modern context and modern interventions on any plausible influenza pandemic.

In short, the model can use a range of different assumptions to simulate a new viral strain that might emerge and tell us what impact this would have on the global population. It can also tell us how a real pandemic that took place sometime in our history would look if it happened today.

2.5.2 Swiss Re Model Overview

This pandemic model is a frequency and severity model. A frequency model estimates the likelihood of events occurring within a given time frame, while a severity model assesses the potential impact or size of each event. Together, they help insurers predict the frequency and financial impact of insurance claims. The frequency is based simply on historical frequencies (3–4% chance of an influenza pandemic occurring in any given year) and the severity model methodology is shown below: Many parameters are hard-coded into the model. Each simulation performed by the model then needs two random variables to be provided, from which it can generate a number of other factors relevant to the eventual outcome. These two variables, which are generated randomly from historically based distributions each time the model is run, are:

- The ability of the pandemic to cause death (its lethality),
- Its ability to spread (expressed as the reproduction value at time zero, R_0)

These two numbers are the ‘seed’ values, which the model uses to generate a variety of other variables. Both parameters are calibrated by the past 3 Influenza pandemics (1918, 1957, 1968) with maximum likelihood method. In the Swiss Re report, the best fitted generalised Pareto distribution was chosen for R_0 and lognormal distribution for lethality. Other pre-defined constant variables are included in the model which are applied to the two main random variables. These variables fall into 3 categories:

- Inception variables and calibrations: the degree of contagiousness by age, the lethality rate by age, other behavior factors
- Demographic characteristics: Age profile of each country

is determined by the underlying contagiousness of those already infected on Day t and the number of infected people on Day t .

Those who are infected exhibit a lethality rate, indicating the likelihood of fatality. At the end of each simulation, the total number of deaths represents the final output for the mortality rate of that simulation. The collective simulations can be utilized to calculate the 99.5% quantile for SCR of CAT Pandemic mortality risk.

2.5.3 Strength and Limitation of Swiss Re Model

Following the model overview, it is essential to examine the model's strengths and limitations to fully appreciate its scope and potential areas for further enhancement. By identifying key advantages, we understand how this model contributes to pandemic mortality risk assessment and its relevance to multinational insurers. At the same time, recognizing limitations provides valuable insights into areas that may require refinement to improve the accuracy and applicability in an evolving risk landscape. These insights will guide the development of a new internal model with more accurate, adaptable, and comprehensive pandemic risk assessment capabilities in this study.

Strength of Swiss Re model:

- The model offers a comprehensive understanding of the standard formula and is amenable to explanation and verification.
- Its adaptability to country-specific demographics (includes demographically useful quinquennial age groups, i.e., banded into groups spanning five years – 30 to 34, 35 to 39, etc) is an advantage for multinational insurers.
- It generates an entire distribution as output, rather than a solitary value.

Limitation of Swiss Re model:

- Small sample size: The model's effectiveness may be hindered by a limited sample size of 3 data points, potentially leading to less robust predictions and a higher degree of uncertainty.
- Exclusion of the latest COVID-19 experience: The Swiss Re model was developed before the outbreak of COVID-19, hence its relevance and accuracy may be compromised by its failure to

incorporate the unique characteristics of the COVID-19 pandemic, such as its high contagion rates and the widespread implementation of quarantine measures, which have significantly impacted previous pandemic dynamics.

- Absence of area and gender factors: The model's scope is restricted by its lack of consideration for area-specific factors and gender-specific factors, limiting its ability to provide a comprehensive assessment of pandemic risk across diverse geographical and demographic risk exposures.

In the following chapters, our study will adopt the foundational framework of the Swiss Re model while addressing the limitations previously identified. Specifically, we will incorporate additional data points for calibration, integrate insights from the COVID-19 experience, and develop specific factors related to area and gender to enhance the model's robustness.

Part III

New Internal Model Methodology

3

Overview of the New Internal CAT Pandemic Model

In this chapter, the focus is on the methodology of a new pandemic model developed as the internal model for CAT Mortality SCR. Firstly, an overview of the model is provided, emphasizing its Frequency-Severity model structure. Following this, we introduce the stochastic and pre-determined parameters. Additionally, the chapter presents the epidemiological model with different health statuses and the transition dynamics within them.

3.1 Objective

The objective of this modeling effort is to capture the risk of excess mortality resulting from a pandemic event. This model aims to generate pandemic scenarios for each country in the Internal Model, considering a wide range of pandemic features, including transmissibility and lethality. For each scenario, the model calculates excess mortality due to pandemic conditions, allowing the construction of a pandemic

excess-mortality quantile curve for each country. Notably, the 99.5th percentile of this curve represents the shock used for the $SCR_{pandemic}$.

It should be noted that the input data, including age structure, gender structure, and area factors, is based on country-level data from the World Bank rather than AXA entities' insurance portfolio, due to confidentiality constraints.

This CAT Pandemic mortality shock represents an additional increase in mortality rates, applied to the base mortality rates for the first year of the projection.

The specifications of the corresponding tool model are:

- In terms of functionality:
 - To be granular enough to derive the most refined shock for all the countries and regions in which AXA has exposure.
 - Integrate exposures from various countries (population by area, age, and gender) in order to reduce the basis risk.
- In terms of accuracy:
 - Remain simple without excessive complexity to be reliable
 - Have observable/understandable behaviors/formulas for more transparency and fewer implementation errors
- In terms of usability:
 - Be simple to use which will ensure a correct set-up when launching the model
 - Have an acceptable runtime
- In terms of maintainability:
 - Be modular enough, to allow to integration of potential future developments (disability, medical expenses, etc.)

3.2 Frequency and Severity Model

3.2.1 Global Approach

By definition, a pandemic event is an extreme and rare event, with a high and unpredictable death rate. To better study frequency and severity characteristics independently, the pandemic modeling approach for Life CAT risk is based on two essential and independent elements:

- **Frequency** is given by a Bernoulli random variable $I \sim \text{Bernoulli}(p)$, which determines if a pandemic has occurred during the year, based on the probability of occurrence p .
- **Severity** is conditional to the occurrence of an event: a random variable S is used to model the severity of the pandemic in terms of a percentage of excess mortality. The probability distribution of S is given through its quantile function $F_S^{-1}(x)$.

Therefore, the pandemic stress is calculated using a Frequency x Severity approach, which results in an excess mortality rate. The pandemic death shock x , as for 1 in 200 year event, is given by:

$$x = \text{VaR}^{99.5\%}(S * I)$$

Let F_X be the Cumulative Distribution Function of random variable X .

Noting p the annual probability of occurrence of a pandemic event, there are $x = \text{VaR}_{(S*I)}^{99.5\%}$, where x verifies $F_{(S*I)}(x) = 99.5\%$. So we can deduce:

$$\begin{aligned} F_{S*I}(x) &= P(I = 0) * P(S * I \leq x | I = 0) + P(I = 1) * P(S * I \leq x | I = 1) \\ &= (1 - p) + p * P(S \leq x) \\ &= (1 - p) + p * F_S(x) \end{aligned}$$

Therefore,

$$\begin{aligned} F_{S*I}(x) &= 99.5\% \\ \iff (1 - p) + p * F_S(x) &= 99.5\% \iff F_S(x) = 1 - \frac{0.5\%}{p} \iff x = F_S^{-1}\left(1 - \frac{0.5\%}{p}\right), \end{aligned} \quad (3.1)$$

where p is the probability of the pandemic occurrence.

This equation that transforms the probability level of combined model to the probability level of severity model will be later used in Chapter 6.

As a result, the CAT shock of pandemic mortality at 99.5% level is given by:

$$x = VaR^{\alpha}(S), \text{ with } \alpha = 1 - \frac{0.5\%}{p}$$

3.2.2 Frequency Model

The frequency is a pivotal assumption in the modeling and thus has been chosen with care based on historical considerations, epidemiological studies, and literature review.

The historical pandemic frequencies from studies are listed in Table 3.1.

Study	Frequency
J.K. Tautenberger and D.M. Morens (Tautenberger & Morens (2009))	2.6%
Global Catastrophes and Trends: The Next Fifty Years (Romaniuk (2011))	3.6%
European Actuarial Consultative Group (EUROPEEN (2006))	3-4%
Our study (see Subsection 2.3.1)	4% (6 Pandemics in the past 150 years)

Table 3.1: Historical pandemic frequency studies

As mentioned in the previous chapter, in the past 150 years duration (1875-2024), there were 6 severe airborne, respiratory pandemics reaching 1 million global deaths, which include four Influenza pandemics (1889, 1918, 1957, 1968 and 2009) and one Coronavirus pandemic (2020). This leads to a frequency of 4%.

Therefore, the study retains a frequency of 4% for the pandemic model..

3.2.3 Severity Model

The severity modeling can be seen as a 3-component model:

- **The Transmissibility model:** The aim of this first component is to derive, for each pandemic scenario, the speed and dynamic of the virus spread in a country. Together with the mitigation

model, we can calculate the number of infected people in a country. The transmissibility model is based on an SIID (Susceptible-Infected-Immune-Deceased) metapopulation model. More details regarding this modeling are provided in the next sections.

- **The Lethality model:** The aim of this component is to derive, for each pandemic scenario, the lethality rate in each country. For each pandemic scenario, knowing the number of infected people per country, we can eventually calculate the mortality rate for each country.
- **The Mitigation model:** The aim of this component is to simulate the government intervention actions or vaccination effects. This is an additional component applying to both Transmissibility and Lethality components.

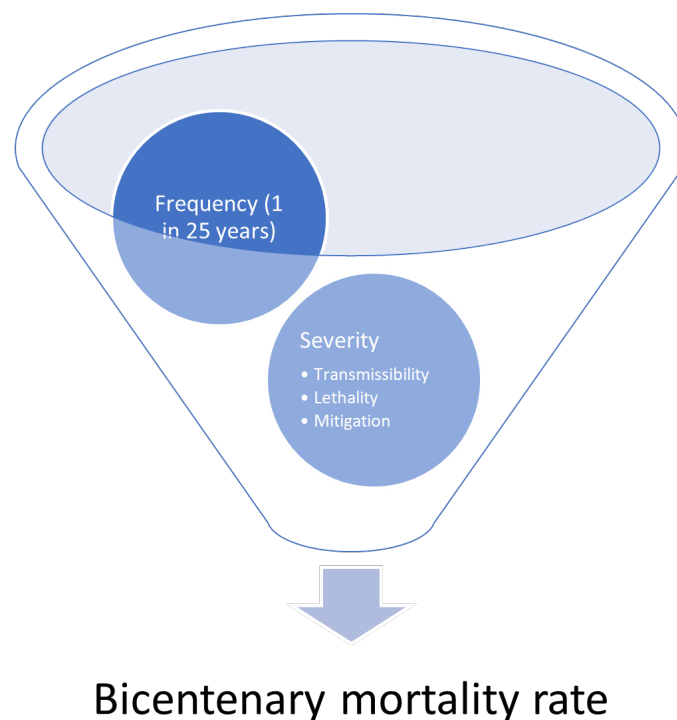


Figure 3.1: Illustration of the Pandemic Model blocks

The retained approach (geographically extended Susceptible-Infectious-Immune-Vaccinated) is accurate from an insurance point of view for the following reasons:

- **Easy modular framework:** With its four compartments, the SIID (Susceptible – Infected – Immune – Death) model allows an easy modular framework that captures data linked to the country

and evaluates the spreading with a compartmental epidemiologic model. It can be easily updated (at the scale of the inputs or the structure). Comparable to reality: The model is designed to reflect the course of a pandemic in the real world. It includes a 4-phase quarantine model, which has been verified through real-life experience with the COVID-19 pandemic.

- **Comparable to reality:** The model is designed to reflect the course of a pandemic in the real world. It includes a 4-phase quarantine model, which has been verified through real-life experience with the COVID-19 pandemic.
- **Justified with extensive literature review and prudent approach:** Some inputs and parameters are more difficult to assess due to the lack of history or the hard accessibility. For instance, vaccine efficiency is difficult to evaluate and has a wide range of possible values. To face that, values with the most consensus from scientific articles and experts' opinions are taken and most of the time with a prudency layer. Sometimes the difficulty is also in the large scale of difference due to the coverage of the whole world.
- **Comprehensive and up-to-date mitigation techniques are included:** As the results show, the two mitigation effects of the model have two different impacts. The vaccination has an effect on transmissibility and lethality while the quarantine has an effect only on transmissibility.
- **Good ratio between accuracy and runtime:** The model also has an acceptable runtime of a few hours.

4

Model Dynamic: Generation of Pandemic Scenarios

4.1 Methodology

The model is designed to effectively reproduce the dynamics of any plausible pandemic scenario, capturing the most significant aspects of its progression. This chapter outlines the process for simulating a pandemic based on specific parameters tailored to selected scenarios.

It is important to note that the model does not encompass every conceivable element of pandemic modeling. Notably, it does not account for the unpredictable nature of pandemic development during the initial days of spread. Additionally, the model operates at the country level, as all indicators and mitigation assumptions are based on national data.

Furthermore, the model accommodates a variety of assumptions to simulate the emergence of new

viral strains and assess their potential impacts on each country's population.

4.1.1 Modeling Timeframe

The model calculates spread at discrete time intervals, each lasting 24 hours (1 day), which comply with pandemic data reporting specifications. It begins on Day 1 with a given number of people infected in any chosen country. The number infected by Day 2 is a mathematical function based on the underlying infectiousness of those already infected on Day 1 and the number of contacts they have with susceptible people. As the days go by, more people become infected, fewer remain susceptible, and an increasingly large proportion of contacts occur with people who have immunity and would not be reinfected. After a certain number of days, the pool of susceptible people is sufficiently depleted that the number of new infections starts to decrease instead of increasing (herd immunity point).

The model projects the pandemic evolution from the beginning of the pandemic to a 3-year length (1095 days). This aligns with the 6 airborne, respiratory pandemics in the past 150 years. For each scenario, the total mortality rate during the 3-year period will be considered as a 1-year death shock for the CAT Pandemic STEC calculation. Accordingly, to simplify the simulation process, initial assumptions set at the start of each scenario remain unchanged during the 3-year period (e.g., Population number, age and gender profile, country-specific factors, etc.). See in Table 4.1

Year(s)	Name	Duration (in years)
1889-1890	Russian flu	< 2
1918-1920	Spanish flu	< 3
1957-1958	Asian flu	< 2
1968-1969	Hong Kong flu	< 2
2009-2010	Swine flu	< 2
2020-2023	COVID-19	< 4

Table 4.1: Historical pandemic durations

4.1.2 Transition Status in Epidemiological Model

The epidemiological model is used to describe the transition between 4 health statuses during an infection, which includes Susceptible, Infected, Immune and Death. See the transition graph in the following Figure 4.1.

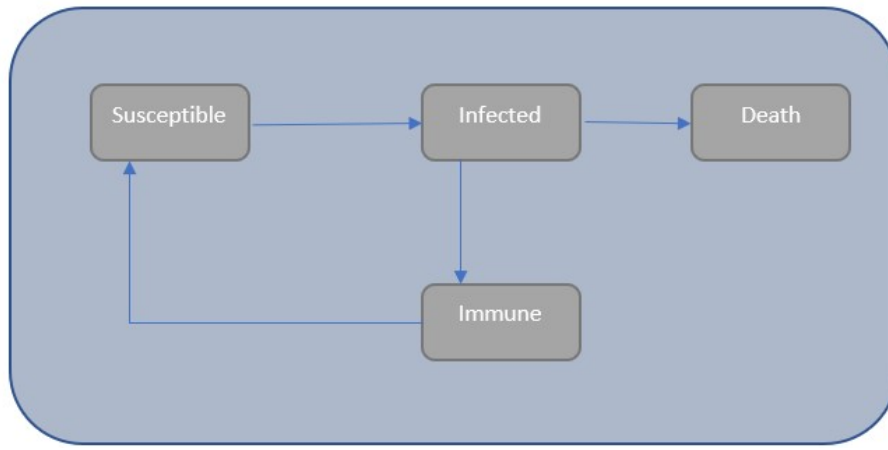


Figure 4.1: Transition between health statuses

From one day to another, members of groups S (Susceptible), Inf (Infected) and Imm (Immune) can remain in the group they already are part of, or move to another status as shown by the direction of the arrow in Figure 4.1

4.2 Input Parameters

To predict the number of deaths caused by a pandemic, the model consists mainly of two components:

- Transmissibility, the ability to spread.
- Lethality, the ability of the pandemic to cause death.

The third component, Mitigation, is in fact included in these 2 components, Transmissibility and Lethality.

All the input parameters in the model can be classified into the components above.

The principle of the model is to generate a large set of random scenarios to compute the death rate in case of many different possible pandemics. Then the 99.5th percentile risk will be determined by ordering these scenarios by increasing the mortality rate, taking into account the 4% frequency assumption.

Among all input parameters, some parameters are stochastic and will take different values in each scenario. They are the major parameters that determine the final output. The Internal CAT Pandemic model was fitted on historical data, from which simulated values are generated for each scenario, covering a wide range of possibilities.

Others are pre-calibrated parameters. They take into account all the other characteristics (e.g., virus nature, environment settings, mitigation actions, etc.). These pre-calibrated parameters mainly explain the variance in mortality among different age profiles, genders, and countries.

4.2.1 Stochastic Parameters

Each simulation performed by the model is based on two essential stochastic parameters. These two parameters, which are generated randomly from historically based distributions for each scenario are as follows (calibration details will be presented in the next Chapter):

Basic Reproduction Number(R_0): This is the major parameter for Transmissibility. It is the reproduction number of a virus at time zero (i.e., at the beginning of Day 1). This represents the average number of people who would subsequently be infected by any newly infected person in an entirely susceptible population (i.e., at the start of a pandemic or epidemic). R_0 is therefore a basic measure of the ability of a virus to spread.

Baseline Lethality Rate (\bar{L}): This is the major parameter for Lethality. It refers to the average number of deaths per infection in the total population (in simple terms, how many people the virus kills as a proportion of those infected).

In addition, three different types of pandemics (Normal flu, Spanish flu, or COVID-19) will be simulated, impacting some other model parameters:

Duration Profile of Infectiousness (f): A discrete probability density function for a given pandemic (Influenza or Coronavirus) describing the duration profile of infectiousness after infection. For instance, if $f(d) = 40\%$, it means that, on average, 40% of the total infections generated by an originally infected individual would happen on d^{th} day since the original infection. By definition, $\sum_d f(d) = 100\%$.

Age-specific Factor of Lethality ($\alpha_{country,shape}$): A factor applied to \bar{L} for each given age profile (age structure of a country in which AXA entity resides. Same for the gender and area factor below.)

and each type of disease. Different diseases have different shapes of lethality curve on age groups (three different scenarios).

4.2.2 Pre-determined Parameters

Some of the model's pre-calibrated parameters (constant values) are applied supplementarily to either the Basic Reproduction Number (R_0) or the Baseline Lethality Rate (\bar{L}) to precisely describe the Transmissibility and Lethality:

Gender-specific Factor of Lethality (δ_{entity}): A constant factor applied to \bar{L} for each given gender composition. Males and Females have a different lethality rate with the same disease. Therefore, in our modeling approach, we take into account this gender-specific difference, given that the gender composition within each entity's profile may vary.

Area-specific Factor of Lethality ($\beta_{country}$): A constant factor applied to \bar{L} for each country. This factor describes the different lethality rates in each country, including a variety of possible factors like health care expense, health resource density, country's preparedness, country's comorbidity profile, area-related socioeconomic risk behaviors, etc.

Parameters include mitigation actions for Quarantine and Vaccination: Quarantine has an impact on transmissibility and Vaccination has an impact on both transmissibility and lethality. Each part consists of a series of parameters which include efficiency values as well as several timing parameters (quarantine start and end date, vaccination start and end date, etc.).

For **Quarantine**, there are R_t^Q (reproduction number during quarantine), R_t^R (reproduction number for reopen period), T^Q (number of days of full quarantine), T^T (number of days of transition between full quarantine and full reopen) and $Trigger^Q$ (threshold on number of infected to start the quarantine).

For **Vaccination**, there are T_s (vaccination start date), T_d (vaccination deployment duration), and C_r

(vaccination coverage limit for country r).

There are two parameters shared by both Vaccination and Normal Infection, Immunity Ratio (γ) and Lethality Reduction Effect (μ).

Immunity Ratio (γ) represents the proportion of infected or vaccinated people who gain full immunity and cannot be re/infected. And for those who are infected or vaccinated, but still could be re/infected, they should have a lower Lethality due to their partial immunity, which is defined by the Lethality Reduction Effect (μ).

As explained by the Centers for Disease and Control Prevention (CDC): "Active Immunity results when exposure to a disease organism triggers the immune system to produce antibodies to that disease. Active immunity can be acquired through natural immunity or vaccine-induced immunity." Therefore, for simplicity reasons, the model assumes both parameters are the same for either being infected or being vaccinated.

4.3 Dynamics of the Model without Mitigation

4.3.1 Notation

For each country, individuals can be grouped according to their health status. More generally, we will adopt the following notation: let X stand for a given health status. $X_r(t)$ will represent the number of people on day t , living in a country r , who are in the health status X .

- **Susceptible ($S_r(t)$):** Number of people who are not immunized against the virus and are susceptible to being infected. They can catch the virus and be sick. At the end of an infection, a part of the infected people, γ , will gain full immunity to future infections and move to the Immune class, and the other part will only gain partial immunity (i.e. lethality reduction effect) and remain in Susceptible class with a lower lethality rate (this portion $1 - \gamma$ can be (re)infected as any other Susceptible).

Number of new partially immune Susceptible on day $t+1$ ($newPartialS(t+1)$) depends on the

number of last-day infections and the immunity rate (proportion of people that gain full immunity after infection).

- **Infected ($Inf_r(t, d)$):** Number of people who are currently infected by the disease. d is an integer with range $d \in D$, where $D = 1, 2, \dots, d_{max}$ which denotes the number of days d since the infection incidence ($d = 1$ means the people just got infected, d_{max} is the maximum duration in Infected class). In the model, infected people will pass through all the stages $1, 2, \dots, d_{max}$. After d_{max} days, people will move to the Immune, Susceptible, or Death class, respectively.

Number of new daily infections on day $t+1$ depends on the number of infected (contagious) people on day t , and on all the variables related to Transmissibility (including the proportion of susceptible people over total population in area r , the Duration Profile of Infectiousness ($f(d)$), and the Basic Reproduction Number (R_0)).

- **Immune ($Imm_r(t)$):** Number of people who gained immunity following vaccination or recovery from a previous infection. Only a proportion of people, γ , who recovered from the disease gain enough immunity to prevent reinfections, which means this proportion will move from Infected class to Immune class at the end of the infection and the remaining proportion, $1 - \gamma$, moves directly back to Susceptible class.

Number of new daily immune on day $t+1$ ($newImm_r(t+1)$) depends on the number of infected people who passed d_{max} days in Infected class on day t and all the variables related to survival rate ($1 - Lethality$) and immunity (γ)

- **Death ($D_r(t)$):** Number of people who were previously infected but died at the end of the infection stage. People who died from the disease move to Death class permanently.

Number of new deaths on day $t+1$ ($newD_r(t+1)$) depends on the number of infected people who passed d_{max} days in Infected class on day t , and all the variables related to Lethality.

- **Total Alive ($N_r(t)$):** This is not a single health status. It is the sum of Susceptible, Infected and Immune. Hence, it only decreases when people die from the disease.

As previously mentioned, individuals can move from one health status to another. This dynamic

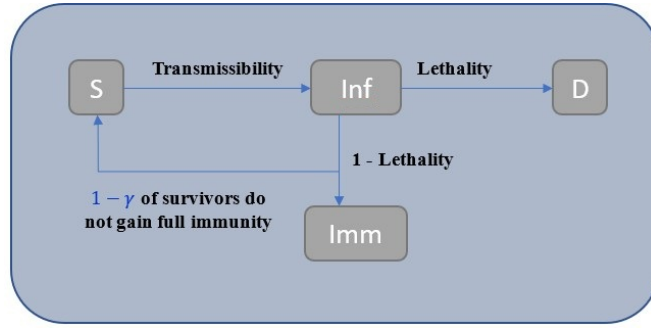


Figure 4.2: Transition between health statuses without mitigation

can be described through differential equations. We assume a discrete time step (on a daily basis), for implementation purposes.

To derive these discrete equations, a chronology is required in the occurrence of the different events that can happen. This chronology has an impact on the specification of the equations (and on the short-term results), but little impact on the overall results.

The chronological order is defined as the following:

- The new Infection occurs
- The last day of Infection transfers to either Immune, Death or Susceptible

After each event, all the affected statuses will be updated.

The following equations present how the different states evolve from day t to day $t+1$. The symbol “ \leftarrow ” means that a value is replaced by another one.

4.3.1.1 New Infection Occurs

Infection event happens at first and the daily new infections will be updated.

Infected: The daily new infections generated by one single infected individual who passed d days since his/her infection should be $f(d) * R_0 * \frac{S_r(t)}{N_r(t)}$, where:

- $f(d)$ is the proportion of the total infections generated by an infected individual in its d^{th} day since the original infection.
- R_0 represents the transmissibility.

- As the Susceptible proportion changes, the transmissibility at day t should be scaled to the proportion of Susceptible $\frac{S_r(t)}{N_r(t)}$.

Hence the newly infected people ($d = 1$) at day $t+1$ should be:

$$Inf_r(1,1) \leftarrow initial_number_of_infected$$

The initial number of infected people has been set to 20. In a later sensitivity test, it is shown that the difference between setting the initial number for 1 and 100 is negligible.

$$\forall t \geq 1, Inf_r(t+1,1) \leftarrow R_o * \frac{S_r(t)}{N_r(t)} * \sum_{d \in D} Inf_r(t,d) * f(d)$$

Infected people who have been infected for less than d_{max} days will be simply shifted to next stage $d+1$ as they are still infected on the following day:

$$\forall d < d_{max}, Inf_r(t+1,d+1) \leftarrow Inf_r(t,d)$$

Infected people who passed exactly d_{max} days will be moved to Death, Immune or Susceptible. Altogether, the total infected people ($d = 1, 2, \dots, d_{max}$) at day $t+1$ should be

$$\begin{aligned} Inf_r(t+1) &\leftarrow Inf_r(t+1,1) + \sum_{d < d_{max}} Inf_r(t+1,d+1) \\ &= R_o * \frac{S_r(t)}{N_r(t)} * \sum_{d \in D} Inf_r(t,d) * f(d) + \sum_{d < d_{max}} Inf_r(t,d) \end{aligned}$$

4.3.1.2 The Last Day of Infection Transfers to Other Status

After the infection is updated, those who were in the last day of infection the day before, need to transfer to new status. Thus, Death, Immune and Susceptible are updated.

Death: The number of new deaths at day $t+1$ should be the number of people who passed exactly d_{max} days infected at day t , multiplied by the effective Lethality. The effective Lethality will be the product $\bar{L} * \alpha_{entity,shape} * \delta_{entity} * \beta_r * \mu(t - d_{max})$ using:

- Baseline Lethality Rate \bar{L} (generated randomly from historically-based distribution)
- Age-specific Factor of Lethality $\alpha_{entity,shape}$
- Gender-specific Factor of Lethality δ_{entity}
- Area-specific Factor of Lethality β_r
- Lethality Reduction Effect $\mu(t - d_{max})$ depends on time and should be applied at the date of infection.

The daily new death is developed from the last day of infection and is computed as the number of infected who passed exactly d_{max} days at day t multiplied by effective lethality.

$$\begin{aligned} newD_r(t+1) &\leftarrow Inf_r(t, d_{max}) * effective_Lethality \\ &= Inf_r(t, d_{max}) * \bar{L} * \alpha_{entity,shape} * \delta_{entity} * \beta_r * \mu(t - d_{max}) \end{aligned}$$

Altogether, the total deaths at day $t+1$ should be the total deaths at day t , and the new deaths

$$D_r(t+1) \leftarrow D_r(t) + newD_r(t+1)$$

Immune: The number of Immune people at day $t+1$ should be increased by the number of people who survived at the end of the infection period, after exactly d_{max} days at day t , and have gained immunity (proportion γ).

The daily new immune is developed from the last day of infection and is computed as

$$\begin{aligned} newImm_r(t+1) &\leftarrow Inf_r(t, d_{max}) * (1 - effective_Lethality) * immune_rate \\ &= Inf_r(t, d_{max}) * (1 - \bar{L} * \alpha_{entity,shape} * \delta_{entity} * \beta_r * \mu(t - d_{max})) * \gamma \end{aligned}$$

Together, the total immune people at day $t+1$ should be:

$$Imm_r(t+1) \leftarrow Imm_r(t) + newImm_r(t+1)$$

Susceptible: The change in number of Susceptible people at day $t + 1$ should be impacted by:

- The inclusion of the new partially immune Susceptible, who are the people at the end of the infection period (after d_{max} days at day t) and who survived but did not gain full immunity.
- The removal of newly infected people at day $t + 1$

New partially immune Susceptible is computed as

$$newPartialS_r(t + 1) \leftarrow Inf_r(t, d_{max}) * (1 - \bar{L} * \alpha_{entity, shape} * \delta_{entity} * \beta_r * \mu(t - d_{max})) * (1 - \gamma)$$

Altogether, the total number of Susceptible people at day $t + 1$ should be

$$S_r(t + 1) \leftarrow S_r(t) + newPartialS_r(t + 1) - Inf_r(t + 1, 1)$$

Lethality reduction effect: The Lethality Reduction Effect μ at day $t+1$ is updated at the end of the day. The proportion of Partially immune Susceptible who recover from the infection and join the Susceptible class but do not gain full immunity ($\frac{newPartialS_r(t+1)}{S(t+1)}$) has a lethality reduced by a reverse Lethality reduction factor $(1 - Lr)$ compared to others. Considering that Partially immune Susceptible have their lethality reduced by only $(1 - Lr)$ means that people do not get multiple reductions of lethality in case of multiple successive infections, which is a prudent assumption. Thus, the Lethality Reduction Effect is a weighted effect that combines this reduced lethality of the new partially immune Susceptible and the already reduced lethality on the rest of the Susceptible.

$$\mu(0) = 1$$

$$\mu(t + 1) = (1 - Lr) * \frac{newPartialS_r(t + 1)}{S(t + 1)} + \mu(t) * \left(1 - \frac{newPartialS_r(t + 1)}{S(t + 1)}\right)$$

Moreover, the lethality reduction effect should be applied at the date of infection so in the formulas for death, immune, and susceptible at day $t+1$, the lethality factor μ to use is $\mu(t - d_{max})$.

4.4 Dynamics of the Model with Mitigation

One advantage of using an epidemiological model is to be able to account for recent developments in terms of mitigation strategies. In this modeling, two kinds of mitigation strategies are considered: Quarantine and Vaccination. These mitigation strategies are incorporated in the model previously shown.

Both Quarantine and Vaccination are intervention actions to slow down the pandemic spread, hence, to reduce the transmissibility. For those who get infected after vaccination, the lethality rate also decreases due to the quick response of body immunity systems. Thus, we show below the impact of the Mitigation part on our model.

4.4.1 Notion

The health statuses are the same as described previously, while the transition between health statuses has changed due to the mitigation actions that affect both transmissibility and Lethality. The illustration Figure 4.3 below shows the transition between health statuses with mitigation:

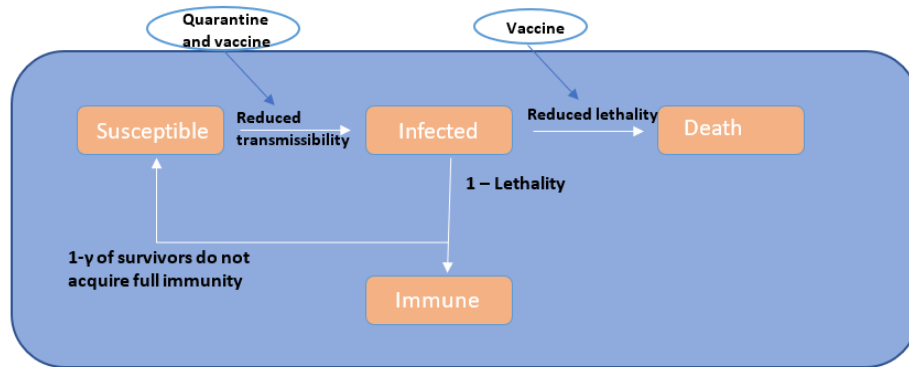


Figure 4.3: Transition between health statuses with mitigation

Before mitigation actions, Transmissibility is determined by two parts:

- Basic Reproduction Number R_0
- Scaling Factor $\frac{S_r(t)}{N_r(t)}$ representing the number of Susceptible divided by the total alive population.

When applying quarantine to the population, people have much less contact with each other, which reduces the chance of being infected. Hence, the Reproduction Number R_t should vary over day t , depending on the strength of quarantine action.

On the other side, vaccination helps the people in Susceptible class to gain immunity, and thus moves a proportion of Susceptible people to the Immune class.

To conclude, mitigation actions impact Effective R_t given that quarantine affects R_t and vaccination reduces $S_r(t)$:

$$Transmissibility(Effective_{Rt}) = R_t * \frac{S_r(t)}{N_r(t)}$$

Vaccination also reduces Lethality by providing partial immunity to those who are vaccinated (a similar reduction can be observed for those who survived a previous infection) but did not gain full immunity and remain in the Susceptible category. This is characterized by the Lethality Reduction Effect μ .

4.4.2 Transition Functions

After adding mitigation, we define the following chronological order of the four events:

- The new Infection occurs
- The last day of Infection transfers to either Immune, Death or Susceptible
- The new vaccination applies
- The update of quarantine status (update Effective R_t)

After each event, all the affected statuses will be updated. Under the four events chronology, Susceptible and Immune will be updated more than once. Thus, we add the event name in front of the status notation to distinguish each update (e.g. Susceptible after vaccination will be *after_vaccination* $S_r(t)$).

4.4.2.1 New Infection Occurs

Infection event happens at first and the daily new infections will be updated.

Infected: The formula for updating Infected status will have different effective reproduction numbers (*Effective* R_t) depending on the 4-phase quarantine model, including Outbreak, Quarantine, The progressive transition between quarantine and reopening, and Full reopening. Thus, newly infected people ($d = 1$) at day $t + 1$ should be

$$Inf_r(1, 1) \leftarrow initial_number_of_infected$$

$$\forall t1, Inf_r(t+1, 1) \leftarrow EffectiveR_t * currently_infected * duration_profile$$

$$= (R_t * \frac{after_vaccination S_r(t)}{N_r(t)}) * \sum_{d \in D} Inf_r(t, d) * f(d),$$

where $R_t * \frac{after_vaccination S_r(t)}{N_r(t)}$ is the effective reproduction number depending on the quarantine phase on day t. The dynamics of R_t will be presented in the next chapter.

Infected people who have been infected for less than d_{max} days will be simply shifted to the next stage $d+1$ as they are still infected on the following day:

$$\forall d < d_{max}, Inf_r(t+1, d+1) \leftarrow Inf_r(t, d)$$

. Infected people who passed exactly d_{max} days will be moved to Death, Immune or Susceptible. Altogether, the total infected people ($d = 1, 2, \dots, d_{max}$) at day t should be

$$Inf_r(t) \leftarrow \sum_{d=1}^{d_{max}} Inf_r(t, d)$$

4.4.2.2 The Last Day of Infection Transfers to Other Statuses

After the infection is updated, those who are on the last day of infection need to transfer to a new status. Thus, Death, Immune, and Susceptible are updated.

Death: The formula for updating the Death status will remain the same. The daily new death is computed as

$$\begin{aligned} newD_r(t+1) &\leftarrow Inf_r(t, d_{max}) * effective_Lethality \\ &= Inf_r(t, d_{max}) * \bar{L} * \alpha_{entity, shape} * \delta_{entity} * \beta_r * \mu(t - d_{max}) \end{aligned}$$

The total deaths at day t+1 should be

$$D_r(t+1) \leftarrow D_r(t) + newD_r(t+1)$$

However, the Lethality Reduction Factor (μ) changes due to the implementation of vaccination (same

for Immune and Susceptible below).

Immune: The formula for updating Immune at this event will remain the same (except for μ).

The daily new immune is developed from the last day of infection and is computed as

$$\begin{aligned} newImm_r^{Infection}(t+1) &\leftarrow Inf_r(t, d_{max}) * (1 - effective_Lethality) * immune_rate \\ &= Inf_r(t, d_{max}) * (1 - \bar{L} * \alpha_{entity, shape} * \delta_{entity} * \beta_r * \mu(t - d_{max})) * \gamma \end{aligned}$$

Together, the total immune people at day t+1 should be:

$$Imm_r(t+1) \leftarrow Imm_r(t) + newImm_r^{Infection}(t+1)$$

Susceptible: The formula for updating Susceptible at this event will remain the same (except for μ).

New partially immune Susceptibility from infection is computed as

$$newPartialS_r^{infection}(t+1) \leftarrow Inf_r(t, d_{max}) * (1 - \bar{L} * \alpha_{entity, shape} * \delta_{entity} * \beta_r * \mu(t - d_{max})) * (1 - \gamma)$$

Altogether, the total Susceptible people at day t+1 should be

$$after_InfectionS_r(t+1) \leftarrow S_r(t) + newPartialS_r^{infection}(t+1) - Inf_r(t+1, 1)$$

4.4.2.3 The New Vaccination Applies

In the third event, vaccination is applied to the model and transfers Susceptible to Immune. Thus, these two statuses are updated again in this event.

Immune: The vaccination transfers Susceptible people directly into Immune without infected period. During the deployment period of vaccination, we set each day the number of newly vaccinated as $V(t)$ and only a proportion γ of the vaccinated gain full immunity and move to Immune, similarly to those who are in the last day of infection. In addition, we assume that the vaccination does not have any effect on Immune class. Since we vaccinate the whole population (alive) and only those in the Susceptible class are really affected (moving to Immune class), we must also multiply the number of newly Immune

by the ratio $\frac{S_r(t)}{N_r(t)}$, to get the daily effective vaccinated immune.

The daily effective vaccinated immune is computed as

$$newImm_r^{vaccination}(t) = V(t) * \frac{after_infectionS_r(t)}{N_r(t)} * \gamma$$

The formula for the total immune people after vaccination at day $t+1$ should be changed to

$$after_vaccinationImm_r(t+1) \leftarrow after_infectionImm_r(t+1) + newImm_r^{vaccination}(t+1)$$

Note that this formula for effective vaccinated immunity assumes that the vaccination is not performed in an organized manner, meaning the people that will be vaccinated on a given day are chosen randomly in the overall population (even if some have already been vaccinated and could be already immune). This is obviously a prudent choice because it is more efficient to vaccinate people who have not been vaccinated before and so have a smaller chance of being already immune. Still, it is not overly prudent because:

- At the start of the vaccination, most people have not been vaccinated yet, so it mostly selects non-vaccinated people anyway
- Vaccinated people might not be immune so vaccinating them again can be useful
- Many non-vaccinated people may already be immune (thanks to previous illness) so vaccinating only those is only partially more efficient

Susceptible: The vaccination transfers Susceptible directly into Immune without infection period. A proportion γ of the vaccinated gain full immunity and moves to Immune. The remaining proportion $1 - \gamma$ of the vaccinated stays in Susceptible. In addition, we multiply by the ratio $\frac{S_r(t)}{N_r(t)}$, since the vaccination affects only the Susceptible, not the already Immune. New partially immune Susceptible from vaccination is computed as

$$newPartialS_r^{vaccination}(t+1) = V(t+1) * (1 - \gamma) * \frac{after_infectionS_r(t+1)}{N_r(t+1)}$$

The formula for the total Susceptible people after vaccination at day $t + 1$ should be changed to

$$after_vaccinationS_r(t + 1) \leftarrow after_infectionS_r(t + 1) - newImm_r^{vaccination}(t + 1)$$

4.4.2.4 Update Quarantine Status (Update Effective R_t)

This last event is at the end of the day and has no change on the status, only the *Effective R_t* will be updated. At the end of the day, $after_vaccinationS_r(t + 1)$ and $after_vaccinationImm_r(t + 1)$ will be the starting number of Susceptible and Immune for the next day (i.e. on day $t + 2$).

Lethality Reduction Effect: The Lethality Reduction Effect μ is updated at once at the end of the day with impacts on new infections and new vaccination events. The function is similar to the one without mitigation as mentioned before.

Initially

$$\mu(0) = 1$$

After infection event

$$after_infection_ \mu(t + 1) = (1 - Lr) * \frac{newPartialS_r^{infection}(t + 1)}{after_infectionS_r(t + 1)} \\ + after_vaccination_ \mu(t) * \left(1 - \frac{newPartialS_r^{infection}(t + 1)}{after_infectionS_r(t + 1)} \right)$$

After vaccination event

$$after_vaccination_ \mu(t + 1) = (1 - Lr) * \frac{newPartialS_r^{vaccination}(t + 1)}{after_vaccinationS_r(t + 1)} \\ + after_infection_ \mu(t + 1) * \left(1 - \frac{newPartialS_r^{vaccination}(t + 1)}{after_vaccinationS_r(t + 1)} \right)$$

4.4.3 Overview of the Pandemic Dynamic Formulas

See the overview of the pandemic dynamic formulas in Table 4.2.

Key Parameters:

Component	Formula	Description
Effective Reproduction Number	$Effective_R_t = R_t \times \frac{S_r(t)}{N_r(t)}$	Transmission rate adjusted for quarantine (R_t) and susceptible population ratio
New Infections	$Inf_r(t+1,1) = Effective_R_t \times \sum_{d \in D} Inf_r(t,d) \times f(d)$	Daily new infections based on current infected and duration profile
New Deaths	$newD_r(t+1) = Inf_r(t,d_{max}) \times \frac{1}{L} \times \alpha \times \delta \times \beta_r \times \mu(t-d_{max})$	Deaths from last day of infection, adjusted by lethality reduction μ
New Immune (Infection)	$newImm_r^{infection}(t+1) = Inf_r(t,d_{max}) \times (1-effective_L) \times \gamma$	Recovery to full immunity from infection
New Immune (Vaccination)	$newImm_r^{vaccination}(t) = V(t) \times \frac{S_r(t)}{N_r(t)} \times \gamma$	Direct vaccination to immunity
New Partial Susceptible (Infection)	$newPartialS_r^{infection}(t+1) = Inf_r(t,d_{max}) \times (1-effective_L) \times (1-\gamma)$	Recovery to partial immunity (remain susceptible)
New Partial Susceptible (Vaccination)	$newPartialS_r^{vaccination}(t+1) = V(t+1) \times (1-\gamma) \times \frac{S_r(t+1)}{N_r(t+1)}$	Partial immunity from vaccination
Lethality Reduction Update	$\mu(t+1) = (1-Lr) \times \frac{newPartialS}{S(t+1)} + \mu(t) \times \left(1 - \frac{newPartialS}{S(t+1)}\right)$	Weighted average of immunity effects

Table 4.2: Pandemic dynamics formula summary

- γ : Immunity rate (proportion gaining full immunity),
- $V(t)$: Daily vaccination rate,
- d_{max} : Maximum infection duration,
- Lr : Lethality reduction factor,
- $\mu(t)$: Lethality reduction effect at time t .

Part IV

Model Calibration and Simulation

5

Parameter Calibration

This chapter illustrates the methods used for the calibration of the parameters in the model. As a reminder, the parameters can be classified into three components:

- **Transmissibility**, which includes:
 - Basic Reproduction Number (R_0)
 - Duration Profile of Infectiousness($f(d)$)
- **Lethality**, which includes:
 - Baseline Lethality Rate (\bar{L})
 - Age-specific Factor of Lethality ($\alpha_{entity,shape}$)
 - Gender-specific Factor of Lethality (δ_{entity})
 - Area-specific Factor of Lethality (β_r)

- Lethality Reduction Effect (μ) from previous infection or vaccination
- **Mitigation**, which includes:
 - for Quarantine:
 - * Threshold triggering quarantine (as a % of Infected over Alive population) ($Trigger^Q$)
 - * Effective R_t during Quarantine (R_t^Q)
 - * Full Quarantine Duration (T^Q)
 - * Transition Duration from full quarantine to full reopen (T^T)
 - * Reduction of R_t during Reopen period (ρ such that $R_t^R = \rho * R_0$)
 - For Vaccination:
 - * Vaccination Start Date after the outbreak (T_s)
 - * Vaccine Deployment Duration (T_d)
 - * Vaccination Coverage Limit (C_r)

Because the precise nature of any future pandemic is unknown, understanding the risk is best achieved by creating a representative set of plausible events for the main parameters (R_0 , lethality, type of strain). We will therefore calibrate distributions for R_0 and lethality based on historical data, which can then be used to generate plausible future pandemics and apply other pre-determined parameters calibrated mainly based on scientific research.

5.1 Transmissibility

Transmissibility determines the spreading speed of a disease among the population. There are three types of factors:

- **Nature of the Pandemic Disease** (R_0 , duration profile of infectiousness): These factors originate from the pandemic disease's characteristics. They include the spreading rate, length of the infectiousness period, and time-dependent infectivity.

- **Environmental and Societal Factors** (age, gender, population density, weather): These factors are dictated by the unique characteristics of the society under study. They may include population density in different age ranges, weather conditions, etc.
- **Mitigation Factors** (Quarantine and Vaccination): Policy-based factors, including the stay at home and quarantine policies, health system reaction, etc.

One indicator that allows to quantify the transmissibility of the virus is the Basic Reproduction Number (R_0): it is the average number of direct infections generated by one infector in an entirely susceptible population (i.e., at the start of a pandemic or epidemic). This indicator is commonly estimated and reviewed in historical pandemic research. The Duration Profile of Infectiousness plays a supplementary role in transmissibility. It shows how fast an infector could infect others.

According to a systematic review and meta-analysis of 27 surveys conducted across 22 countries involving a total of over 28,000 individuals (see [Mousa et al. \(2021\)](#)), there is no significant difference in daily contact numbers between genders or by age (Environmental and Societal Factors) across active age band. As the primary exposure to mortality risk for AXA is within the working age group (25-65 years), it is reasonable to assume same transmissibility for all countries, age groups, and genders.

The climate factor (high temperatures) and the urban environment as environmental and societal factors have been proven to be much less significant to transmissibility than Mitigation Factors (see [Paraskevis et al. \(2021\)](#)), particularly with the recent COVID-19 experience during which strong quarantine actions have been undertaken very early after the outbreak of the pandemic.

Hence, the model neglects the difference in transmissibility between countries before adding Mitigation Factors. The next section will focus on the calibration of R_0 , while Duration Profile of Infectiousness and the Mitigation Factors will be discussed in section 5.1.2 and 5.3.1 respectively.

5.1.1 Basic Reproduction Number

Basic Reproduction Number (R_0) is a baseline parameter for Transmissibility. It is always greater than 1 for an outbreak of pandemic, because it signifies that the disease has the potential to spread and increase in the population.

The event sets are based on R_0 distributions derived using data from the last five airborne, respiratory pandemics in a 150-year period. Table 5.1 and Table 5.2 present the R_0 of the 6 chosen historical pandemics:

Year	Disease	Swiss Re (Swiss (2007))	WHO (Organization et al. (2017))
1889	Russian Flu	-	-
1918	Spanish Flu	2.1	1.2-3.0
1957	Asian Flu	1.6	1.5
1968	Hong Kong Flu	1.9	1.3-1.6
2009	Swine Flu	1.5	1.1-1.8
2020	COVID-19	-	-

Table 5.1: R_0 of previous pandemics in literature (1)

Year	Disease	IFOA (Paul Morden (2013))	Research
1889	Russian Flu	-	2.1 (Valleron et al. (2010))
1918	Spanish Flu	1.5-2.5	-
1957	Asian Flu	1.5-1.7	-
1968	Hong Kong Flu	1.5-2.2	-
2009	Swine Flu	1.5-2	
2020	COVID-19	-	2.9 (Billah et al. (2020))

Table 5.2: R_0 of previous pandemics in literature (2)

The average value from the resources above (using, if necessary, the middle of an interval) is applied as the input for calibrating R_0 , as shown in Table 5.3.

Year	Disease	R_0
1889	Russian Flu	2.10
1918	Spanish Flu	2.07
1957	Asian Flu	1.57
1968	Hong Kong Flu	1.73
2009	Swine Flu	1.55
2020	COVID-19	2.87

Table 5.3: Retained R_0 of previous pandemics

The next step is to calibrate the most credible distribution for R_0 . The model uses Maximum Likelihood Estimation (MLE) method to find the distribution that is the best fit based on the 6 historical values.

Maximum likelihood estimation (MLE) is a statistical method used to estimate the parameters of a probability distribution based on a given set of observations. The basic idea of MLE is to find the values

of the parameters that maximize the likelihood function, which is the probability of observing the given data under the assumed distribution.

Formally, suppose there is a set of n independent and identically distributed observations, denoted as x_1, x_2, \dots, x_n , from a probability distribution with unknown parameters θ . The likelihood function $L(\theta|x_1, x_2, \dots, x_n)$ is defined as the joint probability density (or probability mass) function of the observations evaluated at their respective values given the parameter θ .

The maximum likelihood estimate, denoted as $\hat{\theta}$, is the estimate of θ that maximizes the likelihood function over the parameter space, i.e., $\hat{\theta} = \operatorname{argmax}_{\theta} L(\theta|x_1, x_2, \dots, x_n)$.

Table 5.4 shows the result of maximum likelihood estimation (from the R package *rriskDistributions* (see [Schlattmann \(2016\)](#)), which is commonly used to fit probability distributions) for each possible distribution:

Distribution	Log Loss	AIC	BIC
Normal	-3.76	11.52	11.10
Cauchy	-4.55	13.11	12.69
Logistic	-3.77	11.54	11.13
Exponential	-10.10	22.21	22.00
Chi-square	-9.46	20.93	20.72
Uniform	-	-	-
Gamma	-3.35	10.71	10.29
Lognormal	-3.19	10.39	9.97
Weibull	-4.03	12.06	11.65
F	-9.73	23.45	23.03
Student	-15.91	33.82	33.62
Gompertz	-4.73	13.45	13.04

Table 5.4: Measures for R_0 distribution fitness

Descriptions of the statistical measures:

- Log Loss (Log Likelihood): This is a measure of the probability of observing the data given the parameters of the model. In the context of distribution fitting, a higher (less negative) log-likelihood indicates a model that better explains the observed data. It is directly related to the parameters of the distribution and is sensitive to the overall shape of the distribution.
- AIC (Akaike Information Criterion): A widely used criterion for model selection that deals with the trade-off between the goodness of fit of the model and the complexity of the model. The model with lower AIC offers a better fit.

- BIC (Bayesian Information Criterion): Similar to AIC, it also includes a penalty for the number of parameters in the model, generally giving a higher penalty than AIC. The model with lower BIC offers a better fit.

By process of elimination, the lognormal distribution, which fits best and only generates positive values, is chosen for the 6 historical values of R_0 .

The graph below shows the probability density function for R_0 :

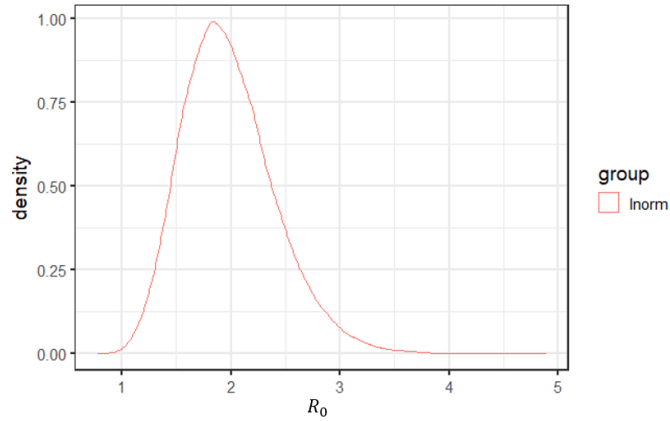


Figure 5.1: Probability density function for R_0

Recall that a random variable X is said to follow a lognormal distribution if its natural logarithm $Y = \ln(X)$ is normally distributed. Its mean m is defined by $m = e^{\mu + \frac{\sigma^2}{2}}$, where μ is the mean of the natural logarithm of the variable, $Y = \ln(X)$, and its standard deviation γ is defined by $\gamma = \sqrt{(e^{\sigma^2} - 1) \cdot e^{2\mu + \sigma^2}}$, where σ is the standard deviation of the natural logarithm of the variable Y . And the maximum likelihood estimator for lognormal distribution based on a sample (x_1, x_2, \dots, x_n) is calculated by the formula below:

$$\hat{\mu} = \frac{\sum_i \ln x_i}{n} \text{ and } \tilde{\sigma} = \sqrt{\frac{\sum_i (\ln x_i - \hat{\mu})^2}{n}},$$

where x_i is the data input and n is the number of data.

In addition, the maximum likelihood estimator is unbiased for the logarithm mean, but biased downwards for the logarithm standard deviation when the data sample size is small. To adjust the logarithm standard deviation to be an unbiased estimator, we replace the denominator n by $n - 1$ in the estimator

equation for logarithm standard deviation, $\hat{\sigma}$:

$$\hat{\sigma} = \sqrt{\frac{\sum_i (\ln x_i - \hat{\mu})^2}{n - 1}}$$

This unbiased estimator increases the standard deviation, which results in a more prudent final output.

Finally, the model retains a lognormal distribution for R_0 with parameters logarithm mean 0.7046 and logarithm standard deviation 0.2064.

5.1.2 Duration Profile of Infectiousness

Duration Profile of Infectiousness quantifies the degree of infectivity depending on the number of days elapsed since the start of the infection, which shows how fast the original infector could infect the Susceptible people (considering a daily time-step). It is a pre-defined parameter that supplements the Basic Reproduction Number.

The event sets are based on the duration profile of Infectiousness derived using data from the last six airborne, respiratory pandemics in a 150-year period. This history includes two types of viruses, SARS-CoV-2 (COVID-19) and Influenza, which will be discussed separately.

The duration profile of Infectiousness can be measured based on serial interval distribution or generation interval distribution. The former is a probability distribution showing the time difference between the dates on which the infector and the infected show symptoms, whereas the latter is the time difference between the dates on which the infector and the infection to others. For simplicity, we assume that the time between infection to others and first symptoms is always the same¹, then the serial interval distribution is identical to the generation interval distribution, which is the time between the infection of a person and the infection of his or her infector.

Duration Profile of Infectiousness should be non-negative, and according to the contact tracing data (a number of infector-infected pairs) (see [Tsang et al. \(2015\)](#)), the serial interval distribution should be right skewed, which aligns with the viral shedding dynamics (see [Carrat et al. \(2008\)](#)). Serial interval or generation interval is often assumed to be gamma distributed when estimating Basic Reproduction

¹Note that this condition can be relaxed in a future study

Number (see [Cori et al. \(2012\)](#)). Thus, we assume the Duration Profile of Infectiousness, $f(d)$, in the model, to be gamma-distributed. As a reminder, $\text{gamma}(\alpha, \lambda)$, can be seen as the sum of α exponential distributions with the same parameter λ , which indicates the waiting time until the α^{th} event happens.

The mean and standard deviation of serial interval distribution from two studies (see [Hart et al. \(2021\)](#) for COVID-19 and [Hahné et al. \(2009\)](#) for Influenza) are retrieved to calibrate the Duration Profile of Infectiousness. Retained values are shown in Table 5.5.

	Mean	Standard deviation
COVID-19	5.5	2.3
Influenza	2.7	1.1

Table 5.5: Mean and standard deviation of Serial Interval for COVID-19 and Influenza

With the retained parameters, the two gamma distributions are plotted in Figure 5.2 (in discrete days).

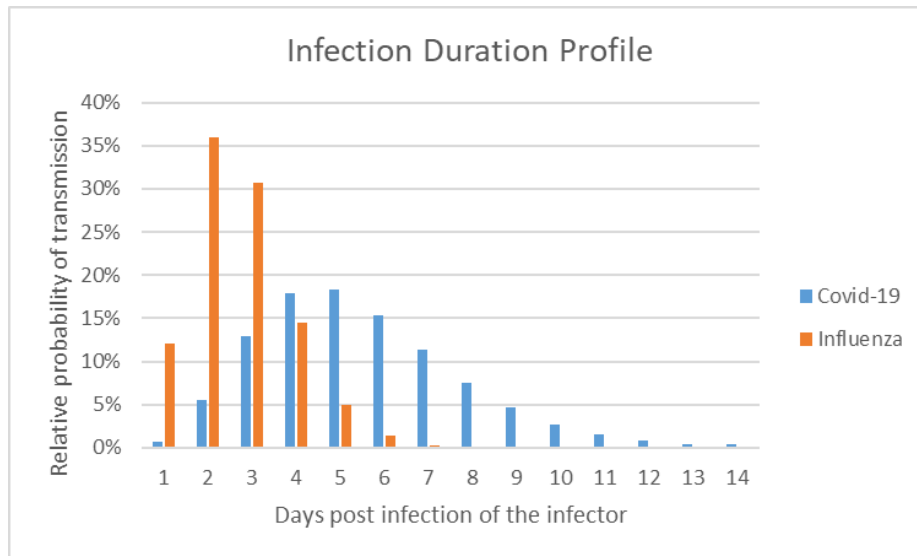


Figure 5.2: Infection Duration Profile for COVID-19 and Influenza

In Figure 5.2, we observe that on average, around 36% of those infected by an Influenza infected individual (orange bar) would be infected on Day 2, about 30% of subsequent infected would be infected on Day 3, around 15% on Day 4, etc.

For simulation, the model uses the historical frequency of the two types of viruses based on the last 150 years and generates two scenarios of Duration Profile of Infectiousness, $f(d)_{\text{COVID}}$ and $f(d)_{\text{Influenza}}$, with a frequency ratio of 1/5 (COVID/Influenza). This is coherent with the scenarios generated for the age lethality factor in the next section.

The number of days of infection (the maximum days of the duration profile), d_{max} , determines the time for each infected remaining in the infected status before moving to the other three statuses. The number of days can vary depending on whether infected people will be transferred to Susceptible (can be reinfected), Immune (recovered with immunity), or Death. Those moving to Death have no impact on further infections, while those transitioning to Susceptible and Immune statuses have a direct impact on the potential for future infections. Those returning to the Susceptible status are susceptible to reinfection, and the sooner they turn to Susceptible, the greater the likelihood of subsequent infections. Conversely, individuals who recover promptly and acquire full immunity contribute to a reduction in future infections. It is suggested by the U.S. Centers for Disease and Control and Prevention (CDC) that the reinfection period could occur at intervals ranging from 7.5 to 18.5 months (see [Tenforde \(2020\)](#)), and the infection symptoms resolve after 3-12 days (see [Memoli et al. \(2020\)](#) and [Edridge et al. \(2020\)](#)).

In conclusion, reinfection takes longer time than recovery in general. Taking the shorter time of reinfection as for recovery, 14 days, will result in a faster reinfection and hence more infection cases, which is a prudent assumption for the pandemic model (can be seen as an upper bound of the model prediction). Therefore, it is prudent to assume the same duration for recovery and reinfection, leading to a 14-day maximum duration of infection, d_{max} , for both influenza and COVID-19.

5.2 Lethality

The lethality of a disease refers to the likelihood that an infected person dies due to the disease.

There are four types of main factors impacting Lethality:

- **Nature of the Pandemic Disease:** The Baseline Lethality Rate (\bar{L}) originates from the pandemic disease's characteristics. It is the average rate of lethality of each disease in the total world population, which is age and area (country) independent.
- **Age-specific Factor:** Age is the major factor that has an impact on the lethality rate. Different age groups have huge differences in lethality rates. The lethality rate by age of most diseases could be described as a U shape (i.e., with lethality peaking in childhood and among the elderly). But some could also have a W shape (i.e., adding another peak at young adult ages) or a J shape (i.e., increasing with age with only one peak for high ages).

- **Gender-specific Factor:** Gender is also a significant factor that has an impact on the lethality rate. Males and females have different underlying biological make-up, which determines both immunological and hormonal profiles that is important in responding to diseases. Although the gender ratios in countries in which AXA is operating are all close to 1/1, the life insurance profile could have quite a different ratio. Therefore, it is necessary to integrate this factor in our model.
- **Area-specific Factors:** Besides the age structure profile and gender ratio difference, there are another significant area (country) related factors that could have impacts on lethality rate, including comorbidity profile, health expense per capita, health resource density, country's preparedness (economics), etc. All these factors are implied in the Area-specific Factor.

Age-specific Factor, Gender-specific Factor and Area-specific Factor are significant factors, hence we calibrate them carefully and separately. Thus, the final lethality for a given region r will be defined as:

$$Lethality_rate_r = \bar{L} * \alpha_{entity,shape} * \delta_{entity} * \beta_r * \mu(t - d_{max}),$$

where the \bar{L} denotes the Baseline Lethality Rate, $\alpha_{entity,shape}$ denotes the Age-specific Factor, δ_{entity} denotes the Gender-specific Factor, β_r denotes the Area-specific Factor and $\mu(t - d_{max})$ denotes the Lethality Reduction Effect (from either infection or vaccination).

5.2.1 Baseline Lethality Rate

The event set is based on Baseline Lethality Rate (\bar{L}) distributions derived using data from the last six airborne, respiratory pandemics in 150 years. The \bar{L} value for each has been sourced from a review of various items of literature.

Tables 5.6 and 5.7 present the \bar{L} of the 6 chosen historical pandemics:

Finally, the average value from the resources above (using, if necessary, the middle of an interval) is summarized as the input for calibrating \bar{L} , as shown in Table 5.8.

Note that for COVID-19, only the original agent is considered as the majority of deaths happened in 2020 in the first and second waves.

Year	Disease	WHO (Organization et al. (2020))	IFOA (Paul Morden (2013))
1889	Russian Flu		« low »
1918	Spanish Flu	2%-3%	>2%
1957	Asian Flu	<0,2%	0,13%
1968	Hong Kong Flu	<0,2%	<0,1%
2009	Swine Flu		0.05%
2020	COVID-19	0,5%-1%	

Table 5.6: Baseline Lethality of previous pandemics in literature (1)

Year	Disease	Public Health Agency of Canada	Research
1889	Russian Flu	0,10%-0,28% (Valleron et al. (2010))	
1918	Spanish Flu	2,5%	>2,5% (Taubenberger & Morens (2006))
1957	Asian Flu	0,01%-0,33% (Payne & McDonald (1958))	
1968	Hong Kong Flu	0,1%	
2009	Swine Flu		0.048% (Nishiura (2010))
2020	COVID-19		0,68% (Meyerowitz-Katz & Merone (2020))

Table 5.7: Baseline Lethality of previous pandemics in literature (2)

Year	Disease	\bar{L}
1889	Russian Flu	0.19%
1918	Spanish Flu	2.5%
1957	Asian Flu	0.15%
1968	Hong Kong Flu	0.13%
2009	Swine Flu	0.05%
2020	COVID-19	0.72%

Table 5.8: Retained Baseline Lethality of previous pandemics

Maximum Likelihood Estimation method is used to calibrate the distribution of \bar{L} . The method is the same as the one that calibrates R_0 .

Table 5.9 shows the result of maximum likelihood estimation (from the R package *rriskDistributions*) for each possible distribution.

We observe that the Lognormal distribution and Exponential Distribution are the distributions with high log losses and the lowest AIC and BIC. Both distributions only generate positive \bar{L} , which aligns with our constraints.

However, maximum likelihood estimation for Exponential distribution is by definition unbiased, unlike the estimation for Lognormal distribution that requires an adjustment. Therefore, the exponential distribution is chosen for \bar{L} , which is the best fit, provides positive values, and contains a fat tail, which embeds some prudence.

Distribution	Log Loss	AIC	BIC
Normal	-6.61	17.22	16.44
Cauchy	-3.92	11.85	11.07
Logistic	-6.49	16.99	16.21
Exponential	-3.48	8.96	8.57
Chi-square	-3.9	9.79	9.4
Uniform	-	-	-
Gamma	-3.43	10.86	10.08
Lognormal	-2.72	9.44	8.66
Weibull	-3.36	10.71	9.93
F	-3.6	11.21	10.42
Gompertz	-3.48	10.96	10.18

Table 5.9: Measures for Baseline Lethality distribution fitness

In the end, the model retains an Exponential distribution for \bar{L} with parameter, $\lambda = 0.5046$.

5.2.2 Age-specific Factor of Lethality

5.2.2.1 The age-dependency of the lethality rate

The lethality rate will generally be age-dependent, and this dependency structure will differ across the different pandemics.

In normal cases, for instance, the pandemics in 1889, 1957, 1968 and 2009, the most vulnerable age groups are the very young and very old people. This is caused by the most common severe complication of Influenza, secondary bacterial pneumonia. The lethality rate among age groups presented a U-shape, which aligns with the human natural death curve by age. However, there are rare cases like pandemics in 1918 and 2020 that presented W-shape and J-shape respectively.

In 1918, the pandemic caused by influenza had a high lethality rate for people aged between 20 and 40. Their deaths are suspected to be mainly due to the over-aggressive immune response to infection. The response – known as a cytokine storm – can lead to a build-up of secretions in the respiratory tract causing respiratory distress. Research with genetically re-engineered 1918 influenza A suggests that this virus could have produced very high levels of chemokines and cytokines (see [Kobasa et al. \(2007\)](#)). The cytokine storm effect and secondary bacterial pneumonia together caused the lethality rate to be a W-shaped curve.

As for COVID-19, the lethality rate for very young people is relatively low compared to what had been seen in influenza. The curve is defined as J-shaped and more details will be provided later in this section.

The 3 age shapes for the 6 airborne, respiratory pandemics is summarized below:

	U-shape	W-shape	J-shape
Pandemics involved	1889, 1957, 1968, 2009	1918	2020

Table 5.10: Age shape on lethality for historical pandemics

The model assumes the probability of each type of curve will follow the historical occurrence:

- 2/3 for U-shape
- 1/6 for W-shape
- 1/6 for J-shape

Note that generally, given the enviromental changes, we usually put more weight on the recent pandemics. However, for the sake of simplicity, we have chosen to retain the frequency data as it appears historically. This approach may be revisited and refined in future studies.

5.2.2.2 Precise Calibration of the Age-mortality Factor by Age-band

Table 5.11 and Figure 5.3 present the retained lethality structure for the 3 age shapes: U, W, and J, based on the recent historical pandemics.

Age-band	U-shape	W-shape	J-shape
<1	362%	435%	0%
1-4	285%	106%	0%
5-14	18%	35%	0%
15-24	16%	85%	1%
25-34	18%	156%	3%
35-44	27%	112%	8%
45-54	64%	84%	23%
55-64	147%	135%	54%
65-74	366%	238%	191%
75-84	585%	350%	666%
85+	804%	462%	1417%

Table 5.11: Retained mortality rates compared to baseline by age-band

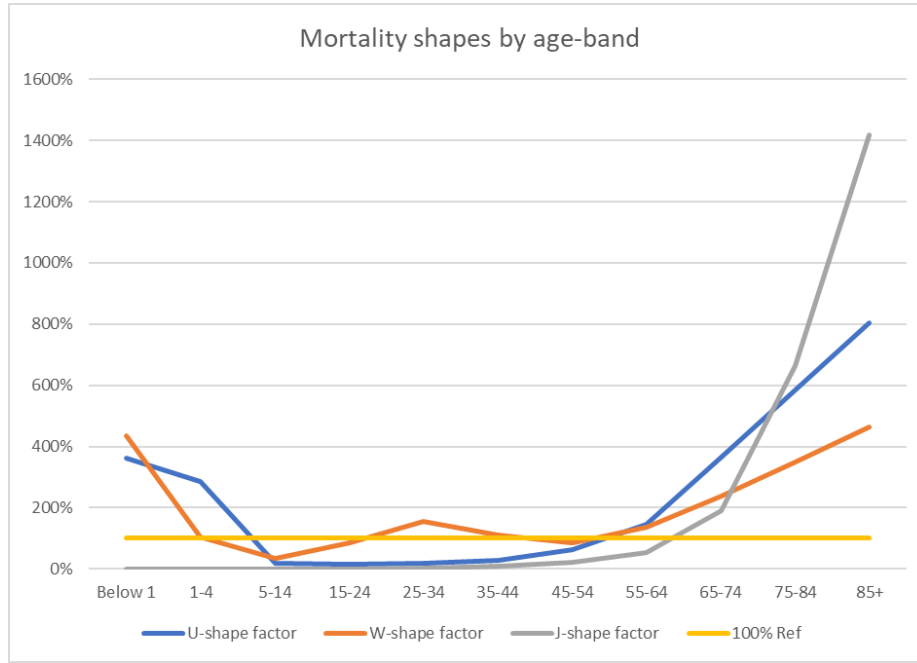


Figure 5.3: Retained mortality shape by age-band

The methodology to output those shapes is detailed below.

The lethality by age band is retrieved from reference data sources: - For the U shape, due to lack of data, we only retrieved the curve for the pandemic in 1957, which is the most severe among the four, using the “Age-Specific Estimates of the Global Pandemic-Related Mortality Burden” table provided by a scientific article about the 1957-1959 influenza pandemic (see [Viboud et al. \(2016\)](#)). - For the W shape, we use the table “fatality of influenza and of pneumonia by age, on all surveyed localities during epidemic of 1918-19” from the Public Health Reports (see [Britten \(1932\)](#)) of 1932. - For the J shape, the research by [O’Driscoll et al. \(2021\)](#) published in Nature presents the COVID-19 Infection-Fatality Rates (IFR) by Sex and Age Group.

Each shape of the lethality curve by age band ($L_{i,shape}$ for age band i) is then normalized using the global mortality of the corresponding lethality curve (\bar{L}_{shape}) to provide a multiplicative age-factor by age-band ($\alpha_{r,i,shape}$ for country r and age band i). It should be noted that in case of uncertainty, it will be prudent to renormalize using a lower global mortality rate, so that the multiplicative age-factor by age-band ($\alpha_{r,i,shape}$) will be higher:

$$\alpha_{r,i,shape} = \frac{L_{i,shape}}{\bar{L}_{shape}}$$

- For the U shape, the reference mortality rate used to calibrate the 1968 global mortality in the previous section, 0.13%, is chosen. This aligns with the study by [Viboud et al. \(2016\)](#), which

gives a slightly higher mortality rate, 0.14%.

- For the W shape, the mortality from the study by [Britten \(1932\)](#) is used to provide the 1918 mortality by age-band (“fatality of influenza and of pneumonia by age, on all surveyed localities during epidemic of 1918-19”), 1.7%. Indeed, this assumption is significantly lower than the retained assumption for global mortality calibration (2.5%) so it is more prudent by using the 1.7%, a lower mortality rate, to renormalize and compute the age-factor.
- For the J shape, the retained global mortality assumption for COVID-19 (0,72%) is chosen for the calibration.

Then, the model calculates the Age-specific Factor for each entity and each shape of the lethality curve:

$$\alpha_{entity,shape} = \sum_i \frac{x_{entity,i}}{\sum_j x_{entity,j}} * \alpha_{r,i,shape},$$

where $x_{entity,i}$ is the sum insured value for each entity for age-band i .

The reason for using the weighted average of the sum insured value for computation instead of the weighted average of the number of policyholders is that the mortality risk exposure differs for each individual across age bands. The single pandemic mortality shock applied to all policyholders for each entity should reflect their age structure of the sum insured value. This approach is crucial for computing the precise financial exposure of the solvency capital requirement.

In the later simulation part, the model uses the historical frequency of the three shapes of the lethality curve and generates scenarios in the ratio of 4/1/1 (U-shape / W-shape / J-shape), which is consistent with the two types of viruses (COVID-19 and Influenza) for the duration profile of infectiousness: J-shape for COVID-19 and W, U- shape for Influenza. In total, there are 3 scenarios generated for the age-specific lethality factor and the duration profile of infectiousness.

5.2.3 Gender-specific Factor of Lethality

5.2.3.1 The Gender-dependency of the Lethality Rate

As suggested by the literature, the lethality rate will generally be gender dependent. Both biological and behavioral differences could explain the difference in lethality.

Males and Females have different underlying biological make-up, which determines both immunological and hormonal profiles that may be important in responding to infection. These differences in the biological responses of males and females might be important in determining clinical outcomes in certain diseases. Take COVID-19 for example, the COVID-19 virus enters cells by binding to the angiotensin-converting enzyme (ACE2) receptor. There are some indications that levels of ACE2 may be higher in males than females and that increased ACE2 activity may be linked to a higher risk of severe COVID outcomes and death (see [Ramírez-Soto et al. \(2021\)](#)).

Behavior differences between genders also play an important role in determining:

- A person's risk of exposure to environments and products that might be unhealthy (e.g. smoking tobacco or drinking alcohol, etc.)
- Response to disease (e.g. patterns and timing of health service use)

5.2.3.2 Calibration of Gender-specific Factor

In the previous section, the baseline lethality distribution is calibrated, which is based on the entire population's gender structure. Now we need to calibrate a gender-specific factor, denoted as δ_e for entity e , that could address the disparity between the baseline lethality for the insurance portfolio and the baseline lethality for the country wherein these entities are situated, due to the differential gender ratio existing between the entities' policyholders and the countries' population. Indeed, the area-specific factor of lethality factor will be computed in the next section and only the policyholder gender structure needs to be considered here.

Thus, for entity e , there are:

$$\delta_e = \frac{\tilde{L}_e}{\tilde{L}_r} = \frac{\text{Proportion}_e^{\text{Male}} * L^{\text{Male}} + \text{Proportion}_e^{\text{Female}} * L^{\text{Female}}}{\text{Proportion}_r^{\text{Male}} * L^{\text{Male}} + \text{Proportion}_r^{\text{Female}} * L^{\text{Female}}},$$

where

- \tilde{L}_e is the lethality based on gender structure for entity e,
- \tilde{L}_r is the lethality based on gender structure for country r,
- $Proportion_r^{Male}$ is the proportion of the male population in country r, same for females,
- $Proportion_e^{Male}$ is the proportion of male sum insured value in entity e, same for female.

The reason we use the weighted average of the sum insured value for computation instead of the weighted average of the number of policyholders is that the mortality risk exposure differs for each individual across genders. The single pandemic mortality shock applied to all policyholders for each entity should reflect their gender profile of the sum insured value. This approach is crucial for computing the precise financial exposure of the solvency capital requirement.

We define the male to female ratio (MFR) such that:

$$L^{Male} = MFR * L^{Female}$$

For a given country r, there is:

$$\begin{aligned}\tilde{L}_r &= Proportion_r^{Male} * L^{Male} + Proportion_r^{Female} * L^{Female} \\ &= (Proportion_r^{Male} * MFR + Proportion_r^{Female}) * L^{Female}\end{aligned}$$

For a given entity e, there is:

$$\begin{aligned}\tilde{L}_e &= Proportion_e^{Male} * L^{Male} + Proportion_e^{Female} * L^{Female} \\ &= (Proportion_e^{Male} * MFR + Proportion_e^{Female}) * L^{Female}\end{aligned}$$

Thus:

$$\delta_e = \frac{Proportion_r^{Male} * MFR + Proportion_r^{Female}}{Proportion_e^{Male} * MFR + Proportion_e^{Female}}$$

For the country gender proportions, the baseline gender ratio for each country is assumed to be 1/1, since all countries in which AXA has exposure have a gender ratio close to 1/1, which means:

$$Proportion_r^{Male} = Proportion_r^{Female} = 0.5$$

Hence the remaining variable to calibrate is the MFR.

Recent medical research analyzing mortality data from 73 countries until May 20, 2021 (see [Ramírez-Soto et al. \(2021\)](#)), which primarily focused on the COVID-19 pandemic, has concluded that the lethality rate between males and females is 1.4/1. A different study, focused on the Influenza epidemic between 2015 and 2018 in Guangzhou, China (see [Li et al. \(2023\)](#)), reports an excess mortality rate between males and females of 1.34/1. In addition, a study of the age-standardized lethality rate during the 1918's Influenza pandemic has concluded a male and female lethality rate ratio of 1.3/1.

Thus, the model assumes an MFR of 1.4 for all pandemics for the matter of prudence, and we have the gender-specific factor:

$$\delta_e = \frac{Proportion_e^{Male} * 1.4 + Proportion_e^{Female}}{0.5 * 1.4 + 0.5} = \frac{Proportion_e^{Male} * 1.4 + Proportion_e^{Female}}{1.2}$$

5.2.4 Area-specific Factor of Lethality

Lethality between different countries varies due to multiple countries' characteristics like health expense per capita, comorbidity profile, health resource density, country's preparedness (economics), etc.

The model uses the entity's country demography as the model input. This assumption is prudent as it is based on the understanding that the insured population generally has better health care and living conditions compared to the general population (see [Erlangga et al. \(2019\)](#)).

The model uses historical data to calibrate the Area-specific Factor of Lethality, which should include or imply the factors listed above. However, most past pandemics are either out of date (country characteristics 50 years ago are completely different from today) or the data was not sufficient (2009 Influenza's Infection Lethality Rate was barely studied among different countries). Thus, the most recent and sufficiently studied pandemic, COVID-19, is chosen to calibrate this factor. A summary of formulas to compute the final factor is shown in Fig 5.4.

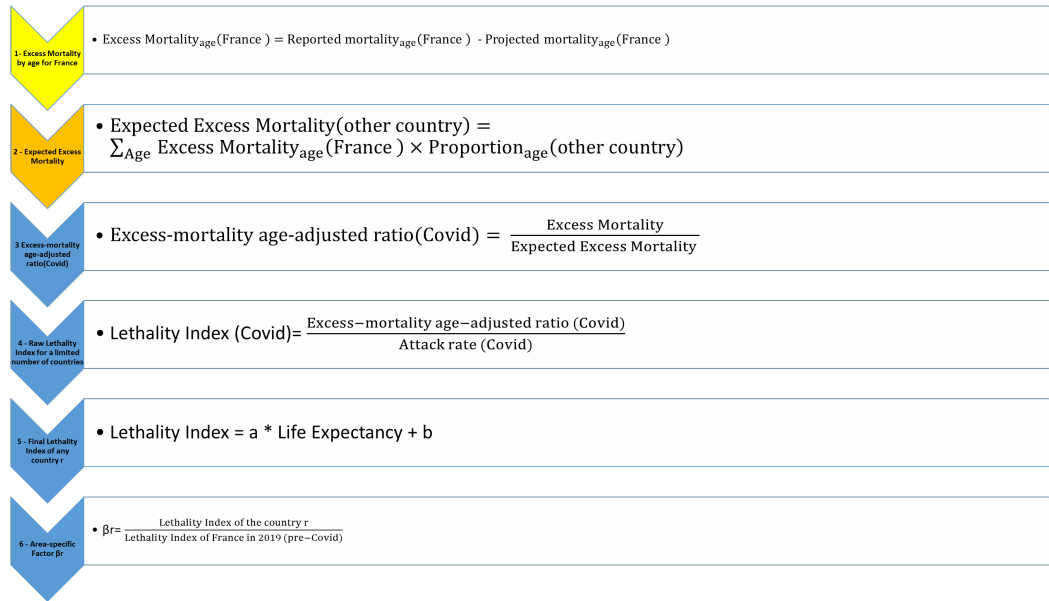


Figure 5.4: Calibration process for Area-specific Factor of Lethality

The first step is to estimate the lethality of COVID-19 in different countries (as a ratio between mortality rate and incidence), removing the age factor from the mortality rate since it is accounted for separately in the model. (Since we assume each country has a 1/1 Male to Female ratio, there is no need to remove the gender factor). The second step is to perform regressions of the lethality on various country's characteristics to determine the best explanatory factors. This regression determines the area-specific factor of lethality for any country.

5.2.4.1 Data Description and Treatment

This treatment is done in three steps.

Step 1 - Choose the Measure for COVID-19 Death

There are two recorded indicators related to the death numbers, COVID-19 deaths and excess mortality during COVID-19. A comparison between the two indicators is shown in Table 5.12:

The COVID-19 deaths indicator is not appropriate because some countries strongly underestimate it by only reporting the deaths of those who have been tested positive. Moreover, even when this is not the case, in the absence of a test it can be difficult to acknowledge with certainty if the death is linked

COVID-19 Deaths	Excess-Mortality
Most countries report this indicator	Some countries report this indicator
Some countries only report deaths that are tested positive	All deaths are recorded
Only includes deaths caused by COVID-19	Includes all cause of deaths

Table 5.12: Comparison on mortality indicators

to COVID-19. Finally, since the model aims at estimating the full risk linked to the Pandemic, it is appropriate to take into account indirect effects that impact excess mortality. Therefore, the model uses excess mortality per Million People (named as “excess-mortality” below) to model the factor. To avoid double counting the Lethality Reduction Effect caused by the vaccine, the model chooses the excess mortality from the beginning of the pandemic outbreak to Jan. 2021 (just before the vaccination period), which is long enough for each country to have a relatively reliable Attack Rate and not include the vaccination effect differences.

Step 2 - Remove Age Impact from COVID-19 Mortality

Different countries have different age structures, and age factor is proven to have a huge impact on Lethality. Hence, the age impact must be removed from the excess mortality before further calibration. Since there are only a few countries that record their excess mortality by age groups, an indirect age-adjustment method (see [Naing \(2000\)](#)) is used (only need one benchmark country to report Excess-mortality by age) to remove the age impact. The model takes France as the benchmark country, and transforms all countries’ excess mortality, denoted as $exM^{country}$, to be the comparable excess mortality (based on the benchmark age structure of France), denoted as $Compare_exM^{otherCountry}$ using the following formula:

$$Compare_exM^{otherCountry} = \sum_{Age} exM_{age}^{France} * Proportion_{age}^{otherCountry} \quad (5.1)$$

Thus, the Excess Mortality Age Adjusted Ratio for a certain country, denoted as $exM_Adj_Rate^{country}$, will be

$$exM_Adj_Rate^{country} = \frac{exM^{country}}{Compare_exM^{country}}$$

With this indirect age-adjustment method, population structure and excess mortality for each country

are required. And as a benchmark, France also needs the excess mortality data by age group (0-14, 15-64, 65-74, 75-84, 85+). The excess mortality model uses the Human Mortality Database and the p-score provided by the research of [Karlinsky & Kobak \(2021a\)](#) to compute the excess mortality.

The p-score measures excess mortality as the difference (in percentage) between the reported and projected number of deaths. This metric is calculated as:

$$p_score = \frac{Reported_Deaths - Projected_Deaths}{Projected_Deaths} * 100,$$

where *Projected_Deaths* is a linear regression model fitted on the last 5 years, 2015-2019. In order to estimate excess mortality, the expected (or baseline) mortality for 2020 was first estimated using historical data from 2015 to 2019 (or as many years from this interval as were available). The following regression model was fitted separately for each country:

$$D_{t,Y} = \alpha_t + \beta \cdot Y + \varepsilon \quad (5.2)$$

where $D_{t,Y}$ represents the number of deaths observed in week (or month, or quarter) t of year Y , β denotes a linear slope across years, α_t serves as separate intercepts (fixed effects) for each week (or month/quarter), and $\varepsilon \sim \mathcal{N}(0, \sigma^2)$ represents a Gaussian noise. This model 5.2 captures both seasonal variations in mortality and a yearly trend reflecting changes in population structure or socio-economic factors over recent years.

Note that past (2015–2019) influenza outbreaks contributed to the estimation of the projected death. As a consequence, this baseline estimation captures the expected mortality without the COVID-19 pandemic, but in the presence of usual seasonal influenza.

Knowing the Reported Deaths (the weekly deaths counts), the Projected Deaths per age group for France is computed as:

$$Projected_Deaths = \frac{Reported_Deaths}{1 + \frac{p_score}{100}}.$$

Then the excess mortality model computes the French cumulated excess mortality count by age group from 01/01/2020 to 28/02/2021 by the difference of Reported deaths by age group and Projected deaths

by age group ²:

$$exM_{age} = Reported_Deaths_{age} - Projected_Deaths_{age}$$

Using the total population by age group in mainland France from the United Nations website the French excess mortality per million for each age group is computed and shown in Table 5.13.

	0-14	15-64	65-74	75-84	85+	Total
Population in millions	11	40	7	4	2	64
Excess-Mortality Count	-336	2'058	5'465	17'653	26'919	51'757
Excess-mortality per million	-30	52	751	4 394	11'971	803

Table 5.13: Excess Mortality per million for each age group

Applying the indirect age-adjustment method to remove the age impact. Using proportion of the population by age group from the United Nations and the benchmark French excess mortality per age group, the model calculates the comparable excess mortality for each country as if they would have the same excess mortality per age group as France using Equation 5.1.

Lastly, the model computes the ratio between real excess mortality and the comparable one adjusted to France age structure as the Excess mortality age-adjusted ratio. Note that for France, the ratio is by definition equal to 1. For countries that have more Excess-Mortality than France after removing the age impact, this factor is higher than 1.

Table 5.14 shows some of the numerical results for the COVID-19 crisis (from 01/01/2020 to 31/01/2021), with France as a benchmark for the Age Adjusted Ratio:

In summary, there are four main classes of countries:

- Finland, Japan, Thailand, South Korea or Philippines did very well to protect their population from death in the first year (Age adjusted Ratio close to 0), some of them even having less deaths than previous years (explained by less flu, less car accidents, etc. due to quarantine).
- Some better performed European countries (France, Germany and Switzerland) had similar mitigation actions or health system in place and thus have a similar ratio in range [0.6;1.4].
- Some lower performed European countries (Spain, Italy, Belgium and UK) had similar ratio around 2.

²This cumulated excess mortality during the period is positive for all countries and regions concerned in our study. It should be cautiously used since for other time period the value could be negative.

Continent	Country	Excess Mortality Mortality per Million	Comparable Excess per Million	Age Adjusted Ratio
Benchmark	France	838	838	1.0
Europe	Finland	25	790	0.0
	Germany	526	882	0.6
	Switzerland	1'034	731	1.4
	Belgium	1'408	748	1.9
	Italy	1'860	959	1.9
	Spain	1'655	820	2.0
	United Kingdom	1'696	702	2.4
Asia	Japan	-283	1'291	-0.2
	Philippines	-29	134	-0.2
	Republic of Korea	-54	545	-0.1
	Thailand	41	459	0.1
North America	U.S.	1'780	547	3.3
	Mexico	3'614	264	13.7
South America	Brazil	1'240	261	4.7
	Peru	3'266	252	12.9
Africa	South Africa	2'094	181	11.6

Table 5.14: Excess Mortality, Comparable Excess Mortality, and Age Adjusted Ratio, organized first by continent and then by Age Adjusted Ratio

- Most American countries (USA, Mexico, Brazil, Peru) and South Africa took a heavy toll with factors much higher, with still an even higher gap between USA and South Africa.

Step 3 - Remove Infection Rate Difference from Age-Adjusted Ratio

For the COVID-19 pandemic, each country had different mitigation actions and hence had different Attack Rates as of Jan. 2021. To analyze the lethality difference between countries, we need to remove the Infection rate difference. Confirmed COVID-19 infection cases are infections that have been confirmed with a test but is far from being the true number of infections because many infected people never got tested. So, although this data is available, it is not relevant to estimate the real number of infections. The [Institute for Health Metrics and Evaluation \(IHME\) \(2020\)](#), an independent global health research center at the University of Washington, developed epidemiological models of COVID-19 to estimate the true infection ratio, which is also referenced by WHO in various articles. Figure 5.5 shows the Daily new estimated COVID-19 infections from the IHME model in France from Jan. 10th 2020 to Jan. 31st 2021:

Daily new estimated COVID-19 infections from the IHME model, France

Estimates of the true number of infections. The "upper" and "lower" lines show the bounds of a 95% uncertainty interval. For comparison, confirmed cases are infections that have been confirmed with a test.

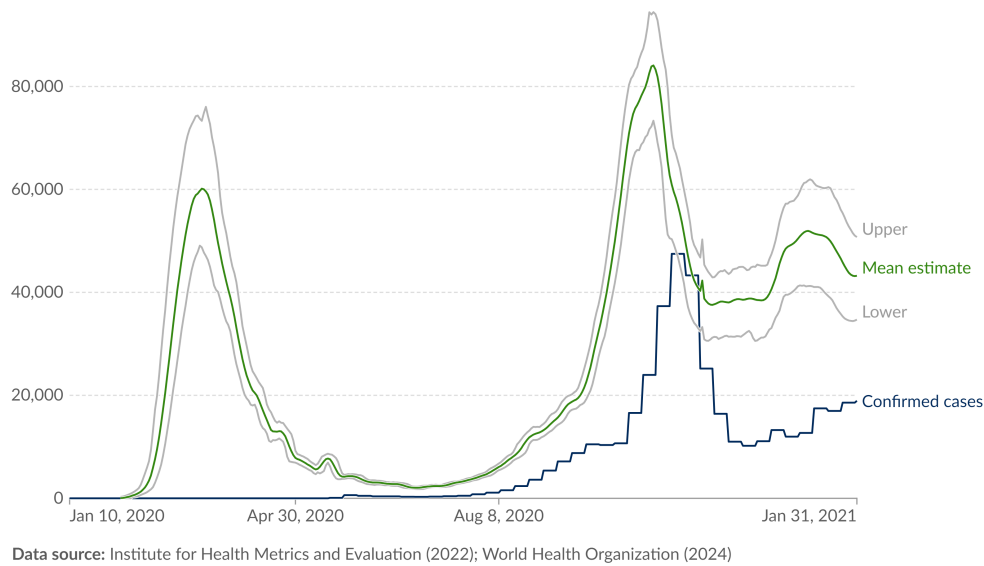


Figure 5.5: Daily new estimated infections of COVID-19 in France by IHME Model

The database of IHME comprises a total of 242 countries and regions. To ensure the accuracy of excess mortality reports and mitigate small sample issues, only countries and regions with a population exceeding 5 million and a cumulative excess mortality rate of over 100 per million people from January 1, 2020, to February 28, 2021, have been selected for calibration inputs. As a result, 48 countries and regions have been selected, including most of AXA's Life risk exposures (except for Japan and Hong Kong, due to the low excess mortality in the first year).

The Lethality Index (removing Infected Ratio in population difference) for each country is defined by the following formula:

$$Lethality_Index = \frac{Age_Adjusted_Ratio}{Infected_Ratio}$$

The lethality results for some countries are shown in Table 5.15.

As a reminder, this lethality index is independent of the age structure of the population (see previous section) and from the speed of propagation of the pandemic.

5.2.4.2 Calibrate Linear Regression on Lethality Index

With the Lethality Index by country, a linear regression model is developed to measure the Area-specific Factor on Lethality. The aim is to isolate and understand the broader socio-economic and health-related

Continent	Country	Age-Adjusted Ratio	Infection Rate	Lethality Index
Benchmark	France	1.00	15%	7
Europe	Finland	0.03	4%	1
	Germany	0.60	9%	7
	Belgium	1.88	20%	10
	Switzerland	1.41	13%	11
	Spain	2.02	15%	13
	United Kingdom	2.41	17%	14
	Italy	1.94	14%	14
North America	United States of America	3.26	20%	16
	Mexico	13.68	54%	25
South America	Brazil	4.75	37%	13
	Peru	12.94	48%	27
Africa	South Africa	11.59	45%	26

Table 5.15: Lethality Index, Age Adjusted Ratio, and Infection Rates, organized first by continent and then by Lethality Index

factors influencing lethality rates across countries. The model can be expressed mathematically as:

$$L_i = \beta_0 + \beta_1 * V_i + \varepsilon_i,$$

where:

- L_i : Lethality Index for country i ,
- V_i could be five different explanatory variables:
 - Life expectancy for country i ,
 - Health Vulnerability Index from the Global Health Security (GHS) Index³,
 - Gini coefficient from the World Bank, measuring income inequality within country i ,
 - Preparedness Index provided by the WHO for country i ,
 - GDP per capita from the World Bank for country i ,
- β_0 : Intercept of the regression model,
- β_1 : Coefficient representing the effect of each explanatory variable on the Lethality Index,

³The GHS Index is a project of the Nuclear Threat Initiative (NTI) and the Johns Hopkins Center for Health Security, developed with Economist Impact. <https://www.ghsindex.org/>

- ε_i : Error term for country i , capturing the effects of unobserved factors.

Given the strong linear correlation between life expectancy and the other four variables, we conduct linear regression analyses on each of the five explanatory variables separately to mitigate potential multicollinearity issues.

These variables collectively represent key dimensions of a country's health system resilience, socio-economic conditions, and preparedness against pandemic events.

We use R-squared value and Root Mean Square Error (RMSE) to measure the fitness of each regression. We recall the R-squared and RMSE below:

R-squared

The R-squared value, denoted as R^2 , is a statistical measure that represents the proportion of the variance for a dependent variable that can be explained by the independent variable(s) in a regression model. For a simple linear regression model, the R-squared value can be calculated as follows:

$$R^2 = 1 - \frac{SS_{\text{res}}}{SS_{\text{tot}}},$$

where:

- SS_{res} (Residual Sum of Squares): $SS_{\text{res}} = \sum_{i=1}^n (y_i - \hat{y}_i)^2$
- SS_{tot} (Total Sum of Squares): $SS_{\text{tot}} = \sum_{i=1}^n (y_i - \bar{y})^2$ Here, \bar{y} is the mean of the observed values.

R^2 ranges from 0 to 1. The closer it is to 1, the better fitting for the linear regression.

Root Mean Square Error (RMSE)

RMSE measures the average difference between the model's predicted values and the actual values. Therefore, a lower RMSE indicates a better model fit. The RMSE is defined mathematically as:

$$RMSE = \sqrt{\frac{1}{n} \sum_{i=1}^n (y_i - \hat{y}_i)^2},$$

where:

- n : The number of data points (countries),
- y_i : The dependent variable (Lethality Index) for country i ,
- \hat{y}_i : The projected value of the dependent variable (projected Lethality Index) for country i .

RMSE is expressed in the same units as the dependent variable, making it interpretable. A lower RMSE value indicates a better fit of the model to the data, as it signifies that the predictions are closer to the actual observed values.

Since R-squared is only applicable to linear regressions, the Root Mean Square Error (RMSE) is employed to compare different types of regressions.

The results are shown in Table 5.16.

Quality of the regressions	Line RMSE (R-squared)	Exp RMSE	Log RMSE
Using Life Expectancy	39.1 (45.5%)	38.6	38.6
Using GHS Indicator	49.1 (13.8%)	51.1	48.8
Using Gini Coefficient	48 (17.8%)	50.0	48.5
Using Preparedness	- (2.0%)	-	-
Using GDP Per Capita	47.1 (20.6%)	48.4	42.0

Table 5.16: Root Mean Square Error (RMSE) using different explaining variables

Note that there are 7 countries among the 48 selected countries that do not have Preparedness indicator. Thus the result only show the R^2 value for linear regression. Table 5.16 indicates that life expectancy is the best explanatory variable under all regression types. Beyond the quantitative measure, life expectancy under linear regression is chosen for three main qualitative reasons:

1. Life expectancy implicitly includes factors such as healthcare expenses, comorbidity profiles, socioeconomic risk behaviors, and other indicators of population health, making it a comprehensive predictor of excess mortality.
2. Linear regression is less sensitive to outliers and is simpler to understand and interpret because it assumes a linear relationship between the independent and dependent variables.
3. Life expectancy has the additional advantages of being readily available, understandable, and stable across data sources.

Thus, the obtained regression on the Lethality Index for country r is:

$$Lethality_Index_r = -1.1929 * LE_r + 105.36,$$

where LE_r is the life expectancy for country r .

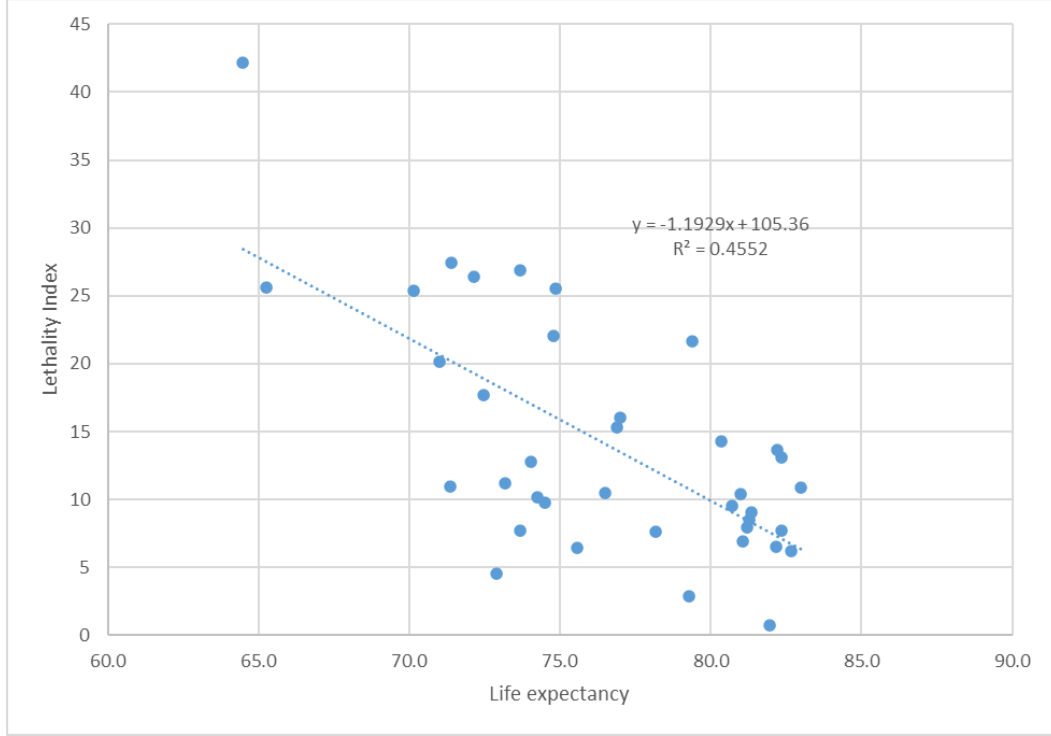


Figure 5.6: Lethality Index as a function of life expectancy

5.2.4.3 Computation of Area Specific Factor of lethality (Choice of a reference country)

In order to estimate the area-specific factor of lethality, β_r , which will be used to adjust mortality computation, the calibration of the baseline lethality (and the age-specific factor) is based on data from around the world. Thus, no area-specific adjustment β_r is needed for countries where the life expectancy is equal to the world's life expectancy. However, since many studies are performed primarily on populations from more developed countries, it is prudent to consider the Life Expectancy of one of the most developed countries as the reference.

Life Expectancy for France is chosen as the reference, as France has an IFR (Infection Fatality Ratio) of approximately 0.65% for COVID-19, close to the global IFR of 0.68% as cited by the same meta-analysis study and within the range of global IFR stated by WHO, 0.5%-1%. The Lethality Index for

France is calculated as follows:

$$Lethality_Index_{France} = -1.1929 * LE_{France} + 105.36 = 6.56$$

The area-specific factor β_r for a country r is defined as the ratio of the projected Lethality Index for that country r to the French projected Lethality Index:

$$\beta_r = \frac{Lethality_Index_r}{Lethality_Index_{France}}$$

By construction, the area-specific factor for France is exactly equal to 1. The area-specific factors for other countries or regions when applying 2020 Life Expectancy are listed below:

Country	β_r
France	1.0
Germany	1.3
Italy	0.9
Spain	0.8
Japan	0.7
Belgium	1.2
Hong Kong SAR, China	0.6
Mexico	2.6
Switzerland	0.8

Table 5.17: Area-specific Factor per country

To conclude this lethality section, we have now defined:

- The baseline lethality rate \bar{L}
- The age-specific factor $\alpha_{entity,shape}$
- The gender-specific factor δ_{entity}
- The area-specific factor β_r

The last factor, lethality reduction effect (from both infection and vaccination) denoted as $\mu(t)$ for day t , will be detailed in Section 5.3. Recall of the lethality rate function:

$$L = \bar{L} * \alpha_{entity,shape} * \delta_{entity} * \beta_r * \mu(t - d_{max})$$

5.3 Mitigation

The mitigation of a pandemic consists in mainly two key components: quarantine, alongside other non-pharmaceutical interventions, and the widespread administration of vaccinations. These critical strategies work together to reduce the transmissibility and lethality of the pandemic.

5.3.1 Quarantine and other Non-Pharmaceutical Interventions

Non-Pharmaceutical Interventions (NPIs) are interventions that are not directly related to the medical world, but that help to reduce the impact of the pandemic. They are classified into three main categories by the Centers for Disease Control and Prevention (CDC):

- **Personal NPIs:** these are NPIs related to single individual
 - Voluntary home isolation (for ill people)
 - Respiratory etiquette
 - Hand hygiene
 - Voluntary home quarantine (for non-ill but exposed people)
 - Face masks use
- **Community NPIs:** these are NPIs related to a group of people
 - School closures and dismissals
 - Social distancing (telecommuting in workplaces, seating people apart, mass gatherings postponements...)
 - Lockdowns (strong restriction policy for people or community to stay at home)
- **Environmental NPIs:** These are NPIs linked to environmental surface cleaning, e.g., cleaning surfaces and objects with detergent-based cleaners or disinfectants.

The global level of NPIs depends on the awareness and attention given by the population. It is realistic to assume that population awareness will increase with the spread of the pandemic, same as the government intervention actions. Our model is mainly based on the latest experience learned from COVID-19

since experience on the Influenza pandemic is limited and the most significant Influenza pandemics happened a long time ago, so government interventions cannot be compared with modern world reactions.

The model applies a simplified quarantine model with 4-phases:

- Outbreak
- Quarantine
- Progressive transition between quarantine and reopen
- Full reopen

It corresponds to several levels of reproduction number: R_0 , R_t^Q (quarantine) and R_t^R (full reopen):

- At the outbreak, the reproduction number is the Basic Reproduction Number R_0 , generated by the Transmissibility model.
- The quarantine is triggered in each country when the infected number reaches a certain level, $Trigger^Q$, then the reproduction number shifts immediately from R_0 to R_t^Q during a certain period of time T^Q .
- After T^Q days, the restrictions are lifted progressively and reproduction number R_t^T shifts linearly from R_t^Q to R_t^R . The reopening will happen progressively during T^T days.
- After T^T days, the R_t^R (reopen) will be lower than R_0 . Even when the governments reduce the restrictions, they may apply face mask requirements and people who are aware of the pandemic still take Personal NPIs. For this reason, the R_t^R (reopen) will be lower than R_0 .

Overall, the following parameters need to be calibrated are:

- Reproduction number during quarantine: R_t^Q
- Reduction of reproduction number during reopen (face masks, personal NPIs...): ρ such that $R_t^R = \rho * R_0$. The final reproduction number during the reopen phase will be $\max(R_t^Q, R_t^R)$, since the reproduction number during the reopen phase should be no smaller than the quarantine one.
- Threshold on number of infected to start the quarantine $Trigger^Q$

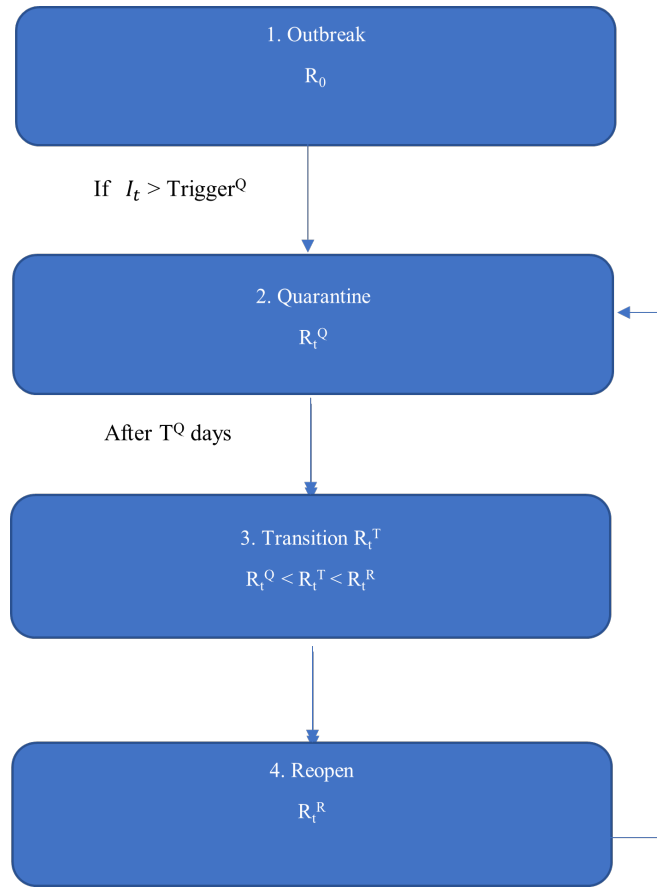


Figure 5.7: The 4 phases of the Quarantine Model

- Number of days of full quarantine T^Q
- Number of days between full quarantine and full reopen T^T

5.3.1.1 Effective Reproduction Number

The model calibrates the Effective R_t , which is computed as $R_t * \frac{S_r(t)}{N_r(t)}$, for all different types of reproduction numbers mentioned previously, because the Effective R_t can be estimated directly on pandemic data, with the R_t value implied in the Effective R_t . After calibrating the Effective R_t , we can retro-calculate the R_t value in our model with the formula: $R_t = \frac{Effective R_t}{\frac{S_r(t)}{N_r(t)}}$

The quarantine during COVID-19 was the latest and most clearly reported experience so far. Our CAT model assumes that if a pandemic happens in the future, the governments will act similarly to what we have seen during COVID-19.

Below is the estimation of Effective R_t for different countries, based on Kalman filter study by [Arroyo-Marioli et al. \(2021\)](#) which has been used by many governments to monitor their quarantine effectiveness.

Note that R_t is implied in the Effective R_t shown in Figure 5.8.

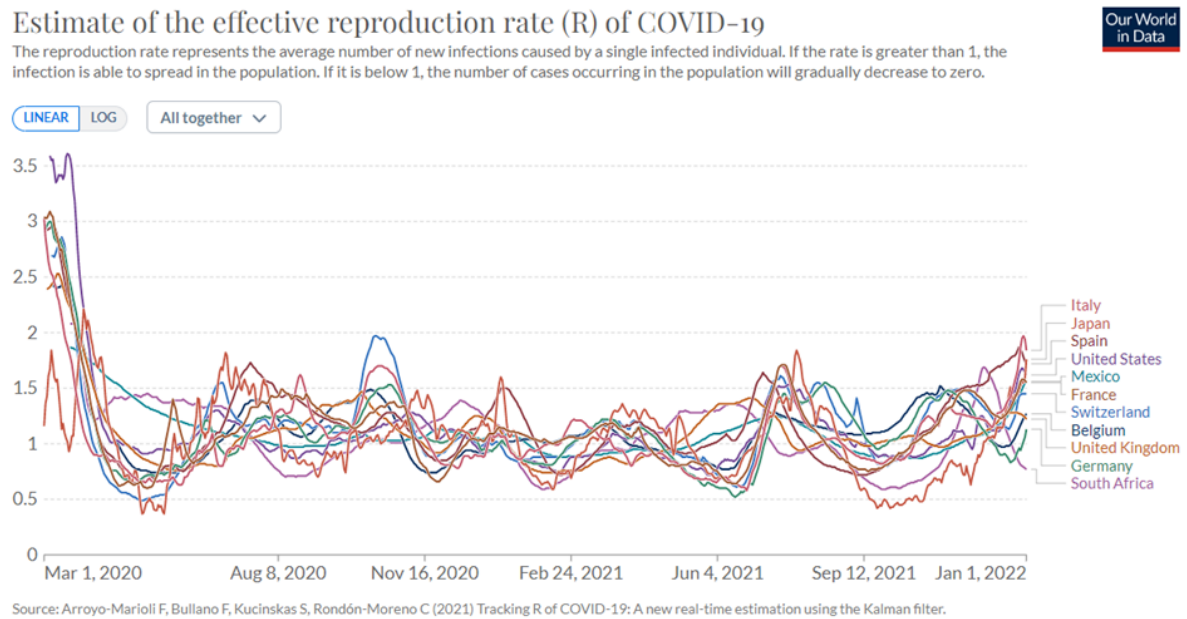


Figure 5.8: Effective R_t of COVID-19 in 2020 and 2021 per country.
Source from: Our World In Data

The effect of the first quarantines was measured by [Flaxman et al. \(2020\)](#) who considered that NPI was sufficient to drive R_t^Q below 1 in considered countries. They also found estimates of R_t^Q to range from a mean of 0.44 (0.26–0.61) for Norway to a mean of 0.82 (0.73–0.93) for Belgium, with an average of 0.66 across the 11 countries.

These conclusions are corroborated by studies from individual countries—France, Spain, Germany, and the UK—over a similar period, which arrive at very similar estimates despite different methodologies and data. The Institut Pasteur estimated using hospitalization records that in France (see in [Salje et al. \(2020\)](#)), the lockdown of March 2020 reduced the reproductive number to 0,67 (Flaxman and al. estimate 0,68); for Germany, the Robert Koch Institute reports R_t^Q of 0,76 using electronically notified cases (Flaxman and al estimate 0,71).

University of Oxford quantitative research [Sharma et al. \(2021\)](#) measured the effect of the first quarantine but also the following ones. They conclude that Effective R_t^Q was reduced to an average of 0,7 [95% CI: 0,5–0,8] across regions in the second wave, compared to an average of 0,7-0,8 in the first wave.

The table below recaps the quarantine Effective R_t^Q :

The conclusions of these studies lead to propose an effective reproduction value during quarantine, effective R_t^Q at 0.75 since this level was reached during the quarantine for the first wave but also the

Research Institution	First Wave	Second Wave
Flaxman et al	0.66	-
Institut Pasteur	0.67 (France)	-
Robert Koch Institute	0.76 (Germany)	-
University of Oxford	0.7-0.8	0.7

Table 5.18: Effective R_t value from research

following one.

The study from the University of Oxford quantitative research also estimates the reduction of reproduction number that remains after the first quarantine measures are lifted: the reduction is between 34 to 49%. For Influenza, the reduction ratio is estimated at 33% by [Cowling et al. \(2009\)](#). So overall, we will consider a reduction of reproduction number by a third during the reopen period, so a scaling factor ρ at 67%.

5.3.1.2 Timing of Quarantines

The World Bank detailed in the table “Sequency of lockdown measures” the dates associated with the relaxation of the first set of lockdown measures (work and mobility restrictions) per country established during April-May 2020. For the countries where AXA was present, the different dates of full lockdown, exit to partial lockdown and exit from full lockdown are retrieved. Then the study computes the minimum, maximum, median, and average duration of the lockdown and of transitory measures between the end of the lockdown and the total reopening of the country. The results are shown in Table 5.19.

	Duration of lockdown (days)	Duration of transition (days)
Min	41	22
Max	58	40
Average	51	31
Median	53	29

Table 5.19: Lockdown and Transition Duration

The CAT pandemic model retains a lockdown duration of 50 days and a transition duration of 30 days.

5.3.1.3 Trigger of quarantine

It is consider that a quarantine will be triggered by a government when too many people are sick at the same time, since this notably puts at risk the hospital’s capacity. We model that as a given proportion of

the population catching the illness over the past two weeks (14 days).

Table 5.20 using IHME reference data (see in [Institute for Health Metrics and Evaluation \(IHME\) \(2020\)](#)) shows an estimation of the number of people who caught COVID-19 over the 14 days before the first lockdown in major European countries. Asian countries are not considered because the pandemic initially hit less strongly, and China initiated a lockdown although the number of infected was very low, so we exclude them in our study.

Country	Number of infected people over the 14 days before the first lockdown	Corresponding proportion of population
France	751'651	1.2%
Italy	463'530	0.8%
Spain	651'012	1.4%
United Kingdom	831'099	1.2%
Germany	270'379	0.3%
Belgium	89'181	0.8%
Switzerland	52'773	0.6%

Table 5.20: Number of infected people over the 14 previous days of first lockdown

Based on these results (average of 0.9%, median of 0.8%), we retain a threshold to start a quarantine at 1.0% of the national population infected over the 14 previous days.

5.3.2 Vaccination

Vaccination is a critical tool for public health systems to mitigate or potentially prevent pandemic waves. However, incorporating vaccination into an epidemiological model requires careful consideration of certain assumptions. Achieving a universal vaccine remains an elusive goal, as viruses continuously evolve, presenting new challenges with each outbreak.

Once a new virus strain is identified, the vaccine development process involves multiple stages: identifying the virus, designing a vaccine candidate, conducting laboratory and clinical trials, and scaling up for mass production.

Since the vaccines need to be tailor-made and since the industry can face some production issues, it will take some time for the vaccine to be available for production. Literature of the production delay has been studied, including both Influenza and COVID-19. Results are shown in Table 5.21.

In summary, Influenza vaccines can be produced more quickly than COVID-19 vaccines because

Source	Vaccination Time since Outbreak
Altevogt et al. (2011)	4-6 months
WHO Pandemic (H1N1) 2009 briefing	6 months
Mathieu et al. (2021)	12 months

Table 5.21: Vaccination time from research

Influenza vaccines are developed annually, with only the strain changing. For our baseline value, we will assume that the vaccine will be available after 13 months (12 months plus 1 additional month for second doses, i.e., 395 days). This assumption uses the longest time frame (from COVID-19) among the information provided. In addition, considering that COVID-19 occurred less frequently than Influenza in past pandemics, the decision to use the longest timeframe for COVID-19 results in more infections, which is a prudent assumption.

5.3.2.1 Distribution of Vaccination

For the vaccine distribution, the model uses assumptions based on the COVID-19 vaccine data provided by public official sources (see in [Mathieu et al. \(2021\)](#)). Figure 5.9 shows the countries' share of people who complete the initial COVID-19 vaccination protocol (2 doses):

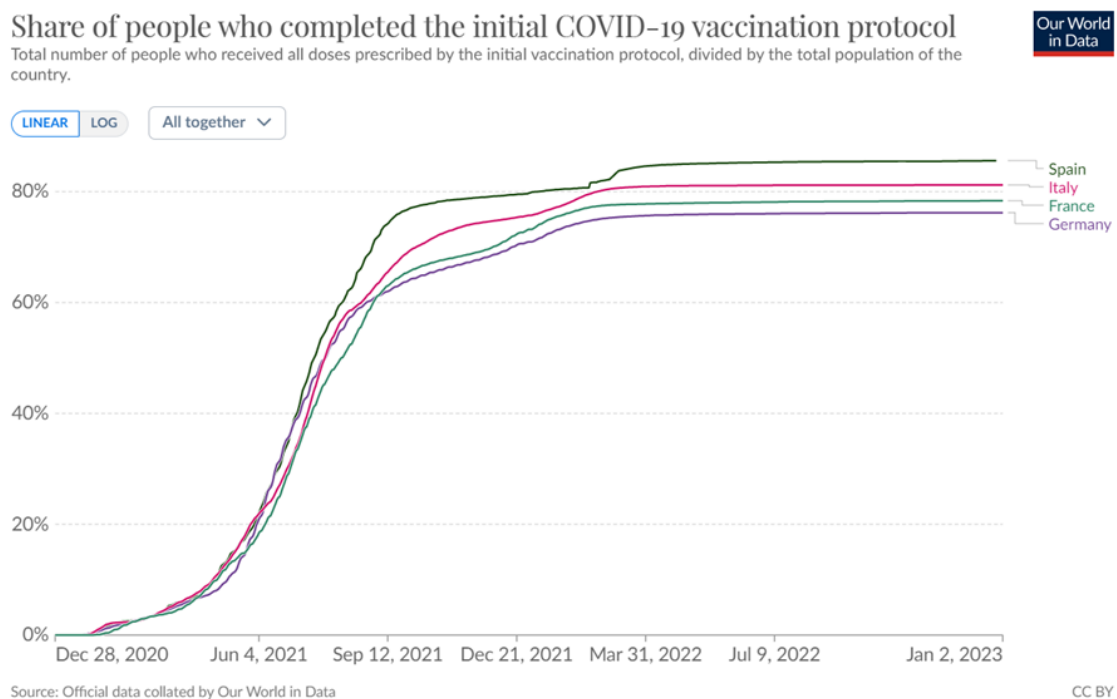


Figure 5.9: Vaccination Distribution during COVID-19
 Source from: Our World In Data

Each country begins with a slow rate and then increases rapidly before reaching the coverage limit (final vaccine coverage plateau). The maximum time from the start to the coverage limit is around 12 months (i.e., 365 days). Note that timing parameters derived from COVID-19 experience are also prudent for Influenza since the vaccination production process for Influenza is relatively more mature than the process for COVID-19.

We assume that vaccines are deployed continuously starting 13 months after the pandemic and that the vaccination level will increase linearly over time for 12 months, so $V_r(t)$, the new vaccinated number on day t will be:

$$\begin{cases} V_r(t) = 0, & \text{if } t < T_s, \\ V_r(t) = 1/T_d * N_r(t-1) * C_r & \text{if } T_s \leq t < T_s + T_d, \\ V_r(t) = 0 & \text{if } t \geq T_s + T_d \end{cases}$$

where

- T_s is the starting time (395 days after the first outbreak)
- T_d is the vaccination duration to reach the coverage limit (365 days)
- C_r is the coverage limit of country r (country-dependent, detailed in the next section)
- $N_r(t)$ is the number of total alive people in country r at time t .

5.3.2.2 Vaccination Coverage Limit

The higher the proportion of people who are vaccinated against the new pandemic, the larger the effects of the vaccination. Thus, the “vaccination coverage”, the proportion of people who are vaccinated, is a key element that must be taken into account in our pandemic model.

The vaccination coverage limit varies between countries. In general, developed countries have higher coverage limits than developing countries.

The model assumes different countries tend to follow the same pattern in terms of coverage limit for the next pandemic as for COVID-19.

Thus, the COVID-19 vaccination coverage at the end of January 2022 is taken into consideration:

- The outbreak on 01/01/2020
- The vaccination starts with a first dose after a year
- The second dose one month later
- The vaccination deployment lasts a year (so the overall process lasts 25 months)

Note that the same countries and indicators as in the Area factor of lethality has been chosen for the calibration of vaccination coverage limit.

The model applies linear, exponential, and logarithmic regressions on the indicators to calibrate the vaccination coverage limit (same method as in Section 5.2.4.2). As previously demonstrated on finding a relationship between the lethality index and country-specific indicators, Root Mean Square Error (RMSE) was used to compare the fit of different regressions.

The results are presented in Table 5.22:

Quality of the regressions	Line RMSE (R-square)	Exp RMSE	Log RMSE
Using Life Expectancy	0.643 (55.94%)	0.649	0.646
Using GHS Indicator	0.808 (30.47%)	0.833	0.797
Using Gini Coefficient	0.962 (1.42%)	0.976	0.966
Using Preparedness Index	- (0.54%)	-	-
Using GDP Per Capita	0.846 (23.91%)	0.876	0.802

Table 5.22: Root Mean Square Error (RMSE) result on vaccination coverage limit

Note that there are 7 countries among the 48 selected countries that do not have Preparedness indicator. Thus, the result only show the R^2 value for linear regression.

Life expectancy generally provides better-fit results (lower RMSE) compared to other indicators; thus, life expectancy is retained as the indicator for the regression analysis. With this consideration, the linear regression demonstrates a lower RMSE when compared with the other two regressions. Therefore, life expectancy under linear regression is chosen to calibrate the Vaccination Coverage Limit. The formula for Vaccine Coverage Limit for country r , denoted C_r , is shown below (restricted between 0% and 100%):

$$C_r = 0.025 * LE_r - 1.308$$

The retained Vaccination Coverage Limits for AXA entities are listed in Table 5.23:

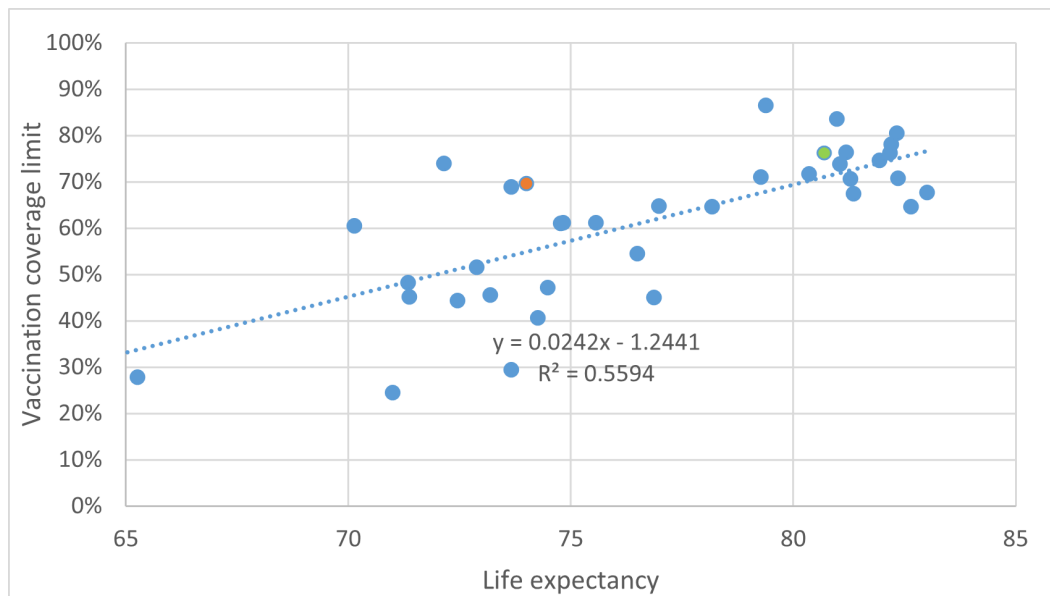


Figure 5.10: Vaccination Coverage as a function of life expectancy

Country or Region	Vaccine Coverage Limit
France	75%
Germany	72%
Italy	75%
Spain	75%
Japan	80%
Belgium	71%
Hong Kong SAR, China	82%
Mexico	45%
Switzerland	77%

Table 5.23: Vaccination Coverage Limit per country

5.3.2.3 Reduction of Transmissibility following Vaccine or Previous Infection

Vaccine efficiency is difficult to assess since it is correlated with the strain of the virus. For example, flu vaccines have more efficacy against H1N1 than H3N2 (67% versus 33% of efficacy respectively based on a study by [Belongia et al. \(2016\)](#)). However, we need to strongly distinguish between yearly flu pandemics and a potential major pandemic. Indeed, these estimates refer to vaccines designed in advance when the future circulating strain is not well known yet and might still evolve due to antigenic changes. In case of a major pandemic, as shown in the examples below, vaccines will be designed specifically against the pandemic strain and are expected to be more efficient. The drawback is that they will take longer to be available, but this is being modeled.

Based on the analysis by [Gagliani et al. \(2016\)](#), on the H1N1 virus that circulated in 2013-2014 and

was identical to the 2009 pandemic virus, we retrieved the effectiveness rates for Influenza in Table 5.24:

Age Band	Retained effectiveness
9-17	61%
18-49	55%
50-64	64%
≥65	59%

Table 5.24: Vaccine effectiveness for H1N1 Influenza

These results show a Vaccine efficiency of around 60% and look prudent, compared to the Vaccine efficiency observed during the 2009 pandemic itself (78,4% in patients < 65years; 71,9% overall [Valenciano et al. \(2011\)](#)).

Concerning COVID-19, comprehensive studies including different vaccines towards different variant types are summarized by the Institute for Health Metrics and Evaluation [Institute for Health Metrics and Evaluation \(IHME\) \(2020\)](#) and shown in the Figure 5.11:

Vaccine	Effectiveness at preventing											
	Ancestral		Alpha		Beta		Gamma		Delta		Omicron	
	Severe disease	Infection	Severe disease	Infection	Severe disease	Infection	Severe disease	Infection	Severe disease	Infection	Severe disease	Infection
AstraZeneca	94%	63%	94%	63%	94%	69%	94%	69%	94%	69%	71%	36%
CanSino	66%	62%	66%	62%	64%	61%	64%	61%	64%	61%	48%	32%
CoronaVac	50%	47%	50%	47%	49%	46%	49%	46%	49%	46%	37%	24%
Covaxin	78%	73%	78%	73%	76%	72%	76%	72%	76%	72%	57%	38%
Johnson & Johnson	86%	72%	86%	72%	76%	64%	76%	64%	76%	64%	57%	33%
Moderna	97%	92%	97%	92%	97%	91%	97%	91%	97%	91%	73%	48%
Novavax	89%	83%	89%	83%	86%	82%	86%	82%	86%	82%	65%	43%
Pfizer/BioNTech	95%	86%	95%	86%	95%	84%	95%	84%	95%	84%	72%	44%
Sinopharm	73%	68%	73%	68%	71%	67%	71%	67%	71%	67%	53%	35%
Sputnik-V	92%	86%	92%	86%	89%	85%	89%	85%	89%	85%	67%	44%
Other vaccines	75%	70%	75%	70%	73%	69%	73%	69%	73%	69%	55%	36%
Other vaccines (mRNA)	91%	86%	91%	86%	88%	85%	88%	85%	88%	85%	67%	45%

Figure 5.11: COVID-19 Vaccination Effectiveness

The vaccine efficiency against infection is very high, especially for the two main distributed vaccines in France, Pfizer and Moderna. Those vaccines show an efficiency between 84% and 92%, except against the variant Omicron for which it falls to 44% and 48% respectively. Still, this last variant appeared a very long time after the start of the pandemic, so the vaccines were not designed for this strain. Moreover, it was much less severe. This can explain why there was no rush to design new vaccines against this

strain. In conclusion, the 60% vaccine efficiency against infection retained for the Flu and COVID-19 is reasonable.

Concerning reduction of transmissibility after previous contamination, for COVID-19, a study was performed by Lancet and estimated that prior infection led to a 93% lower incidence of new infection compared to participants that had not been previously infected. Another study [Sheehan et al. \(2021\)](#) showed that protection offered from prior infection was 81.8% and against symptomatic infection was 84.5%.

In summary, **the model assumes a 60% vaccination effectiveness against infection as well as 60% immunity ratio after a prior infection.**

5.3.3 Reduction on Lethality from Vaccination or Previous Infection

Lethality Reduction Effect, $\mu(t - d_{max})$, is used to quantify the impact on the average population lethality accounting for both partially immune (those who are vaccinated or suffered a previous infection, but did not gain full immunity) and non-immune Susceptible. In this context, for each partially immune individual, the Reverse Lethality Reduction Factor, denoted as $(1 - LR)$, is employed.

According to the systematic review from [Ferdinands et al. \(2021\)](#), adults with influenza-associated hospitalization, vaccinated patients had 31% reduced risk of death compared with unvaccinated patients. For COVID-19, the vaccination reduction effect against infection was 89.1% whereas it was 99.0% against death, according to a literature review from [Zheng et al. \(2022\)](#). as of the date of 15th Oct. 2021. This leads to a lethality reduction factor of

$$LR = 1 - (1 - 99\%)/(1 - 89.1\%) = 91\%.$$

Further comprehensive studies including different vaccines towards different variant types are summarized by the Institute for Health Metrics and Evaluation (IHME) and shown in Table 5.11. The probability of avoiding severe infection (a proxy for death) when infected can be computed in a similar way as above for the flu. It leads to a lethality reduction factor of at least $(1 - (1 - 97\%)/(1 - 92\%)) = 63\%$ for Moderna, and $(1 - (1 - 95\%)/(1 - 86\%)) = 64\%$ for Pfizer, except for the Omicron virus, which, as described in the previous section, is not representative of the efficiency of vaccines (appeared after

the vaccines, less deadly so no new vaccines produced).

Although the COVID-19 pandemic gives a more realistic case study (vaccines were designed after the virus strain was known, as expected in a major pandemic) and shows a Lethality reduction factor above 60%. **The model sets the partially immune individual's Lethality reduction factor, namely LR , at 30% (hence $(1 - Lr)$ is set at 70%), to be in line with yearly flu.**

As previously when assessing reduction of transmissibility, we assume that recovery from illness decreases the future mortality risk in the same level as a vaccine. This aligns with the principle of the digital EU COVID-19 certificate.

6

Model Simulation

Pandemic modeling requires sophisticated approaches to capture the complex dynamics of disease spread and its impact over multiple years. The purpose of model simulation is to generate various pandemic scenarios from the initial outbreak (day 0) up to three years (day 1095), allowing for a comprehensive exploration of potential outcomes under different conditions and initial parameters of each outbreak virus. This approach enables the estimation of distribution for the mortality impact, or death shock, associated with pandemic events. By simulating a wide range of scenarios, it becomes possible to analyze the variability in death rates and to identify factors that may contribute to higher or lower mortality outcomes in future pandemics.

The simulation tracks multiple compartments including susceptible, infected, immune, and deceased populations, while incorporating time-varying transmission rates (effective R_t). A key component of this framework is the interaction between three stochastic parameters:

- The Basic Reproduction Number (R_0)

- Baseline Lethality Rate (L_m)
- The virus type which combines duration profile of infectiousness and the shape of age-specific factors.

Historical combinations of the virus type with Duration Profile of Infectiousness ($f(d)_{Influenza}, f(d)_{Covid}$) and the shape of Age-specific Factor (U, W, J-shape) exist with probability determined by occurrence frequency:

- Influenza with U-shape curve, denoted as ($f(d)_{Influenza}$, U-shape) of probability $\frac{4}{6}$ (4 pandemics: 1889, 1957, 1968, 2009)
- Influenza with W-shape curve, denoted as ($f(d)_{Influenza}$, W-shape) of probability $\frac{1}{6}$ (1 pandemic: 1918)
- COVID-19 with J-shape curve, denoted as ($f(d)_{Covid}$, J-shape) of probability $\frac{1}{6}$ (1 pandemic: 2020)

In this chapter, the Quasi-Monte Carlo (QMC) Method is used to simulate different scenarios with the distribution assumptions, then we compute the 99.5% quantile, $Q_{99.5\%}$, for the CAT pandemic mortality shock.

6.1 Quasi-Monte Carlo

6.1.1 Main Principle

The Quasi-Monte Carlo (QMC) method is a deterministic variation of the traditional Monte Carlo (MC) simulation approach. While the standard Monte Carlo method relies on pseudo-random sampling to approximate expectations, this stochastic nature can lead to high variance and slower convergence rates, typically of order $\mathcal{O}(N^{-1/2})$ for N samples. In contrast, the QMC method employs low-discrepancy sequences that more uniformly cover the sample space, improving convergence to approximately $\mathcal{O}\left(\frac{(\log N)^d}{N}\right)$ in d dimensions (see in [Dick & Pillichshammer \(2010\)](#)).

6.1.2 Overview of Implementation Steps

We briefly recall the inverse probability method, which is used to generate samples from a specified distribution. This serves as a foundation for the implementation steps that follow.

Suppose we have n independent random variables drawn from a uniform distribution:

$$U_1, U_2, \dots, U_n \sim \text{i.i.d. Uniform}(0, 1)$$

Then, we can obtain n independent samples from the distribution F_X by applying the inverse CDF:

$$X_i = F_X^{-1}(U_i), \quad i = 1, \dots, n$$

The resulting sample:

$$X_1 = F_X^{-1}(U_1), \quad X_2 = F_X^{-1}(U_2), \quad \dots, \quad X_n = F_X^{-1}(U_n)$$

are i.i.d. random variables from the distribution with CDF F_X .

The implementation of QMC for simulating mortality scenarios involves the following structured steps:

1. Generation of Low-Discrepancy Sequences:

Define deterministic, uniformly spaced probability levels over $[0, 1]$ for key stochastic parameters as input variables for the QMC simulation:

- For the basic reproduction number R_0 , define n probabilities:

$$u_n^{(i)} = \frac{2i-1}{2n}, \quad i = 1, 2, \dots, n$$

- For the lethality rate \bar{L} , define m probabilities:

$$u_m^{(j)} = \frac{2j-1}{2m}, \quad j = 1, 2, \dots, m$$

These correspond to the midpoints of n and m evenly partitioned intervals over $[0, 1]$.

2. Transformation via Inverse Cumulative Distribution Functions (CDFs):

Each probability is then transformed to the quantiles using the inverse CDF (quantile function) of the corresponding input variables:

$$R_0^{(i)} = F_{R_0}^{-1}(u_n^{(i)}), \quad \bar{L}^{(j)} = F_{\bar{L}}^{-1}(u_m^{(j)}),$$

where $F_{R_0}^{-1}$ and $F_{\bar{L}}^{-1}$ are the inverse distribution functions (recall that we have lognormal distribution for R_0 and exponential distribution for \bar{L}) chosen to model each variable.

3. Construction of Scenario Matrix and Mortality Estimation:

Formulate the cross-product of the variable sets to simulate multiple mortality scenarios:

$$\left\{ (R_0^{(i)}, \bar{L}^{(j)}, Vtype_k) : i = 1, \dots, n; j = 1, \dots, m; k = 1, 2, 3 \right\}$$

where $Vtype$ is the virus type that combines the duration profile of infectiousness and the shape of age-specific factor, $[f(d), a_{\text{entity, shape}}]$.

This results in a total of $n \times m \times 3$ variable sets. Each combination represents a unique simulation case to compute the projected mortality rate under a given pandemic scenario.

6.1.3 Define The Relationship Between The Variables

The relationship between the transmissibility, lethality and virus type of a pandemic is complex and the 3 parameters are not necessarily directly correlated. A virus with high transmissibility can spread widely without needing to be highly lethal, while a very lethal virus might reduce its transmission by incapacitating or killing its hosts quickly, limiting its spread.

For example, during the COVID-19 pandemic, the SARS-CoV-2 virus showed increasing transmissibility, especially with variants like Omicron, but did not necessarily become more lethal. High transmissibility often means the virus can spread efficiently, even from asymptomatic or mildly ill individuals,

as was the case with COVID-19. This allows it to infect many people without requiring severe illness in every case.

On the other hand, viruses that are too lethal, such as SARS (2002-2003), often struggle to sustain large outbreaks because they kill or incapacitate hosts too quickly, which limits opportunities for transmission. This is why many highly lethal viruses like Ebola tend to cause more localized outbreaks.

The evolution of viruses often follows a balance between transmissibility and lethality. This virulence–transmission trade-off hypothesis was developed by [Anderson & May \(1982\)](#), which indicates that it is difficult for the two to be high simultaneously. Viruses that are highly lethal may reduce their own spread because they incapacitate or kill hosts before they can effectively transmit the virus. And COVID-19 was observed partially following this trade-off.

Nevertheless, for the simplicity, in our CAT Pandemic model we assume that the three parameters transmissibility, lethality and virus type of a pandemic are independent, which gives us a more prudent model (include extreme scenarios with high lethality and high transmissibility at the same time to produce more deaths) than following the virulence-transmission trade-off¹.

Therefore, the probability of each scenario is the product of the probability of the three variables in the corresponding set, $(R_o^{(i)}, \bar{L}^{(j)}, Vtype_k)$.

Finally, the outputs are sorted in ascending order and we calculate the cumulative probability of the excess mortality rate for each entity/country, which is a discrete distribution of $n*m*3$ points.

6.2 Simulation Convergence

Selecting the sequence length for the two random parameters is essential to determining the total number of scenarios.

The simulation process is performed in R codes. Additional tests are performed to select the best size of the two sequences among these criteria:

- **Convergence of the simulation:** The simulation should converge to a stable (and accurate) result. This means that the output should not fluctuate significantly when the number of scenarios

¹Future research could investigate the virulence–transmission trade-off and the potential dependence between relevant epidemiological variables, as these relationships may evolve over time and differ from those observed during earlier studies, such as the work of [Anderson & May \(1982\)](#).

increases or decreases slightly.

- **Computational time:** The simulation should be efficient and not take too long to run. Therefore, the number of scenarios should not be so large that it causes the simulation to become too computationally intensive.

With the pandemic frequency of 4% (one per 25 years), the 87.5% quantile of severity part is transformed to the final 99.5% quantile of Frequency-Severity model as shown in Formula 3.1 from the previous chapter.

Ultimately, to achieve an optimal balance between computational efficiency and convergence accuracy, we selected 60 sequences for each key parameter, the basic reproduction number (R_0) and baseline lethality. Including the three virus type scenarios, this approach yields a total of 10'800 scenarios. Convergence test results are presented in the Appendix B.

Part V

Model Output Analysis

7

Statistical Analysis of Simulated Pandemic Mortality Rates with Extreme Value Theory

The analysis of the simulated pandemic mortality rates presents unique challenges due to the heavy-tailed and asymmetric nature of the data. The simulation study in the previous chapter, comprising over 10,000 scenarios, reveals characteristics that cannot be adequately captured by traditional statistical distributions. This chapter presents a sophisticated approach to modeling these extreme events using a hybrid Generalized Pareto Distribution (LN-E-GPD) in the [Dacorogna et al. \(2023\)](#) framework. This addresses the challenge of achieving automatically global optimization instead of local one that arises when relying solely on gradient-based methods.

Our input to improve the optimization method is to introduce a genetic algorithm (GA) as a preliminary step, then combine it with the Levenberg Marquardt (LM) method used in [Dacorogna et al. \(2018\)](#). This GA method facilitates a more robust optimization process compared to the pure LM method, which relies

on manually selected initial parameters (see in [Dacorogna et al. \(2023\)](#)).

Before getting into more advanced models, we recall that Extreme Value Theory (EVT) provides a robust mathematical foundation for modeling rare, high-impact events, making it suitable for analyzing extreme mortality rates in pandemics. EVT aims to understand the behavior of extreme deviations from average values, particularly in heavy-tailed data settings, as observed in extreme pandemic scenarios.

We refer to Appendix E for a brief survey on univariate EVT (see in [Kratz \(2019\)](#)) and the Peaks-Over-Threshold (POT) Approach.

For our study, we use an unsupervised modeling method on Generalized Pareto Distribution (GPD), which will be introduced in next section, instead of manually choosing the threshold as the POT approach.

7.1 An Unsupervised Modelling Method – Hybrid Generalized Pareto Distribution (LN-E-GPD)

7.1.1 Introduction of Unsupervised Modelling Method

A key objective of Extreme Value Theory (EVT) is to estimate the tail of a distribution, a task closely associated with determining an appropriate threshold from which a Generalized Pareto Distribution (GPD) can be modeled. Estimation methods for EVT can be divided into two main categories. The first includes traditional methods employing the Peak Over Threshold (POT) technique, in which the threshold is selected graphically—often relying on subjective visual inspection. The second category consists of unsupervised algorithmic methods, where thresholds are determined through parameter calibration.

The hybrid model approach implements an unsupervised method that automatically determines the ”tail” threshold. The main concept of the unsupervised method is briefly described here (with details in [Debbabi & Kratz \(2014\)](#) and [Debbabi et al. \(2016\)](#), with overviews in [Kratz \(2019\)](#) and [Dacorogna et al. \(2023\)](#)). This method was developed for fitting multi-component data with heavy tails, aiming to automatically determine the threshold (that we name tail-threshold), denoted by u_2 , above which the Generalized Pareto Distribution (GPD) models the tail, as well as the tail index. Unlike traditional Extreme Value Theory (EVT) approaches, which use only tail data and make defining u_2 less direct,

this method utilizes all data to establish a model for the entire distribution, which can be seen as an advantage.

The iterative algorithm diverges from standard statistical methods like maximum likelihood or method of moments, as it relies on solving a set of non-linear least squares problems using the Levenberg-Marquardt (LM) technique (Levenberg (1944)), which integrates elements of both Gauss-Newton and gradient descent methods to find the desired minimum.

Since 2014, the method has been refined through testing on simulated and real data, such as cyber data, to enhance its accuracy and applicability. The algorithm calibrates a general hybrid model by separately modeling the mean and extreme behaviors with specific limiting distributions, supported by asymptotic theorems. A key improvement was the addition of an exponential "bridge" between the main and extreme components (assuming continuity in the hybrid distribution) to better capture extreme behavior with the GPD.

This bridge prevents the GPD from fitting intermediate statistics, focusing instead on the largest values. It also enables automatic threshold selection for extreme observations based on the Pickands-Balkema-de Haan theorem. The resulting model is flexible, fitting a wide range of heavy-tailed, non-negative data without needing dataset-specific adjustments.

7.1.2 Defining the Hybrid Generalized Pareto Distribution

Our study utilizes the refined hybrid model by Dacorogna et al. (2023), denoted as LN-E-GPD (Lognormal-Exponential-Generalized Pareto Distribution) to better capture the characteristics for asymmetric positive data. It is characterized by its probability density function (pdf) h expressed as:

$$h(x; \theta) = \gamma_1 f(x; \mu, \sigma) \mathbf{1}_{(x \leq u_1)} + \gamma_2 e(x; \lambda) \mathbf{1}_{(u_1 \leq x \leq u_2)} + \gamma_3 g(x - u_2; \xi, \beta) \mathbf{1}_{(x \geq u_2)}$$

where $f(\cdot; \mu, \sigma)$ denotes the lognormal (LN) probability density function (pdf) with mean $\mu \in \mathbb{R}$ and standard deviation $\sigma > 0$, defined for all $x > 0$ by

$$f(x; \mu, \sigma) = \frac{1}{x\sigma\sqrt{2\pi}} e^{-\frac{(\log x - \mu)^2}{2\sigma^2}},$$

e : the exponential pdf with intensity λ (defined on \mathbb{R}^+) by

$$e(x; \lambda) = \lambda \exp(-\lambda x),$$

g : the pdf of the GPD defined with tail index $\xi > 0$ (heavy-tail condition) and scale parameter $\beta > 0$, while $\gamma_i, i \in \{1, 2, 3\}$, are the non-negative weights (for h to be a pdf) with $\gamma_1 + \gamma_2 + \gamma_3 \geq 1$, and u_1 and u_2 are the two junction points between the components, with $u_1 \leq u_2$.

The relations between the parameters of the model are defined using the heavy-tailed framework and the C^1 assumption on the pdf that imposes smooth transitions from one component to another to reduce the number of parameters. For heavy-tailed data, we have $\xi > 0$ and the asymptotic (for high threshold) relation $\beta = \xi u_2$, which we are going to use in the algorithm. The C^1 assumption is translated by $\gamma_1 f(u_1; \mu, \sigma) = \gamma_2 e(u_1; \lambda)$, $\gamma_2 e(u_2; \lambda) = \gamma_3 g(0; \xi, \beta)$, and similar equalities when considering the derivative of f , e , and g , respectively. Therefore, after some computation, there is:

$$\begin{cases} \beta = \xi u_2; & \lambda = \frac{1+\xi}{\beta}; & \gamma_2 = \left[\xi e^{-\lambda u_2} + \left(1 + \lambda \frac{F(u_1; \mu, \sigma)}{f(u_1; \mu, \sigma)} \right) e^{-\lambda u_1} \right]^{-1}; \\ \lambda \sigma^2 u_1 - \log u_1 = \sigma^2 - \mu; \\ \gamma_1 = \gamma_2 \frac{e(u_1; \lambda)}{f(u_1; \mu, \sigma)}; & \gamma_3 = \beta \gamma_2 e(u_2; \lambda). \end{cases} \quad (7.1)$$

These relations help reduce the size of the vector of parameters to be estimated from 10 to 4, namely $[\mu, \sigma, u_2, \xi]$. Then, the iterative algorithm for the LN-E-GPD model is run to estimate those 4 parameters by minimizing the distance between the empirical cumulative distribution function (CDF) and the CDF generated by the model parameters, denoted H :

$$H(x; \theta) = \begin{cases} \gamma_1 F(x; \mu, \sigma) & \text{if } x \leq u_1, \\ \gamma_1 F(u_1; \mu, \sigma) + \gamma_2 \left(e^{-\lambda u_1} - e^{-\lambda x} \right) & \text{if } u_1 < x \leq u_2, \\ 1 - \gamma_3 \left(1 + \xi \frac{(x - u_2)}{\beta} \right)^{-1/\xi} & \text{if } x \geq u_2. \end{cases}$$

In this paper, the model parameters are estimated through an iterative algorithm adapted from the method developed for the original hybrid model (G-E-GPD, with Gaussian replacing the lognormal distribution, as detailed in [Debbabi et al. \(2016\)](#)), with its convergence examined both analytically and numerically. The main procedure follows the principles outlined in [Kratz \(2019\)](#), Section 2.4.1, where the initial parameters of the body of the distribution and the threshold u_2 are set. This initialization

enables the estimation of the tail index in the first iteration. Subsequently, the tail index is held constant while the remaining parameters are estimated. This iterative process—alternating between body and tail estimation—is performed using the Levenberg-Marquardt (LM) technique to jointly minimize two distance metrics: one comparing the empirical and model distributions across the entire dataset, and the other focusing on the tail, until convergence criteria are met.

While this fundamental approach remains relevant to the proposed model, a key challenge arises in the selection of initial parameters, particularly when choosing between modeling the bulk data with a Gaussian or a lognormal distribution. In the G-E-GPD model, initializing the Gaussian mean at the mode of the distribution is effective for achieving convergence. However, this strategy is not applicable for the lognormal distribution. Additionally, the Levenberg-Marquardt (LM) technique is prone to falling into local minima, further enhancing the importance of initialization to ensure robust optimization.

7.2 A New Optimization Algorithm for Hybrid GPD

Our study focuses on using the Genetic Algorithm (GA) to address the initialization challenges encountered in calibrating the LN-E-GPD model. GA method is rooted in the broader field of metaheuristic optimization, which emerged as an alternative to deterministic optimization methods like gradient descent and Newton’s methods.

7.2.1 Overview of Genetic Algorithm (GA)

Genetic Algorithms, inspired by the principles of natural selection and genetic evolution, became a promising approach for tackling these challenges. Originating from the work of [Holland \(1992\)](#), GA was initially applied to optimization and search problems where traditional methods struggled. By simulating a “population” of solutions that evolve over generations, GA can explore a much broader parameter space, which is particularly beneficial in complex, multimodal functions like those in the LN-E-GPD model.

The application of GA method to statistical model initialization, particularly in hybrid and heavy-tailed models like the LN-E-GPD, leverages the advantage of exploring broader parameter space. With its ability to find near-optimal solutions without requiring gradients, GA offers a robust alternative for

establishing reliable starting values for parameters that are otherwise hard to estimate. Once initialized by GA, the model can then be fine-tuned using LM, combining GA's global search capability with the precision of gradient-based optimization in local refinement.

In this context, GA method acts as an essential pre-processing step, enabling complex hybrid models to be effectively calibrated, extending their application across datasets where traditional optimization alone may fail to converge accurately if not examining carefully (manually) the initialization step.

To address the initialization challenges inherent to calibrating the LN-E-GPD model, the GA method is used to systematically optimize starting parameter values before applying the Levenberg-Marquardt (LM) technique for final parameter estimation. By leveraging GA's exploratory capabilities, a more robust initial parameter set can be generated, minimizing the chances of premature convergence to local minima.

This type of algorithm aims to find optima by manipulating a constant-sized population. The population consists of candidate points called "chromosomes." Each chromosome is made up of "genes," representing a potential solution to the optimization problem.

The fixed population size creates a competitive environment among chromosomes. Thus, with each iteration of the algorithm, a new population of chromosomes is generated, known as a new "generation." Each generation contains the same number of chromosomes and undergoes a form of natural selection: only the chromosomes best suited to their environment survive. Over generations, the chromosomes tend to converge toward the optimum of the objective function.

The GA optimization process has 4 major components:

- **Initialization-** This is the process of generating the initial population of potential solutions. A diverse initial population ensures a broad exploration of the solution space, helping the GA avoid local optima and enhancing the chance of finding a global optimum.
- **Selection-** Choose individuals from the current population based on their fitness to create the next generation. This step drives the algorithm toward better solutions by giving higher chances of reproduction to individuals with better fitness, balancing the exploration and exploitation of the search space.
- **Crossover-** In crossover, pairs of selected individuals combine their genetic material to produce

offspring. By mixing traits from two solutions, crossover creates diversity and allows the algorithm to explore new solutions that might inherit beneficial features from both parents.

- **Mutation-** Mutation introduces random changes to individual solutions in the population. This step helps maintain diversity within the population, preventing premature convergence by allowing the algorithm to explore new regions of the search space.

After generating the initial population, the algorithm iterates through the three other components, Selection, Crossover and Mutation, to update new populations for evaluation in the next round. These cycles continue until the algorithm meets one or more stopping criteria: reaching the maximum number of generations, achieving a convergence threshold, exceeding a specified time limit, or observing no improvement over a predefined number of generations.

7.2.2 Key Configuration for Each Component in GA

In this section, we discuss the various components of the Genetic Algorithm (GA) used for real-value optimization in this thesis. GA's 4 major components, population initialization, selection, crossover, and mutation, can significantly impact optimization performance and require careful consideration. The methods available for each component and some seminal references are listed in Tables 7.1, 7.2, 7.3 and 7.4.

Method	Description
Random Sampling (Holland (1992))	Population initialized with uniformly random values within bounds.
Latin Hypercube Sampling (LHS) (McKay et al. (2000))	Ensures diverse coverage of the search space.

Table 7.1: GA Population Initialization Methods

Method	Description
Linear ranking selection (Baker (2014))	uses rank-based probabilities for selection
Non-linear ranking selection	introduces non-linear selection pressure
Roulette wheel selection (Holland (1992))	probability proportional to fitness
Tournament selection (Goldberg & Deb (1991))	selects the best from a tournament of k individuals
Least-squares selection	based on minimizing the least square error
Sigma scaling selection (Rooker (1991))	adjusts fitness by the standard deviation

Table 7.2: GA Selection components

Method	Description
Single-point crossover (Deb et al. (1995))	combines two parents at a single point
Weighted average crossover	averages parent values with weights
Linear arithmetic crossover (Michalewicz (1996))	combines parents linearly
Blend crossover (Eshelman & Schaffer (1993))	combines parents based on a specified mid point
Laplace-based crossover (Yao et al. (1999))	combines parents with Laplace distribution

Table 7.3: GA Crossover components

Method	Description
Random arithmetic mutation (Holland (1992))	uniform random mutation within variable bounds
Non-uniform mutation (Michalewicz (1996))	decreasing randomness over generations
Random replace mutation (Goldberg & Deb (1991))	Random replace of selected genes within bounds
Power-based mutation	controlled by exponent parameter

Table 7.4: GA Mutation components

For this study, we focus on components that require minimal fine-tuning to ensure robustness and ease of implementation. **This is why we selected two methods for each component—LHS and random sample for population initialization, linear ranking and roulette wheel for selection, blend and single point for crossover, random replace and random arithmetic for mutation—resulting in a total of 16 combinations.** These sets were then compared to evaluate their performance.

The general steps of GA method are defined below:

Model Parameters and Objective Function

For the LN-E-GPD model, the parameter set includes elements $[\mu, \sigma, u_2, \xi]$ for both the body (lognormal) and the tail (GPD) components (the parameters for the exponential bridge distribution are implied by 7.1). The objective function for GA is designed to minimize the differences between the empirical data and the theoretical model distribution, focusing especially on aligning both the entire distribution and the tail component. This is achieved by comparing the empirical cumulative distribution function (CDF) with the CDF generated by the model.

Two Methods of Generating Initial Population

The initialization of the population is a critical step in genetic algorithms, as it sets the foundation for exploring the solution space effectively. In this study, two distinct population initialization methods were implemented: **Random sampling**, and **Latin Hypercube Sampling (LHS)**. Random Sampling

ensures a simple and random selection of samples across the input space, while LHS enhances this diversity by systematically stratifying the input space instead of randomly selecting, thereby improving the optimization performance through more efficient exploration of the input variable space.

- **Latin Hypercube Sampling (LHS):** Consider generating a four-variable set, represented as

$$\{\mathbf{X}_1, \mathbf{X}_2, \mathbf{X}_3, \mathbf{X}_4\}$$

Divide Each Variable's Range: For a given variable X_i , with a defined range of $[a_i, b_i]$, the intervals divided from this range can be defined as:

$$\text{Interval}_j^i = \left[a_i + \frac{(j-1)(b_i - a_i)}{N}, a_i + \frac{j(b_i - a_i)}{N} \right], \quad j = 1, 2, \dots, N$$

Sampling: For each variable X_i , one sample is drawn from each interval. Let $u_{i,j}$ be a random sample drawn uniformly from the Interval_j^i :

$$x_{i,j} = a_i + \frac{(j-0.5)(b_i - a_i)}{N} + (b_i - a_i) \cdot u_{i,j}, \quad u_{i,j} \sim U(0, 1)$$

Constructing the Sample Matrix: After sampling, the samples for each variable are combined into a matrix where each row represents a unique combination of samples across all variables. The resulting sample vectors are:

$$\{\mathbf{x}_1, \mathbf{x}_2, \dots, \mathbf{x}_M\}$$

where M is the total number of sampled points, and each \mathbf{x}_k is a vector of the sampled values from all four variables: $\mathbf{x}_k = (x_{1,k}, x_{2,k}, x_{3,k}, x_{4,k})$

This structure improves algorithm efficiency by offering a diverse and representative starting population, increasing the likelihood of finding a global optimum and often leading to faster convergence.

- **Random Sampling:** Random sampling is one of the simplest and most commonly used techniques for population initialization in genetic algorithms. This method generates a random (uniform) pop-

ulation of real values within a specified range, denoted as $[min_{value}, max_{value}]$. Each individual in the population is created independently, allowing for broad exploration of potential solutions without any correlation between the selected variables.

In random sampling, the values for each input variable are drawn uniformly from their respective ranges. For instance, if we have 4 variables X_1, X_2, X_3, X_4 , we draw samples from distribution of X_i as follows:

$$X_i \sim U(min_{value}, max_{value}) \quad \text{for } i = 1, 2, \dots, 4,$$

where $U(a, b)$ represents the uniform distribution over the interval $[a, b]$. This approach ensures that all values within the defined range are equally likely to be selected.

While random sampling is effective in generating an initial population, it may lead to uneven sampling of the solution space. This could result in clusters of individuals, potentially leaving other regions underrepresented. Therefore, while this method is straightforward to implement, it may not guarantee the same level of diversity as more structured methods like LHS, especially in high-dimensional spaces. Consequently, the choice between random sampling and LHS should depend on the specific requirements of the optimization problem at hand.

Two Methods of Selection

The selection process in a Genetic Algorithm is critical for guiding the population toward optimal solutions by favoring individuals with higher fitness values. For this study, two selection methods were implemented: **Linear Rank Selection** and **Roulette Wheel Selection** due to their relative ease of implementation and representativeness of the six methods (ranking method and probability method). Each method differs in how it assigns reproductive opportunities, aiming to balance exploration and exploitation in the solution space.

- **Linear Ranking Selection:** This method assigns selection probabilities based on the rank of individuals within the population, rather than their raw fitness scores. First, the population is sorted from the best to worst-performing individuals. Each individual is then assigned a rank r (where $r = 1$ for the best and $r = N$ for the worst in a population of N individuals).

The probability of selecting an individual with rank r , denoted as $p(r)$, is computed as:

$$p(r) = \frac{2}{N} * \left(s - (s - 1) * \frac{r - 1}{N - 1} \right)$$

where s is a selective pressure variable (with $1 < s \leq 2$). The choice of s controls the probability skew toward better-ranked individuals, with higher values of s increasing selection pressure.

Linear Rank Selection has the advantage of preventing highly fit individuals from dominating too early, thus maintaining diversity in the population.

- **Roulette Wheel Selection:** This is also known as fitness-proportionate selection, which assigns selection probabilities directly proportional to individual fitness values. Each individual's probability of being selected, p_i , is defined as:

$$p_i = \frac{f_i}{\sum_{j=1}^N f_j}$$

where f_i represents the fitness of individual i , and N the total population size.

In practice, the selection process is visualized as a “roulette wheel” where each individual occupies a segment of the wheel proportionate to its fitness. Higher-fitness individuals thus occupy larger segments, increasing their likelihood of selection. This method is effective in rewarding highly fit individuals but may lead to premature convergence if high-fitness individuals dominate too quickly.

Both methods provide distinct advantages: Linear Rank Selection maintains population diversity by limiting early domination, while Roulette Wheel Selection encourages rapid improvement by amplifying the influence of fitter individuals.

Two Methods of Crossover

Crossover is a fundamental genetic algorithm (GA) operator that combines genetic material from two parent solutions to create offspring. This process facilitates the exchange of information between in-

dividuals, allowing beneficial traits to propagate through the population. In this study, two crossover methods are employed: **Blend Crossover** and **Single-Point Crossover** because they offer straightforward implementation and fine-tuning while effectively encapsulating the core principles of crossover operations.

- **Blend Crossover:** The Blend Crossover (BLX Crossover) method is designed for continuous variables, allowing offspring genes to inherit values within a range influenced by the parent genes. This method enhances exploration by introducing controlled randomness.

Let the parents be represented as two vectors:

$$\mathbf{p}^{(1)} = (p_1^{(1)}, p_2^{(1)}, \dots, p_n^{(1)}) \quad \text{and} \quad \mathbf{p}^{(2)} = (p_1^{(2)}, p_2^{(2)}, \dots, p_n^{(2)}).$$

The offspring genes are generated using the formula:

$$p'_j = p_j^{(1)} + r \cdot (p_j^{(2)} - p_j^{(1)})$$

where:

- p'_j is the gene of the offspring at position j ;
- r is a random number sampled from a uniform distribution within $[-\alpha, 1 + \alpha]$, where α is a user-defined parameter that controls the extrapolation beyond the parents' range.

The BLX crossover is advantageous because it helps:

- **Encourage Diversity:** The offspring can explore regions beyond the direct interpolation of the parent genes;
 - **Control Variability:** The parameter α allows balancing between exploration and exploitation.
- **Single-Point Crossover:** This method is a classic crossover technique widely used in genetic algorithms, particularly for binary and discrete representations. It selects a single crossover point and exchanges genetic material between two parents at that point.

Given two parent solutions:

$$\mathbf{p}^{(1)} = (p_1^{(1)}, p_2^{(1)}, \dots, p_n^{(1)}) \quad \text{and} \quad \mathbf{p}^{(2)} = (p_1^{(2)}, p_2^{(2)}, \dots, p_n^{(2)})$$

The crossover process is performed as follows:

- Select a random crossover point c in the range $[1, n - 1]$.
- Create offspring by swapping genetic material after this point:

$$\mathbf{p}' = (p_1^{(1)}, p_2^{(1)}, \dots, p_c^{(1)}, p_{c+1}^{(2)}, \dots, p_n^{(2)})$$

$$\mathbf{q}' = (p_1^{(2)}, p_2^{(2)}, \dots, p_c^{(2)}, p_{c+1}^{(1)}, \dots, p_n^{(1)})$$

Single-Point Crossover is beneficial because:

- **Maintains Structure:** Large portions of the parents' genetic material are retained, ensuring meaningful inheritance.
- **Computational Efficiency:** The method is simple and computationally inexpensive.

Two Methods of Mutation

The mutation process in genetic algorithms introduces variability into the population by altering the genes of individual solutions. This mechanism helps to maintain genetic diversity, preventing premature convergence and enabling the exploration of new solutions. In this study, two mutation methods are employed: **Random Arithmetic Mutation** and **Random Replace Mutation**. We choose the two methods because they provide a balance between simplicity and effectiveness in introducing diversity into the population. Arithmetic Mutation allows for smooth variations in the parameter values, facilitating gradual exploration of the search space, while Random Replace Mutation introduces significant changes by replacing individuals with new random values, ensuring a broad exploration of potential solutions.

- **Random Arithmetic Mutation:** This method modifies individual genes of a solution by adding a random value, which introduces variability while preserving the overall structure of the solution.

Let $\mathbf{p} = (p_1, p_2, \dots, p_n)$ be an individual solution with n genes. The mutation of gene j is defined mathematically as follows:

$$p'_j = p_j + \mu \cdot \delta$$

where p'_j is the mutated gene j , μ is a mutation factor, typically set between 0 and 1, δ is a random number drawn from a normal distribution $\mathcal{N}(0, \sigma)$, with σ is the standard deviation controlling the mutation's scale.

The mutation factor μ adjusts how much influence the random value δ has on the original gene, allowing for fine-tuning of the mutation's impact.

Random Arithmetic Mutation is beneficial because it allows for:

- **Continuous Exploration:** It allows for small adjustments to the genes, promoting gradual exploration of the solution space;
 - **Preserves Feasibility:** By modifying genes rather than replacing them entirely, it is more likely to maintain feasible solutions.
- **Random Replace Mutation:** This method is used primarily for permutations or ordered sets, where two genes within an individual solution are randomly selected and swapped. This technique introduces diversity by changing the order of genes, which can significantly alter the individual's traits.

Let $\mathbf{p} = (p_1, p_2, \dots, p_n)$ be an individual solution. The random replace Mutation can be expressed as follows:

- Select two distinct indices i and j uniformly at random from $\{1, 2, \dots, n\}$.
- Swap the genes at these indices:

$$p'_i = p_j$$

$$p'_j = p_i$$

where p'_i and p'_j are the mutated genes after the swap.

Random Replace Mutation is advantageous because:

- **Enhances Diversity:** By changing the order of genes, it creates entirely new configurations that may lead to better solutions;
- **Simple Implementation:** The method is straightforward to implement and computationally efficient, making it suitable for large populations.

Boundary Settings

The lower and upper boundaries of the parameters (ξ, μ, σ , and u_2) for the Genetic Algorithm (GA) method and the Latin Hypercube Sampling (LHS) initial population were set as follows:

$$\text{lower} = (0.01, \text{round}(\min(\log(\text{data}))), 0, 0)$$

$$\text{upper} = \left(1, \text{round}(\max(\log(X))), 5\sqrt{\log(1 + CV^2)}, \text{quantile}(X, 0.95)\right)$$

where:

- X denotes the data sample to fit with.
- CV is the coefficient of variation of data sample (computed by standard deviation over the mean, $CV = \frac{\sqrt{(X-\bar{X})^2}}{\bar{X}}$).
- $\xi \in [0.01; 1]$: The shape parameter ξ is constrained between 0.01 and 1 to avoid too heavy distributions with no finite mean, since the pandemic generally has a finite mean, consistent with the findings for instance of Corral et al. (see [Corral \(2021\)](#))¹.
- $\mu \in [\text{round}(\min(\log(\text{data}))), \text{round}(\max(\log(\text{data})))]$: The location parameter μ is set between the minimum and maximum log-transformed values of the data to ensure it includes the possible μ .
- $sd \in [0; 5 * \sqrt{\log(1 + CV^2)}]$: The scale parameter sd is non-negative and has an upper bound based on the coefficient of variation (CV), ensuring a reasonable range while preventing excessive

¹Further research could be conducted to investigate the upper bound of 2, which may facilitate the calibration of heavy-tailed data, such as that associated with earthquake damages

variance in the model. The factor of 5 is chosen to allow flexibility concerning the heavy tail given by GPD component.

- $u_2 \in [0; \text{quantile}(\text{data}, 0.95)]$: The threshold parameter u_2 is bounded between 0 and the 95% quantile of the data with this upper bound chosen to capture meaningful extreme values while avoiding unrealistic high-end extrapolations².

These boundaries were chosen to ensure numerical stability, prevent overfitting, and allow the GA method (and LHS) to efficiently explore a practical parameter space.

7.2.3 Jackknife Method to Choose Best Configuration Set

To assess the robustness of the various parameter settings employed in this genetic algorithm (GA), a jackknife-like approach was implemented. The goal of this method is to evaluate the stability and consistency of the model's output parameters by iteratively excluding subsets of data and observing the impact on parameter estimates. Robust parameter configurations are those that produce stable results across different subsets, indicating that the chosen settings are not overly sensitive to specific data points or small variations in the dataset.

We also performed Monte Carlo (MC) simulations on the 16 parameter sets of the genetic algorithm (GA) method and conducted hyperparameter study (see Appendix A). This combination allowed us to analyze additional datasets and confirm the parameter sets selected using the Jackknife method, thereby enhancing the variability and robustness of the algorithm's performance.

The analysis was conducted across 16 different combinations of GA parameter settings derived from the following configurations:

- Two initialization methods: Latin Hypercube Sampling (LHS) and random sample population,
- Two selection methods: linear rank and roulette wheel,
- Two crossover methods: blend (BLX) and single point,
- Two mutation methods: random arithmetic and random replace.

²Further research could explore the potential for a higher value for the lower bound, such as $q_{75\%}$, to achieve a narrower range. For the sake of simplicity, our study adopts a lower bound of 0.

These combinations allow for a comprehensive comparison of different GA configurations to determine which setting provides the most reliable outcomes.

For each combination of parameter settings, the following steps were executed to perform the jackknife analysis:

- **Data Exclusion:**

In each run, 10% of the data was randomly excluded, and this process was repeated across ten iterations per parameter configuration. This exclusion method ensures that each subset is unique and allows us to analyze how each configuration performs under slightly altered conditions. By excluding portions of the data, we simulate variations in the dataset, which helps to reveal any dependency on specific data points. This approach is particularly valuable for assessing model stability in pandemic mortality modeling, where data can be highly skewed or sparse at the extremes.

- **Parameter Evaluation:**

After each iteration, the output parameters from the genetic algorithm were recorded. For each parameter combination, the standard deviation and mean of the estimated parameters across the ten runs were calculated. The standard deviation normalized by the mean (i.e., the coefficient of variation) was used as an indicator of volatility for each parameter combination. Lower volatility indicates greater stability and robustness, suggesting that the configuration is less affected by minor variations in the data.

- **Robustness Ranking:**

Each configuration was ranked based on the stability of its output parameters. Configurations with lower coefficients of variation were considered more robust, as they consistently produced similar parameter estimates across different subsets. This ranking process provided a clear comparison, highlighting which combination of initialization, selection, and mutation methods led to the most stable parameter estimates.

The jackknife method not only allows for the identification of the best configuration set in terms of parameter stability but also provides insight into the reliability of the GA as a whole. By rigorously

testing each configuration's sensitivity to data variations, this method ensures that the final chosen configuration will produce robust estimates even when faced with new or slightly different data. In the context of pandemic mortality modeling, where extreme values are particularly impactful, the ability to maintain consistent parameter estimates across varied data samples is crucial for accurate and reliable risk assessment.

7.2.4 Combine Genetic Algorithm with Levenberg-Marquardt Method

Once the Genetic Algorithm (GA) has identified an optimal or near-optimal set of initial parameters, the Levenberg-Marquardt (LM) method is employed to further refine the LN-E-GPD estimates for greater precision.

The Levenberg-Marquardt method is particularly suited for this task, as it combines aspects of both the Gauss-Newton method and gradient descent. This makes it highly effective at minimizing the least-squares error between the empirical cumulative distribution function (CDF) of the observed data and the model's predicted CDF. The LM method adapts between a gradient descent approach, which is beneficial for rough regions of the error surface, and a Gauss-Newton approach, which is more efficient in well-behaved regions, allowing for rapid convergence to a precise local minimum.

Optimization Process with LM

The optimization process with LM is organized into two iterative substeps, as described in [Dacorogna et al. \(2023\)](#), each focusing on different subsets of parameters to ensure a robust and stable solution. This alternating optimization strategy is crucial for complex models, as it allows each parameter group to be refined in a controlled manner, avoiding interdependencies that could lead to instability.

After GA initializes the parameters ξ , μ , σ , and u_2 , the LM algorithm alternates between optimizing (μ, σ, u_2) while keeping ξ fixed, and updating ξ with (μ, σ, u_2) held constant. This iterative approach gradually improves the accuracy of each parameter. The two substeps within this iterative process are given in [Dacorogna et al. \(2023\)](#); we recall them here for completeness:

1. **Optimize (μ, σ, u_2) :**

In this step, with the shape parameter ξ held fixed, LM minimizes the least-squares error between

the model's cumulative distribution function $H(y; \theta)$ and the empirical cumulative distribution function $H_n(y)$. This yields optimized values for (μ, σ, u_2) at each iteration k .

$$\hat{p}^{(k)} \leftarrow \arg \min_{\mu, \sigma, u_2} \left\| H(y; \theta \mid \xi^{(k-1)}) - H_n(y) \right\|_2^2,$$

where $\xi^{(k-1)}$ is fixed, and θ represents the current parameter values (μ, σ, u_2, ξ) in the model. The LM algorithm iteratively adjusts (μ, σ, u_2) to minimize the discrepancy between $H(y; \theta)$ and $H_n(y)$, refining the location, scale, and threshold parameters while keeping the shape parameter ξ constant.

2. Update ξ :

After optimizing (μ, σ, u_2) , the next step is to update the shape parameter ξ while holding the other parameters fixed. This process ensures that the tail behavior, governed by ξ , is accurately fitted to the data.

$$\xi^{(k)} \leftarrow \arg \min_{\xi > 0} \left\| H(y; \theta \mid (\mu, \sigma, u_2)^{(k)}) - H_n(y) \right\|_2^2,$$

where (μ, σ, u_2) are fixed at their values obtained in the preceding optimization step. By isolating ξ in this step, the algorithm can focus on refining the tail characteristics of the distribution without interference from other parameter updates.

Stopping Criteria

The algorithm iterates until it satisfies the following stop condition:

$$\left(\underbrace{d\left(H(y; \theta^{(k)}), H_n(y)\right) < \varepsilon}_{\text{Condition C1}} \quad \text{and} \quad \underbrace{d\left(H(y_{q_\alpha}; \theta^{(k)}), H_n(y_{q_\alpha})\right) < \varepsilon}_{\text{Condition C2}} \right) \quad \text{or} \quad \underbrace{k = k_{\max}}_{\text{Condition C3}}$$

where ε is a positive real that is small enough, y_{q_α} represents the observations above a fixed high quantile q_α of arbitrary order $\alpha \geq 0.8$ associated with H and $d(a, b)$ denotes the distance between a and b , chosen in this study as the Mean Squared Error (MSE); it can be interpreted as the Crámer-von-Mises test of goodness of fit.

To ensure a reliable fit of data not only for the main behavior but also for the tail, we force the algorithm

to stop only when the MSE between the hybrid cdf and the empirical one is small enough, using on one hand all data (Condition C1), and on the other hand only extreme order statistics above q_α (Condition C2) (we chose $\alpha = 0.8$ in our simulations and examples). Otherwise, the algorithm stops when a fixed number k_{\max} of iterations ($k_{\max} = 10^3$ in our simulations and examples) is reached (Condition C3).

Benefits of the Combined GA and LM Approach

Through this hybrid GA and LM optimization process, the model achieves both a globally informed initialization and locally refined parameter estimates, enhancing the overall robustness and accuracy of the model fitting. The GA provides a strong starting point by exploring a wide range of parameter values, reducing the risk of becoming trapped in local minima. LM then fine-tunes these initial estimates to achieve a precise fit to the empirical data, capturing the heavy-tailed and extreme behavior characteristic of pandemic mortality rates.

7.3 Results and Analysis

7.3.1 Results of Jackknife Method

The General Algorithm configuration was computed using the GA package in R by [Scrucca \(2013\)](#), with parameters set to their default values for each specific method to ensure better comparability. See the result of jackknife in Table 7.5.

- Note: Pop = Initial Population, Sel = Selection Method, Mut = Mutation Method, Cross = Crossover Method
- LHS = Latin Hypercube Sampling, rw = roulette wheel, lr = linear rank, rs = random substitute, ra = random add
- SP = Single Point crossover, BLX = Blend crossover
- Lower relative standard deviation values indicate better stability and reliability.

The jackknife results present relative standard deviations across four metrics for 16 different genetic algorithm configurations. Lower values indicate better stability and reliability across jackknife resampling iterations.

Parameter Setting	$\frac{sd_{\xi}}{mean_{\xi}}$	$\frac{sd_{\mu}}{mean_{\mu}}$	$\frac{sd_{\sigma}}{mean_{\sigma}}$	$\frac{sd_{u2}}{mean_{u2}}$
Pop:LHS, Sel:rw, Mut:rs, Cross:SP	8.2%	0.8%	1.4%	8.7%
Pop:LHS, Sel:rw, Mut:ra, Cross:SP	8.9%	1.2%	2.0%	9.4%
Pop:LHS, Sel:rw, Mut:ra, Cross:BLX	9.0%	1.3%	2.0%	9.3%
Pop:LHS, Sel:lr, Mut:rs, Cross:BLX	10.2%	1.3%	2.3%	11.3%
Pop:random, Sel:rw, Mut:rs, Cross:BLX	11.7%	1.2%	1.9%	12.3%
Pop:LHS, Sel:lr, Mut:ra, Cross:SP	12.9%	1.7%	2.6%	17.5%
Pop:random, Sel:lr, Mut:rs, Cross:SP	16.8%	1.3%	2.1%	25.2%
Pop:random, Sel:rw, Mut:rs, Cross:SP	21.4%	1.2%	2.2%	27.5%
Pop:random, Sel:lr, Mut:rs, Cross:BLX	24.7%	1.4%	2.5%	26.5%
Pop:random, Sel:lr, Mut:ra, Cross:BLX	28.6%	1.4%	2.5%	46.6%
Pop:random, Sel:lr, Mut:ra, Cross:SP	28.9%	2.1%	3.5%	38.6%
Pop:LHS, Sel:rw, Mut:rs, Cross:BLX	32.6%	1.8%	2.9%	49.7%
Pop:LHS, Sel:lr, Mut:rs, Cross:SP	32.8%	1.9%	3.3%	54.1%
Pop:LHS, Sel:lr, Mut:ra, Cross:BLX	46.1%	5.0%	12.3%	210.5%
Pop:random, Sel:rw, Mut:ra, Cross:SP	65.0%	4.0%	9.2%	277.5%
Pop:random, Sel:rw, Mut:ra, Cross:BLX	316.3%	2.8%	5.6%	299.1%

Table 7.5: Comparison of different settings with standard deviation to mean ratios

Top Performing Configurations

The most stable configuration is **Pop:LHS, Sel:rw, Mut:rs, Cross:SP** with the lowest overall standard deviation to mean ratios (0.082, 0.008, 0.014, 0.087), followed closely by **Pop:LHS, Sel:rw, Mut:ra, Cross:SP** and **Pop:LHS, Sel:rw, Mut:ra, Cross:BLX**. These results suggest the superiority of Latin Hypercube Sampling and roulette wheel selection in particular.

Component-wise Analysis

1. **Latin Hypercube Sampling (LHS)** consistently outperforms random sampling, with 7 of the top 8 configurations using LHS. This superiority stems from its stratified coverage that ensures uniform parameter space exploration through structured randomness, avoiding the clusters and gaps typical of pure random sampling.
2. **Roulette wheel (rw) selection** Roulette wheel selection appears to be more stable than linear rank selection. When paired with LHS, roulette wheel selection occupies the top 3 positions. Its proportional selection pressure creates a natural balance between exploration and exploitation, preserving valuable genetic diversity while still favoring fitter individuals. The randomness inherent in the

selection process also reduces the risk of premature convergence.

3. **Random replace (rs) mutation** generally produces lower standard deviations than random add (ra), particularly for the ξ metric. By maintaining parameter values within their intended bounds and providing controlled step sizes, it prevents the potential drift and extreme values that can occur with additive mutations, which makes the search less efficient in scenarios where fine adjustments are more beneficial.
4. **Indifferent crossover Method:** Neither Single Point (SP) nor Blend (BLX) crossover demonstrates clear superiority across all configurations. However, SP shows slightly better results when paired with LHS and roulette wheel selection.

Synergistic Effects

The combination of LHS, roulette wheel selection, and random replace mutation creates exceptional stability through complementary approaches to randomness management – LHS distributes it evenly across the parameter space, roulette wheel balances it proportionally to fitness, and random replace contains it within defined parameter bounds.

The metrics show the largest variation across configurations, suggesting the worst-performing configuration, (**Pop:random, Sel:rw, Mut:ra, Cross:BLX**). It shows dramatically higher relative standard deviation for ξ (3.163) compared to all other configurations, indicating a potential instability issue with this specific combination.

Recommendations

Based on the jackknife results:

1. Prefer **LHS** over random sampling for initial population generation
2. Use **roulette wheel** selection rather than linear rank selection
3. Favor **random replace** mutation over random add mutation when stability is critical
4. SP and BLX crossover are indifferent by jackknife result, but we choose **SP** crossover since it is used in the best configuration set

The significant performance gap between the best and worst configurations underscores the importance of proper algorithm parameter tuning when implementing evolutionary optimization methods. The superior performance of the LHS/roulette wheel/random replace combination demonstrates how theoretically sound methodological choices translate directly into empirical stability advantages.

7.3.2 Result of Model Parameter Fitting on CAT Pandemic Model Outputs

The final estimated parameters is obtained from the hybrid Genetic Algorithm (GA) and Levenberg-Marquardt (LM) optimizer. Before applying the combined method to the outputs of the CAT Pandemic model, we evaluated its performance using simulated data, demonstrating the stability and superiority of the combined method in comparison to the Pure LM method (see in Appendix A). For the study on CAT Pandemic model outputs, it analyses the tail index and compares the performance of this hybrid approach against traditional distributions (Normal, Lognormal, and Exponential) and a pure LM method on Hybrid-GPD. Performance is assessed using the Root Mean Square Error (RMSE) for the overall fit and the tail region (values above threshold u_2).

The GA+LM optimization yields the final estimates for the parameters, which is shown in Table 7.6.

Model	μ	σ	γ_1	u_1	λ	γ_2	ξ	u_2	β	γ_3
LN-E-GPD	-6.662	1.883	1.4	0.11%	894.1	0.815	0.559	0.312%	0.00174	0.0780
				q(67.5%)				q(92.1%)		

Table 7.6: Parameter values for the LN-E-GPD model

The tail index, ξ , is a critical parameter for characterizing the extremal behavior of the distribution. A positive value of ξ indicates a heavy-tailed distribution. The GPD fitted above u_2 exhibits a shape parameter $\alpha = 1/\xi = 1.80$, indicating a heavy tail with a finite first moment but no finite variance.

Table 7.7 shows the results from jackknife method, which demonstrates the fit is robust. The choice of the parameters are with relative low variation, 2.0%, 1.5%, 2.7% and 3.2% for ξ , μ , σ and u_2 respectively.

	ξ	μ	σ	u_2
Estimation	0.574	-6.662	1.883	9.301%
95% Confidence Range	[0.552;0.596]	[-6.860;-6.463]	[1.782;1.983]	[9.284%;9.322%]

Table 7.7: Variability of the parameters estimation using the Jackknife method

To evaluate the effectiveness of the GA+LM optimizer, we compare its performance against two traditional distribution models—Normal and Lognormal—as well as the pure LM optimization method. The evaluation criteria are as follows:

- **Overall RMSE:** Root Mean Square Error calculated across the entire dataset, measuring the general fit of the model.
- **Tail RMSE:** RMSE calculated for observations in the tail region (values above u_2), assessing the model's ability to capture extreme values.

To ensure comparability, both the pure LM method and the GA+LM method were run for 100 iterations of the LM algorithm. The initial parameters for the pure LM method were set as follows: $\xi = 0.5$, μ as the median of the log-transformed data, sd as the standard deviation of the log-transformed data, and u_2 as the 95% quantile of the data.

The RMSE values for each model and method are summarized in Table 7.8.

Model	Overall RMSE (%)	Tail RMSE (%) (above u_2)
Normal Distribution	11.8	2.0
Lognormal Distribution	3.1	2.9
Pure LM Method	0.364	0.718
GA+LM Optimizer	0.357	0.628

Table 7.8: RMSE comparison for overall and tail regions

The GA+LM optimizer demonstrates significantly lower RMSE values in both the overall and tail regions when compared to traditional distributions, and it also outperforms the pure LM method slightly. While traditional distributions like the Lognormal show reasonable overall fit (3.1% RMSE), tail behavior improves (2.9% RMSE), highlighting the importance of a hybrid distribution that captures both body and tail behavior. The GA+LM optimizer achieves a 2% improvement in overall RMSE and a 14% improvement in tail RMSE compared to the pure LM method, demonstrating a better optimal solution found in the searching space.

From the log-scale survival plot in Figure 7.1 and log-scale survival plot at the tail in Figure 7.2, the lognormal distribution (best-fit solo distribution) performs worse than both Pure LM and GA+LM, especially in capturing extreme tail behavior. It fits the middle range well but diverges in the tails.

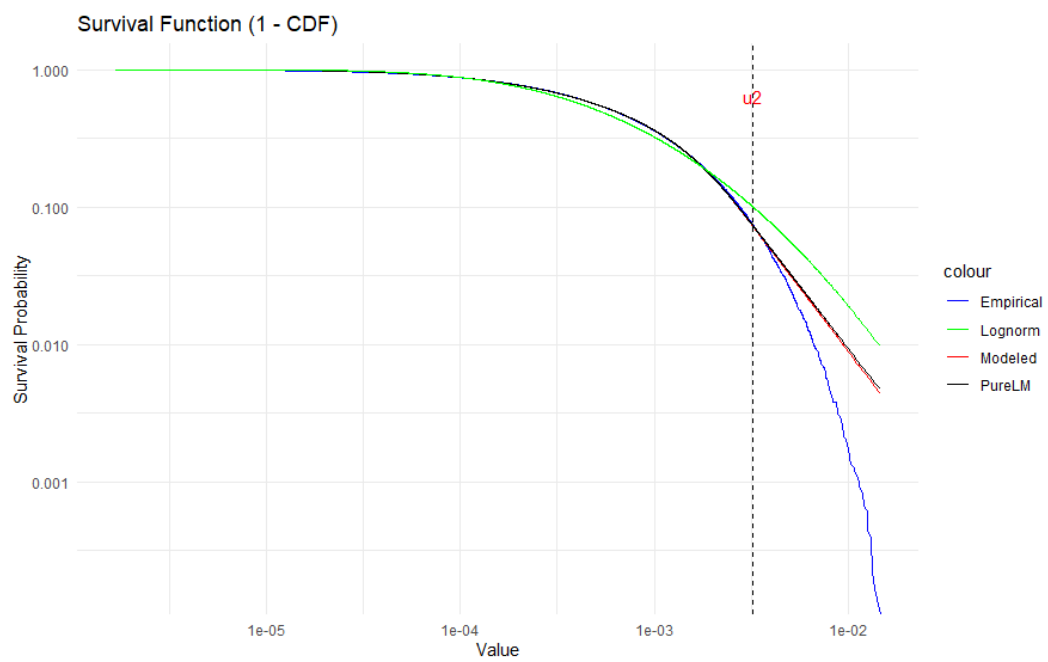


Figure 7.1: Survival graph in log scale

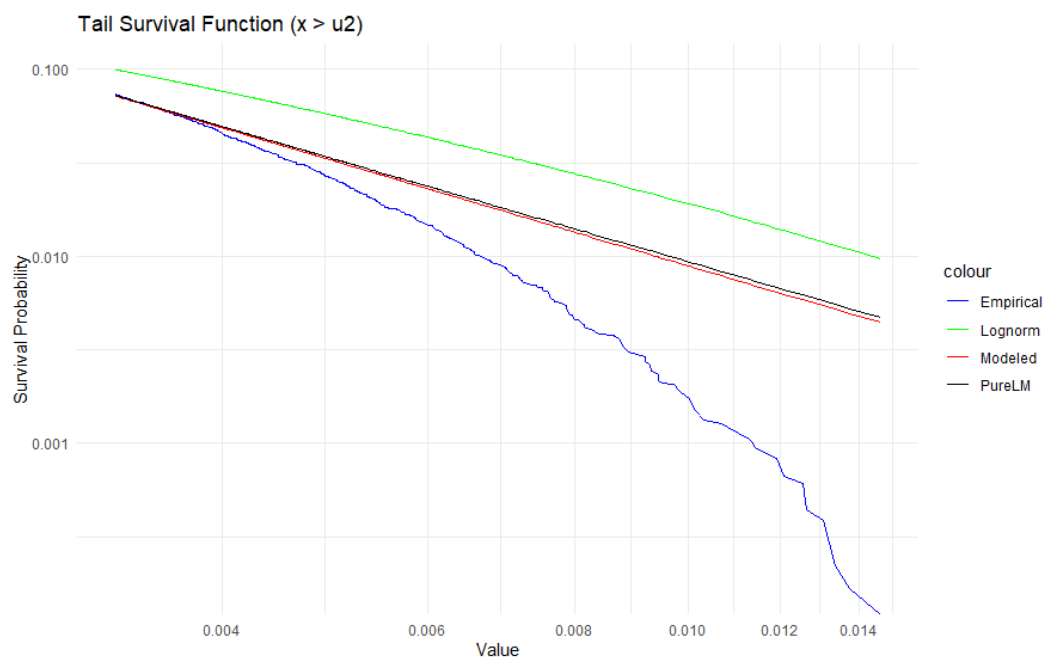


Figure 7.2: Survival graph at tail ($>u_2$) in log scale

Both Pure LM and GA+LM show similar tail index performance, but Pure LM demonstrates instability across simulated data samples (see Appendix A). In contrast, GA+LM is more stable, even in extreme data scenarios.

At the tail part, GA+LM shows a heavier tail than the empirical pandemic data. This is due to the smooth transition constraint (see in Subsection 7.1.2). For the sake of prudence, we use the GA+LM output with the heavier tail as the final output of our CAT Pandemic model.

The results demonstrate that the GA+LM optimizer achieves superior performance in both overall and tail RMSE compared to traditional distributions and the pure LM method where no manual search has been performed for obtaining the best initialization parameters. This outcome suggests that while pure LM optimizer, lacking the global search of GA, may converge to local minima, resulting in suboptimal parameter estimates, the GA+LM approach can provide an accurate fit across the entire dataset and is particularly effective in capturing tail events.

7.3.3 Results Analysis and Validation

The pandemic mortality output, derived from the Hybrid GPD model fitted using the GA+LM optimizer, is compared against the mortality shock component in the standard SCR formula and the two most severe pandemics recorded in the past 150 years, namely COVID-19 and the 1918 Influenza.

7.3.3.1 Comparing the Model with Standard SCR Formula

The study conducts a comprehensive comparison between the mortality output obtained with the hybrid GPD model, optimized with the GA+LM approach, and the mortality shocks specified by the standard Solvency Capital Requirement (SCR) formula, 0.15%. This comparison is carried out across multiple dimensions, including various countries and regions in which AXA operates and distinct age groups.

The SCR formula serves as a benchmark for capital adequacy in response to mortality risks. This framework is essential for insurers, as it dictates the capital buffers necessary to withstand extreme mortality events, ensuring solvency and risk management under catastrophic scenarios. The internal model developed in this study, by contrast, is designed to offer a more tailored and empirically calibrated approach, potentially capturing geographic-specific and demographic-specific factors that may be underrepresented in the single mortality shock standard SCR formula.

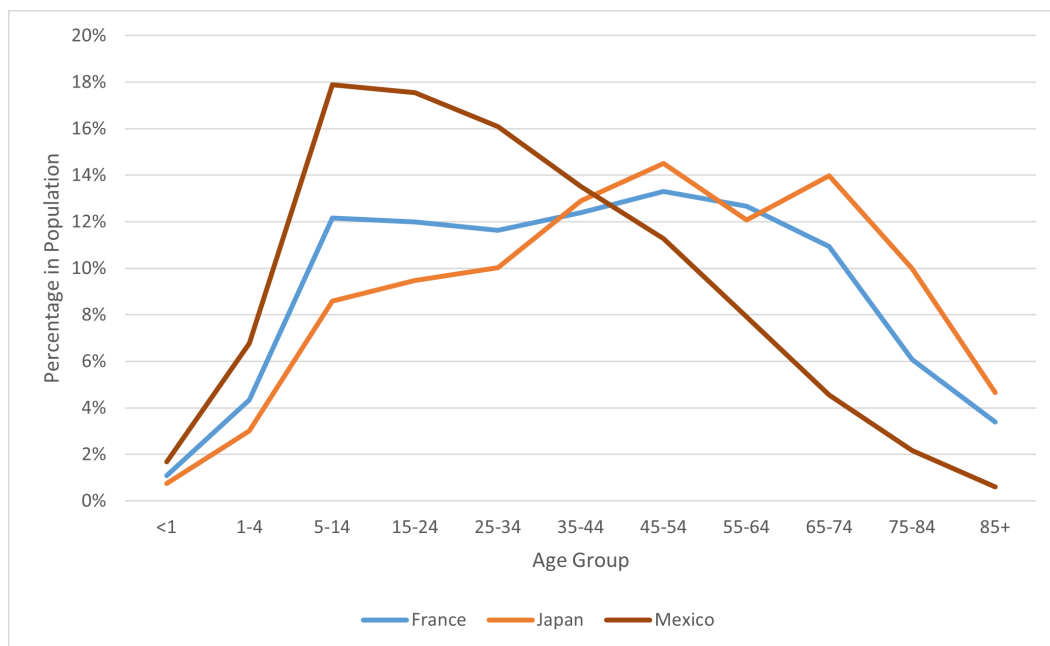


Figure 7.3: Demographic input for data in 2019

Detailed demography data of each country or region is presented in Appendix C. The demographic for France, Japan and Mexico are presented in Figure 7.3

The blue curve corresponding to France exemplifies the demographic characteristics prevalent in most Western European countries. Notably, from the age group 5-14 to 65-74, the demographic distribution are at similar level. In contrast, the brown curve representing Mexico reflects the demographic landscape of South or Central American countries, where a significant portion of the population is still concentrated in younger age groups. Conversely, the orange curve for Japan portrays a demographic profile characterized by elder age groups.

The 99.5% death shock from the final model compared to standard SCR formula is shown in Figure 7.4.

Note that the inputs of the model death shocks are using country or region demography data, (age, gender structure), which includes more older age people than most of the insurance portfolios (except for pension or annuity products).

The data depicted in Figure 7.4 underscores the significance of incorporating country and regional demographic data, as it reveals that the majority of death shocks exceeds the standard SCR shock, with an average model shock (same weight for each country or region) of 0.253% compared to standard SCR shock 0.15%. This underscores the importance of leveraging an internal model to accurately forecast

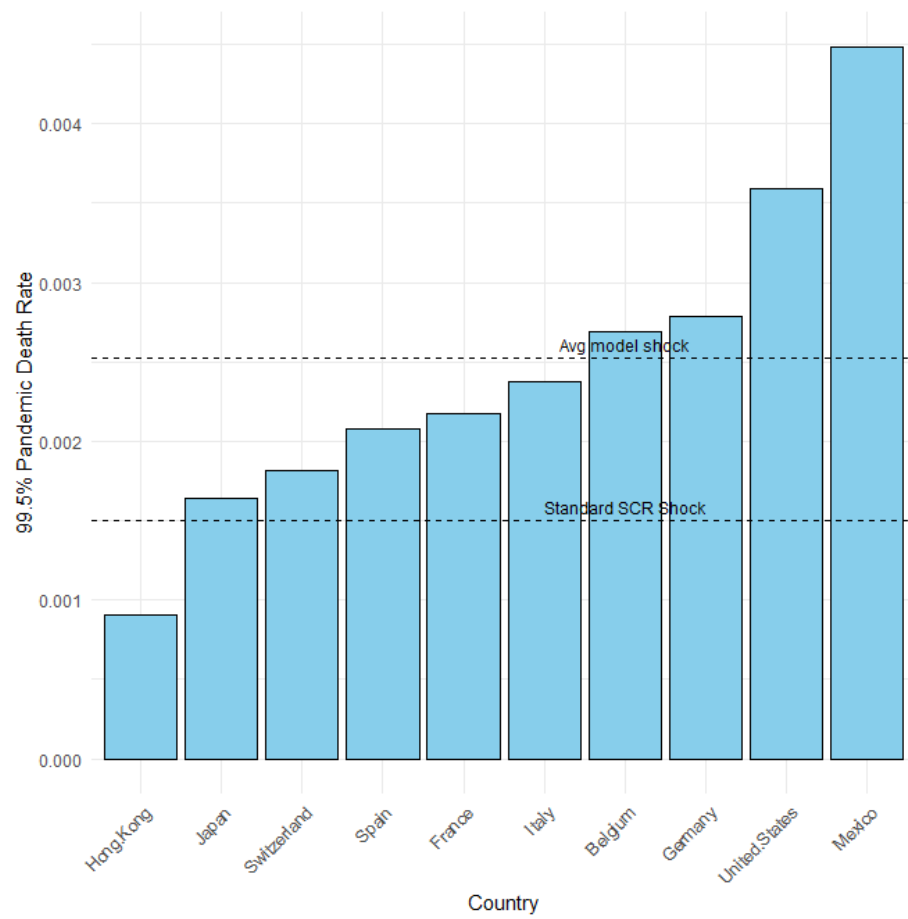


Figure 7.4: Comparison with Standard SCR shock

pandemic mortality rates. Notably, Hong Kong exhibits the lowest mortality rate, reflecting its high life expectancy. In contrast, Japan demonstrates a similar life expectancy to Hong Kong, yet experiences a two-fold higher shock due to its higher proportion of older age groups. Furthermore, Western European countries exhibit a slightly higher shock than Japan, a trend attributed to their marginally lower life expectancy. On the other hand, Mexico has a shock twice that of Western European countries, a consequence of its lower life expectancy, which in turn impacts the level of healthcare treatment available once infected.

7.3.3.2 Comparing the CAT Pandemic Internal Model with Real Pandemic Death (COVID-19 and 1918 Influenza)

To comprehensively assess the functionality of our final CAT Pandemic model and confirm the precision of mortality rate predictions, we conducted a comparative analysis between the model's output and the actual pandemic outcomes (COVID-19 and 1918 Influenza) across different countries.

To replicate the actual pandemics with the CAT Pandemic model, at the simulation stage, instead of using random samples drawn from each parameter's distribution, we use determined inputs for R_0 (2.87 for COVID-19 and 2.07 for 1918 Influenza) and Baseline Lethality (0.72% for COVID-19 and 2.5% for 1918 Influenza)³. In this way, the output from the pandemic model would only be one determined scenario instead of 10'800 scenarios, hence we obtain one mortality rate for each pandemic, rather than a probabilistic forecast.

This comparative evaluation allowed us to gain insights into the model's performance and its ability to accurately capture the dynamics of pandemic mortality rates in real-world scenarios.

Event	Country	Real Death Data	Model Output Death	Delta ($1 - \frac{Model}{Real}$)
COVID-19	France	122'204	144'425	-18%
	Germany	189'981	262'174	-38%
	Spain	136'356	100'252	26%
	Italy	240'288	154'067	36%
	Mexico	690'990	339'013	51%
	U.S.	1'250'000	999'800	20%
1918 Influenza	U.S.	550'000	583'223	-6%

Table 7.9: Comparison of real pandemic death data and model output

³Values were derived from the retained values in Chapter 5

Note that all death numbers for COVID-19 represent the cumulative excess mortality till 1st Jan 2023, computed by [Karlinsky & Kobak \(2021b\)](#) using data from the Human Mortality Database. The estimated death count for the 1918 Influenza in the U.S. is based on the study by [Stern et al. \(2010\)](#). The vaccination component is deactivated for the 1918 Influenza prediction.

Overall, the mortality output of the internal pandemic model developed in this study demonstrates its capability to approximate real-world pandemic mortality levels with reasonable accuracy. For France, Spain, and the United States, the differences between the model's mortality predictions and observed data are less significant. However, the model shows significant underestimation for Mexico and Italy and an overestimation for Germany. These variances are likely influenced by differences in quarantine effectiveness and public health response among countries—factors that the model does not explicitly account for, due to its aggregated, high-level structure.

Regarding the 1918 Influenza pandemic, while historical data is limited, the model's mortality estimates closely approximate values cited in scientific research. This consistency with historical estimates further validates the model's robustness in capturing extreme mortality events, even with sparse data.

In summary, the pandemic mortality model demonstrates a certain level of predictive accuracy, producing mortality estimates on the correct order of magnitude for a broad range of scenarios. Given that the model incorporates numerous aggregated factors, such as age distribution and geographic variation, to capture mortality risk in a hypothetical 99.5% quantile pandemic event, it is expected that some variability will exist when replicating a specific historical pandemic. This variability highlights the inherent challenges in predicting complex, multifactorial events but does not detract from the model's utility in Solvency II Framework and strategic risk management. By providing reliable mortality projections at an extreme quantile level, this model offers a valuable tool for assessing and managing pandemic-related risks in an actuarial context.

7.3.4 Limit of the Study

This study, while providing valuable insights into pandemic mortality risk, has certain limitations that influence the model's accuracy and applicability. First, the model predicts pandemic mortality at an aggregate level rather than at an individual level. This aggregation inherently introduces volatility, as individual-level variations in susceptibility, exposure, and health status are not captured. Consequently,

the model may miss nuanced trends, leading to fluctuations in mortality estimates across different population segments.

The second limitation is the lack of parameters to differentiate quarantine effectiveness across countries. Variations in the stringency and enforcement of quarantine measures significantly impact pandemic outcomes, and not accounting for these differences limits the model's ability to accurately project mortality rates for countries with vastly different public health responses.

The third limitation is that the model does not distinguish transmission dynamics across age groups. Age-specific transmission patterns can play a crucial role in determining pandemic spread and mortality, as contact rates, susceptibility, and immunity responses often vary significantly by age. This lack of age-specific transmission differentiation could lead to less precise mortality estimates, especially in populations with pronounced age-related vulnerabilities.

The fourth limitation of this study is that the model does not account for time-dependent pandemic features, which can significantly influence the dynamics of disease spread and impact. By assuming equal weight for all historical pandemics, the model overlooks the potential changes in transmissibility, lethality, and public health responses that may have evolved over time. Recent pandemics often provide critical insights into contemporary factors such as healthcare infrastructure, population immunity, and social behavior, which may not be adequately represented by historical data alone. Consequently, this assumption may limit the model's ability to accurately reflect current and future pandemic scenarios, as it fails to recognize the increasing relevance of more recent pandemic experiences.

Future research could address these limitations by incorporating data on lockdown effects on age-specific contact patterns and behavior, which would enable a more granular approach to estimating age-group transmission dynamics (see in [Bosetti et al. \(2021\)](#)). Additionally, integrating quarantine effectiveness metrics—such as the Stringency Index or Google Community Mobility data—could enhance the model's capacity to reflect country-specific variations in public health interventions (see in [Zhu et al. \(2020\)](#)). To enhance the time-dependent characteristics of pandemics, various indicators—such as climate, social environment, population health profiles, healthcare infrastructure, economic factors, and pathogen evolution—can be incorporated into the analysis (see the method in [Hambuckers & Kneib \(2023\)](#)). Such refinements would improve the model's robustness, making it more adaptable to diverse scenarios and more precise in predicting mortality impacts across different demographic and geographic

contexts.

Part VI

Conclusion

The evolving complexity of pandemic risks demands a more comprehensive approach than a single mortality shock provided by the standard SCR formula to accurately capture demographic and geographic distinctions in insurers' portfolios. This thesis advances the field in three key dimensions:

First, it enhances the established Swiss Re pandemic model by incorporating granular geographical factors through indirect age-adjustment methods and calibrating against expanded datasets and numerous research. Notably, the model integrates concrete mitigation impacts derived from COVID-19 experiences, making it more relevant for real-world applications.

Second, a new hybrid optimization algorithm is developed, combining genetic algorithms with Levenberg-Marquardt methods, to enhance the calibration of the LN-E-GPD model for pandemics. This advancement enables more accurate fitting of both the body and tail of pandemic mortality rate distributions, with potential applications extending beyond pandemic modeling to other multi-dimensional optimization challenges.

Third, the model's validation against historical pandemic data substantiates its practical utility for insurance companies in multiple aspects of risk management, from contract pricing to portfolio optimization. The framework also provides a quantitative foundation for policymakers to evaluate intervention strategies during pandemic events.

Future research could further refine the model by incorporating additional metrics such as stringency indices and mobility data to better differentiate quarantine effectiveness across countries. This enhancement would provide deeper insights into how varying quarantine measures across countries influence the trajectory of pandemic spread, enabling more precise modeling of infection dynamics.

In conclusion, this work bridges a critical gap between theoretical pandemic modeling and practical risk management needs, offering insurance companies and policymakers a more robust toolkit for navigating future pandemic events.

Part VII

Appendices



Simulation Study of GA Algorithm and LM Optimizer

To assess the robustness and accuracy of our optimization methods, we conducted a Monte Carlo (MC) simulation study comparing the top four GA+LM configurations selected previously based on the jackknife analysis against the pure LM method. Additionally, we analyse the convergence of the best GA+LM method on various sample sizes.

An advantage of MC techniques is to minimize numerical noise and focus on model performance. We performed 100 MC simulations for each configuration to obtain the mean result for each parameter estimate and its standard deviation. The standard deviation provides insight into numerical variation, which differs from confidence intervals, as the latter were computed using the jackknife method in our case.

Compare between top4 GA+LM methods against Pure LM

We tested our GA+LM and pure LM methods on simulated datasets. Each dataset has a size of 10000 samples and was generated using the predefined hybrid distribution model with known parameters: $\xi = 0.8$, $\mu = 0$, $\sigma = 5$, and $u_2 = 4.38$, ($u_1 = 2$). For each scenario:

- We applied the GA+LM method using the top four configurations identified from the jackknife analysis.
- We applied the pure LM method for baseline comparison.
- We computed the mean and standard deviation of the estimated parameters over 100 simulations.
- We compute the average of the log-likelihood ratio \mathcal{D} of $h(\mathbf{y}^q; \theta)$ by $\hat{h}(\mathbf{y}^q; \hat{\theta}^q)$, over the 100 simulations:

$$\mathcal{D} = \frac{1}{Nl} \sum_{q=1}^N \sum_{p=1}^l \log \left(\frac{h(y_p^q; \theta)}{\hat{h}(y_p^q; \hat{\theta}^q)} \right) \quad (\text{A.1})$$

where

- h represents the true hybrid probability density function (pdf) with known parameters θ .
- \hat{h} represents the estimated probability density function with estimated parameters $\hat{\theta}^q$.
- \mathbf{y}^q denotes the q -th test dataset (out of N total test datasets).
- y_p^q refers to the p -th data point within the q -th test dataset, where there are l data points per test dataset.
- θ is the vector of true parameters of the model.
- $\hat{\theta}^q$ represents the estimated parameters obtained from the q -th dataset.
- $\frac{1}{Nl} \sum_{q=1}^N \sum_{p=1}^l$ represents averaging over all N test datasets and all l data points.

It is obvious that the smallest the value of \mathcal{D} is, the most trustworthy is the algorithm.

As a reminder, for both methods, the LM part runs for 100 rounds. The initial parameters for the pure LM method were set as follows: $\xi = 0.5$, μ as the median of the log-transformed data, sd as the standard deviation of the log-transformed data, and u_2 as the 95% quantile of the data. And the lower

and upper boundaries of the parameters (ξ, μ, sd , and u_2) for the Genetic Algorithm (GA) method and the Latin Hypercube Sampling (LHS) initial population were set as follows:

$$\text{lower} = (0.01, \text{round}(\min(\log(\text{data}))), 0, 0)$$

$$\text{upper} = \left(1, \text{round}(\max(\log(X))), 5\sqrt{\log(1 + CV^2)}, \text{quantile}(X, 0.95)\right)$$

Optim Method	ξ (target: 0.8)		μ (target: 0)		σ (target: 5)		u_2 (target: 4.38)		Log-Likelihood Ratio \mathcal{D}
	Mean	Var	Mean	Var	Mean	Var	Mean	Var	
LHS,BLX,RA,RW	0.794	0.008	-0.034	0.065	4.973	0.016	4.526	0.706	3.4×10^{-5}
LHS,BLX,RS,RW	0.804	0.009	-0.029	0.065	4.975	0.016	4.516	2.040	7.0×10^{-5}
LHS,SP,RS,RW	0.798	0.004	0.015	0.064	5.002	0.017	4.434	0.319	1.0×10^{-5}
LHS,SP,RA,RW	0.800	0.006	-0.032	0.063	4.974	0.015	4.476	0.757	2.8×10^{-5}
PureLM	0.930	0.008	0.076	0.081	5.040	0.019	3.628	0.072	9.4×10^{-4}

Table A.1: Comparison of optimization methods performance

Method notation: LHS = Latin Hypercube Sampling, BLX = Blend Crossover, SP = Single Point Crossover, RA = Random Add Mutation, RS = Random Replace Mutation, RW = Roulette Wheel Selection

Based on the comparison of optimization methods, we observe that the selected genetic algorithm for pandemic model consistently outperforms the Pure Levenberg-Marquardt method. In particular, the LHS,SP,RS,RW configuration (Latin Hypercube Sampling with Single Point crossover, Random Replace mutation, and Roulette Wheel selection) demonstrates superior performance across these metrics.

The PureLM method shows significant instability in simulation data samples, as evidenced by:

- Mean estimate of ξ at 0.93, substantially deviating from the target value of 0.8
- Considerably higher variance for μ and σ compared to GA-based methods
- Log-likelihood ratio \mathcal{D} of 9.4×10^{-4} , which is approximately 100 times larger than the best GA method

These simulation results aligns with the best configuration found with the jackknife method using pandemic mortality data. It also demonstrate that genetic algorithms with appropriate configuration significantly outperform traditional optimization methods like Levenberg-Marquardt for this particular application, offering more stable and accurate parameter estimation with better overall model fit.

Analyse the convergence of the best GA+LM on various sample size

We tested the convergence of the best GA+LM method on simulated datasets with varying sample sizes ($n = 500, 1000, 5000, 10000$), using the same parameters as before.

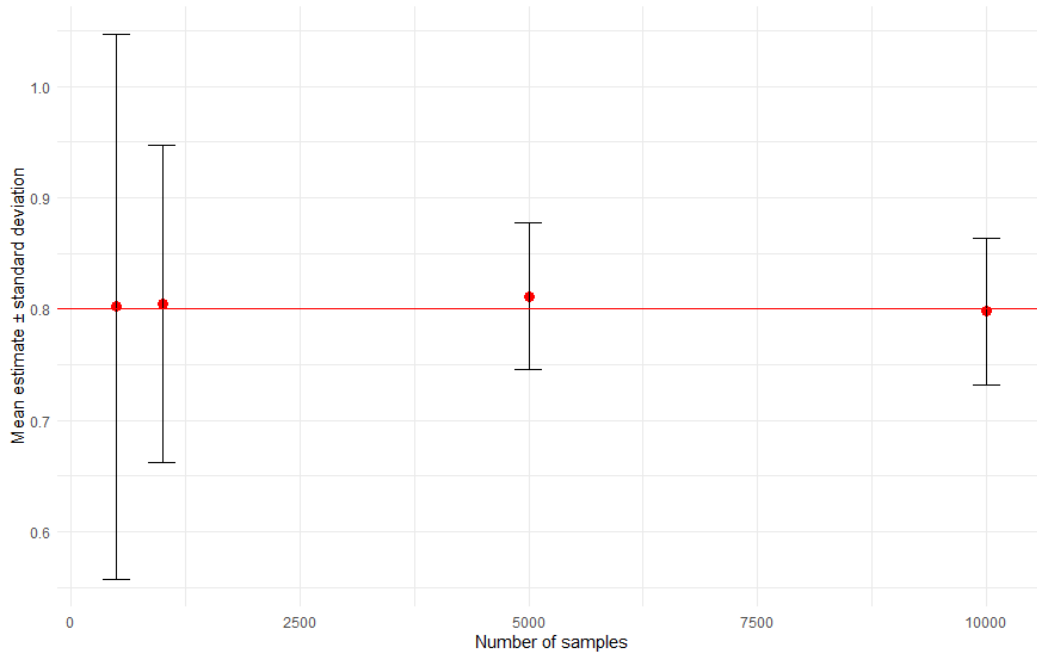


Figure A.1: Variance of estimated ξ

The analysis demonstrates that reliable estimation of the parameter ξ is achieved with 10,000 observations, where the standard deviation has significantly decreased and stabilized. At this sample size, the estimation procedure provides both accuracy (mean estimate close to true value) and precision (reduced variance).

While substantial improvements in precision are observed when increasing from 1,000 to 5,000 samples, the incremental gain in precision from 5,000 to 10,000 samples is more modest but still meaningful.

B

Convergence Study on Quasi Monte Carlo Simulation

Analysis of Quasi Monte Carlo Simulation Convergence Study

As mentioned in the end of Part 3, we performed a convergence study on the Quasi Monte Carlo simulation based on the number of two core parameters, R_0 and Baseline Lethality. See the simulated 99.5% quantile (87.5% quantile of severity model) in Table B.1.

Commentary on Convergence Behavior

The quasi Monte Carlo (QMC) simulation study examines pandemic mortality rates using different parameter grid resolutions for R_0 (basic reproduction number) and baseline lethality. We observe several

Simulation Setup	Sample Size	Mortality Rate
$R_0 \times$ Baseline Lethality	N points	Estimated Value
200×200	40'000	0.002192861
100×100	10'000	0.002195259
80×80	6'400	0.002201033
60×60	3'600	0.002172769
80×40	3'200	0.002189748
40×80	3'200	0.002200000
50×50	2'500	0.002190000
40×60	2'400	0.002185000
60×40	2'400	0.002185000
40×40	1'600	0.002195000
30×30	900	0.002231000
20×20	400	0.002156000
10×10	100	0.002311000

Table B.1: Pandemic mortality rates from Quasi Monte Carlo simulation with varying parameter settings

key patterns in the convergence behavior:

Convergence Analysis

- **Asymptotic Behavior:** The estimated mortality rates appear to converge to approximately 0.00219 as the sample size increases, with the highest resolution simulation (200×200) yielding 0.002192861.
- **Stability Threshold:** Notable stability in estimates is achieved at approximately 3,200 sampling points (corresponding to 80×40 or 40×80 configurations), with estimated values consistently falling within the range of 0.00217–0.00220.
- **Error Characteristics:** The simulation demonstrates non-monotonic convergence, typical of QMC methods. The error does not strictly decrease with increasing sample size but exhibits an overall downward trend in variability.
- **Parameter Grid Symmetry:** Interestingly, asymmetric parameter grids (e.g., 80×40 vs. 40×80) produce slightly different results (0.002189748 vs. 0.002200000), suggesting different sensitivities to the resolution of R_0 versus lethality parameters.
- **Low Resolution Behavior:** At very low resolutions (10×10 , 20×20), we observe higher variance in the estimates (0.002311 and 0.002156, respectively), deviating more significantly from

the apparent limit value.

Choice of 60×60 Grid Configuration

The 60×60 grid configuration (3,600 sampling points) represents an optimal balance between computational efficiency and estimation accuracy. This configuration achieves results within approximately 1% of the highest resolution estimate (200×200) while requiring only 9% of the computational resources. The diminishing returns observed when increasing resolution beyond this point further supports this choice. Notably, the Quasi Monte Carlo approach employed here provides faster convergence rates than traditional Monte Carlo simulation, allowing us to achieve reliable estimates with fewer sampling points. This efficiency, combined with the non-monotonic convergence pattern typical of QMC methods, indicates that the slight deviation of the 60×60 grid estimate (0.002172769) from the apparent limit value (≈ 0.00219) is well within acceptable error margins for pandemic modeling applications.



National or Regional Input Age Structure

Age Group	France	Japan	Hong Kong	Germany	Italy	Spain
< 1	1%	1%	1%	1%	1%	1%
1-4	4%	3%	3%	4%	3%	3%
5-14	12%	9%	8%	9%	9%	10%
15-24	12%	9%	9%	10%	10%	10%
25-34	12%	10%	14%	13%	11%	12%
35-44	12%	13%	16%	12%	13%	16%
45-54	13%	15%	15%	15%	16%	16%

Table C.1: Age distribution by country or region (Part 1)

Age Group	Belgium	Mexico	Switzerland	Morocco	United States
< 1	1%	2%	1%	1%	1%
1-4	4%	7%	4%	4%	5%
5-14	12%	18%	10%	10%	13%
15-24	11%	18%	11%	11%	13%
25-34	13%	16%	14%	14%	14%
35-44	13%	14%	14%	14%	13%
45-54	14%	11%	15%	15%	13%
55-64	13%	8%	13%	13%	13%
65-74	10%	5%	10%	10%	9%
75-84	6%	2%	6%	6%	5%
85+	3%	1%	3%	3%	2%

Table C.2: Age distribution by country or region (Part 2)



Solvency II Framework Details

As a major insurance company headquartered in France, AXA Group is subject to both French and European regulations. This thesis focuses on the current Solvency II framework that governs the operations of AXA Group and its subsidiaries.

The predecessor of Solvency II, the Solvency I framework, was established with the adoption of the First Non-Life Directive (73/239/EEC) in 1973 [Council of The European Communities \(1973\)](#) and the First Life Directive (79/267/EEC) in 1979 [Council of The European Communities \(1979\)](#). However, this framework faced criticism on several fronts. Firstly, the solvency requirements under Solvency I only considered underwriting risks, disregarding other potential sources of risk that could impact solvency. The calculation of capital requirements was overly simplistic, using a ratio based on reserves, premiums, and claims. Additionally, the methodologies for calculating capital requirements varied significantly across Europe, resulting in non-comparable results, particularly problematic for multinational insurance groups with operations across the continent and internationally. Lastly, the Solvency I framework placed

little emphasis on internal control.

In response, the European Union (EU) and its predecessors have endeavored to establish a unified regulatory system that aligns with the evolving understanding of risks associated with insurance activities. The Solvency II framework, detailed in Directive 2009 (2009/138/EC) [The European Parliament and The Council of the EU \(2009\)](#), represents a comprehensive reform of insurance regulation within the EU, focusing primarily on the risk management and capital requirements of European insurers. Following a vote by the EU Parliament on March 11th, 2014, Solvency II came into force on January 1st, 2016.

A Structure with Three Pillars

The Solvency II framework consists of three “pillars”:

- **Pillar 1** comprises quantitative requirements including risk-based capital requirements that firms will be required to meet with assets and liabilities valued on a market-consistent basis. In Pillar 1 the new solvency system contains two capital requirements defining the upper and lower end of a ladder of supervisory intervention. The Solvency Capital Requirement (SCR) is the level above which there is no supervisory intervention for financial reasons. The Minimum Capital Requirement (MCR) is the level below which the supervisor’s strongest actions are taken (e.g. removal of the insurer’s authorization). The SCR may be calculated using a standard formula or, subject to prior supervisory approval, an insurer’s internal model, or a combination of the two. The MCR is calculated using a linear formula and must fall between 25% and 45% of the SCR. Capital add-ons may be imposed by the supervisor in exceptional circumstances where it concludes that the risk profile of the insurer deviates significantly from the assumptions underlying the SCR or the system of governance deviates significantly from the standards required. Supervisor-imposed add-ons increase the SCR.
- **Pillar 2** comprises qualitative requirements focusing on governance, risk management and required functions and includes the supervisory review process. Insurers are required to carry out an Own Risk and Solvency Assessment (ORSA) and this is required to be reviewed by the su-

pervisor. Pillar 2 includes “prudent persons” investment principles. Supervisors can also impose capital additions for governance failings.

- **Pillar 3** comprises reporting and disclosure requirements including a public Solvency and Financial Condition Report (SFCR) and a private Regulatory Supervisory Report (RSR). The aim of public disclosures is to harness market discipline by requiring firms to publish certain details of their risks, capital and risk management.

As explained above, in Pillar 1 the solvency system contains two capital requirements defining the upper and lower end of a ladder of supervisory intervention. The Solvency Capital Requirement (SCR) is the level above which there is no supervisory intervention for financial reasons. The Minimum Capital Requirement (MCR) is the level below which the supervisor’s strongest actions are taken (e.g. removal of the insurer’s authorization)

Solvency Capital Requirement (SCR)

The Solvency Capital Requirement is calculated by combining a number of separate risk charges, allowing for diversification credits using correlation matrices or other methodologies. The SCR is calibrated to the Value-at-Risk of the basic own funds of an insurance or reinsurance undertaking subject to a confidence level of approximately 99.5% over a one-year time horizon.

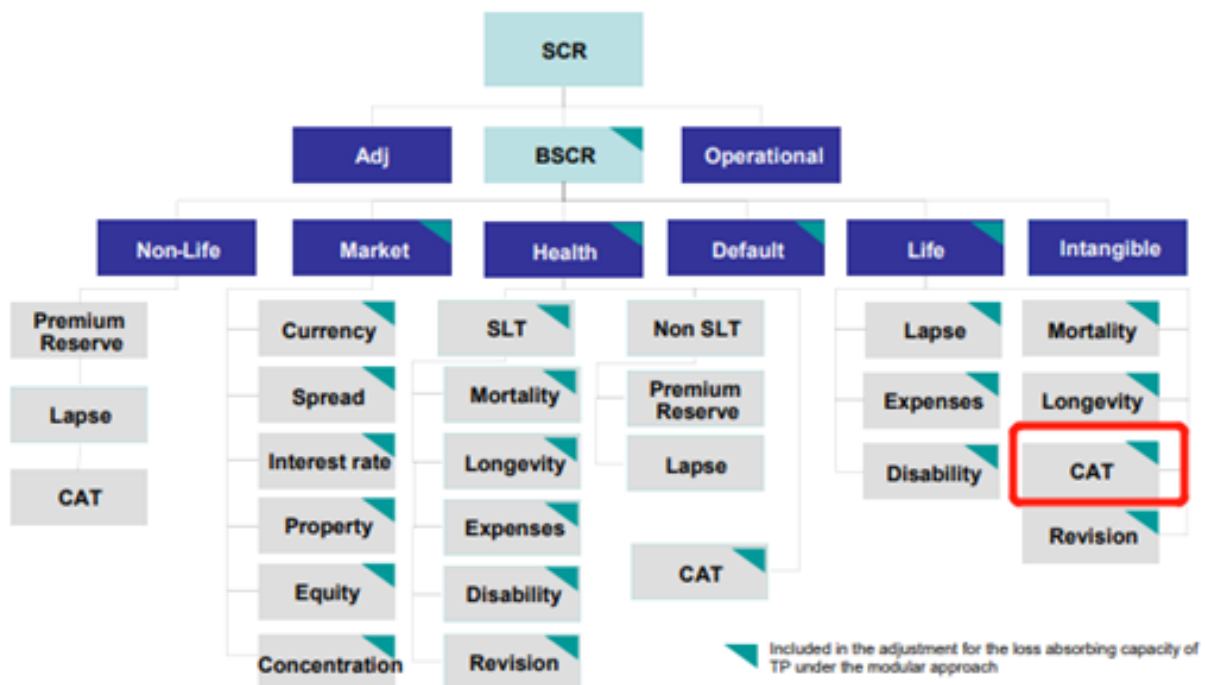
The SCR for each individual risk is then determined as the difference between the net asset value (for practical purposes this can be taken as assets less best estimate liabilities) in the unstressed balance sheet and the net asset value in the stressed balance sheet. These individual risk capital amounts are then combined across the risks within the module, using a specified correlation matrix and matrix multiplication. Solvency II provides a range of methods to calculate the SCR which allows undertakings to choose a method that is proportionate to the nature, scale and complexity of the risks of the undertaking.

The SCR may be calculated using:

- A standard formula with simplifications
- A standard formula

- A standard formula with undertaking-specific parameters. If the standard formula is used, non-life underwriting risk factors may, subject to prior supervisory approval, be replaced with undertaking-specific parameters (“USPs”) which are calculated using an undertaking’s own claims experience
- The combination of the standard formula for some risk factors and a partial internal model for the remaining risk factors
- A fully internal model. The use of an insurer’s (full or partial) internal model is subject to prior supervisory approval.

The structure of the SCR risk charges in the standard formula is summarized in the following diagram.



3

Figure D.1: SCR risk diagram



A Brief Survey of Extreme Value Theory

Fundamental Theorem of Extreme Value Theory

The Fundamental Theorem of Extreme Value Theory, often called the Fisher–Tippett–Gnedenko theorem, is a cornerstone in the statistical analysis of extreme values. It establishes that for a sufficiently large sample size of independent and identically distributed (i.i.d.) random variables, the maximum values in these samples converge to a specific family of distributions, known collectively as the Generalized Extreme Value (GEV) distribution. This convergence property provides a basis for modeling extreme events, regardless of the original distribution of the data, as long as certain conditions are met.

The GEV distribution combines three types of distributions:

- **Gumbel Distribution** (Type I),
- **Fréchet Distribution** (Type II),

- **Weibull Distribution** (Type III).

These types cover all possible tail behaviors of extreme events, with the shape parameter ξ determining which type of distribution is most appropriate. This parameter represents the tail behavior of the GEV distribution, and each form corresponds to a specific value or range of ξ :

- **Gumbel Distribution:** When $\xi = 0$, the distribution is asymptotically Gumbel, suitable for modeling light-tailed phenomena where extreme values decay exponentially. The Gumbel distribution is often applied in natural phenomena like annual maximum rainfall, where extreme values are bounded but do not exhibit heavy tails.
- **Fréchet Distribution:** When $\xi > 0$, the distribution is heavy-tailed and converges to the Fréchet form. This is particularly useful for extreme events that exhibit a power-law behavior, such as large financial losses, catastrophic natural disasters, as in this study, pandemic mortality rates where extreme values can be extraordinarily high and unbounded.
- **Weibull Distribution:** When $\xi < 0$, the Weibull distribution is appropriate, representing data with a finite upper bound. This form is often applied to scenarios where the maximum value is physically limited, such as certain engineering stress limits or failure times.

The cumulative distribution function (CDF) of the GEV distribution is expressed as:

$$F(x) = \exp \left(- \left(1 + \xi \frac{x - \mu}{\sigma} \right)^{-\frac{1}{\xi}} \right)$$

for $1 + \xi \frac{x - \mu}{\sigma} > 0$, where:

- ξ : Shape parameter, which controls the "tail heaviness" of the distribution and dictates which of the three types (Gumbel, Fréchet, Weibull) the GEV converges to.
- σ : Scale parameter, reflecting the spread of the distribution. Larger values of σ indicate a broader range of extreme outcomes.
- μ : Location parameter, which shifts the distribution along the x-axis and determines the central tendency of the extreme values.

In practical applications, the GEV distribution allows us to model block maxima, which is the maximum value observed within fixed blocks of time or space (e.g., annual maximum mortality rate). In the context of pandemic modeling, the GEV distribution provides a useful framework for understanding the upper extremes of mortality rates across multiple simulated pandemic scenarios. It allows us to focus specifically on the "worst-case" outcomes, capturing the rare yet impactful events that are critical for risk assessment in public health planning.

Peaks-Over-Threshold (POT) Approach

The Peaks-Over-Threshold (POT) approach is another fundamental technique within Extreme Value Theory, offering an alternative to the GEV block maxima method. Instead of focusing on the maximum value within predefined intervals, the POT approach examines all data points that exceed a specified threshold. This approach is particularly well-suited for modeling datasets with frequent extreme values, as it retains more information about the tail than methods that rely on block maxima alone.

In the POT framework, extreme values are modeled using the Generalized Pareto Distribution (GPD). This distribution is defined for values that exceed a certain threshold u and is characterized by two parameters: a scale parameter σ and a shape parameter ξ . The CDF of the GPD is:

$$F(y) = 1 - \left(1 + \xi \frac{y}{\sigma}\right)^{-\frac{1}{\xi}}$$

where $y = x - u$ represents the exceedance over the threshold u . The parameters σ and ξ play similar roles as in the GEV framework, with ξ controlling the heaviness of the tail. Depending on the value of ξ , the GPD captures various types of tail behavior:

- If $\xi = 0$, the GPD resembles the exponential distribution, suitable for light-tailed data where extreme values are frequent but not excessively large.
- If $\xi > 0$, the GPD exhibits a heavy tail, suitable for phenomena with large, unbounded extremes, such as pandemic mortality rates.
- If $\xi < 0$, the distribution is bounded, indicating a natural limit to extreme values.

Choosing an appropriate threshold u is crucial in the POT method, as it affects the accuracy and stability of the fitted model. Too low a threshold may include non-extreme values, diluting the focus on extreme behavior, while too high a threshold may reduce the number of observations and lead to statistical inefficiency. Various techniques exist for threshold selection, including graphical methods (e.g., mean residual life plots) and quantitative methods (e.g., minimizing the Kolmogorov-Smirnov distance).

Listing of figures

1	Structure du modèle épidémiologique	v
2	Comparaison avec le choc standard de la SCR	xv
3	Epidemiological model structure	xviii
4	Comparison with Standard SCR shock	xxvii
1.1	Pandemic impact on asset and liability	6
2.1	Swiss Re's Pandemic Model structure	19
3.1	Illustration of the Pandemic Model blocks	27
4.1	Transition between health statuses	31
4.2	Transition between health statuses without mitigation	36
4.3	Transition between health statuses with mitigation	40
5.1	Probability density function for R_0	53
5.2	Infection Duration Profile for COVID-19 and Influenza	55
5.3	Retained mortality shape by age-band	61
5.4	Calibration process for Area-specific Factor of Lethality	66
5.5	Daily new estimated infections of COVID-19 in France by IHME Model	71
5.6	Lethality Index as a function of life expectancy	75
5.7	The 4 phases of the Quarantine Model	79
5.8	Effective R_t of COVID-19 in 2020 and 2021 per country. Source from: Our World In Data	80

5.9	Vaccination Distribution during COVID-19 Source from: Our World In Data	83
5.10	Vaccination Coverage as a function of life expectancy	86
5.11	COVID-19 Vaccination Effectiveness	87
7.1	Survival graph in log scale	121
7.2	Survival graph at tail ($>u_2$) in log scale	121
7.3	Demographic input for data in 2019	123
7.4	Comparison with Standard SCR shock	124
A.1	Variance of estimated ξ	135
D.1	SCR risk diagram	144

References

- Adalja, A., Watson, M., Toner, E., Cicero, A., & Inglesby, T. (2019). The characteristics of pandemic pathogens.; 2018.
- Altevogt, B. M., Nadig, L., & Stroud, C. (2011). *The 2009 H1N1 influenza vaccination campaign: summary of a workshop series*. National Academies Press.
- Anderson, R. M. & May, R. M. (1982). Coevolution of hosts and parasites. *Parasitology*, 85(2), 411–426.
- Arroyo-Marioli, F., Bullano, F., Kucinskas, S., & Rondón-Moreno, C. (2021). Tracking r of covid-19: A new real-time estimation using the kalman filter. *PloS one*, 16(1), e0244474.
- Baker, J. E. (2014). Adaptive selection methods for genetic algorithms. In *Proceedings of the first international conference on genetic algorithms and their applications* (pp. 101–106).: Psychology Press.
- Belongia, E. A., Simpson, M. D., King, J. P., Sundaram, M. E., Kelley, N. S., Osterholm, M. T., & McLean, H. Q. (2016). Variable influenza vaccine effectiveness by subtype: a systematic review and meta-analysis of test-negative design studies. *The Lancet Infectious Diseases*, 16(8), 942–951.
- Billah, M. A., Miah, M. M., & Khan, M. N. (2020). Reproductive number of coronavirus: A systematic review and meta-analysis based on global level evidence. *PloS one*, 15(11), e0242128.
- Bosetti, P., Huynh, B.-T., Abdou, A. Y., Sanchez, M., Eisenhauer, C., Courtejoie, N., Accardo, J., Salje, H., Guillemot, D., Moslonka-Lefebvre, M., et al. (2021). Lockdown impact on age-specific contact patterns and behaviours, france, april 2020. *Eurosurveillance*, 26(48), 2001636.
- Britten, R. H. (1932). The incidence of epidemic influenza, 1918-19. *Public Health Rep*, 47(6), 303–375.
- Carrat, F., Vergu, E., Ferguson, N. M., Lemaître, M., Cauchemez, S., Leach, S., & Valleron, A.-J. (2008). Time lines of infection and disease in human influenza: a review of volunteer challenge studies. *American journal of epidemiology*, 167(7), 775–785.
- Cori, A., Valleron, A.-J., Carrat, F., Tomba, G. S., Thomas, G., & Boëlle, P.-Y. (2012). Estimating influenza latency and infectious period durations using viral excretion data. *Epidemics*, 4(3), 132–138.
- Corral, A. (2021). Tail of the distribution of fatalities in epidemics. *Physical Review E*, 103(2), 022315.
- Council of The European Communities (1973). First council directive 73/239/eec of 24 july 1973 on the coordination of laws, regulations and administrative provisions relating to the taking-up and pursuit of the business of direct insurance other than life assurance.
<https://eur-lex.europa.eu/legal-content/EN/TXT/?uri=CELEX%3A31973L0239>.

- Council of The European Communities (1979). First council directive 79/267/EEC of 5 March 1979 on the coordination of laws, regulations and administrative provisions relating to the taking up and pursuit of the business of direct life assurance.
<https://eur-lex.europa.eu/legal-content/EN/TXT/?uri=CELEX%3A31979L0267>.
- Cowling, B. J., Chan, K.-H., Fang, V. J., Cheng, C. K., Fung, R. O., Wai, W., Sin, J., Seto, W. H., Yung, R., Chu, D. W., et al. (2009). Facemasks and hand hygiene to prevent influenza transmission in households: a cluster randomized trial. *Annals of internal medicine*, 151(7), 437–446.
- Dacorogna, M., Debbabi, N., & Kratz, M. (2018). *Analyse exploratoire des plaintes de crimes cyber renseignées à la C3N de la PJGN*. Technical report, Research report to the PJGN, 1-24.
- Dacorogna, M., Debbabi, N., & Kratz, M. (2023). Building up cyber resilience by better grasping cyber risk via a new algorithm for modelling heavy-tailed data. *European Journal of Operational Research*, 311(2), 708–729.
- Deb, K., Agrawal, R. B., et al. (1995). Simulated binary crossover for continuous search space. *Complex systems*, 9(2), 115–148.
- Debbabi, N. & Kratz, M. (2014). A new unsupervised threshold determination for hybrid models. In *2014 IEEE International Conference on Acoustics, Speech and Signal Processing (ICASSP)* (pp. 3440–3444).: IEEE.
- Debbabi, N., Kratz, M., & Mboup, M. (2016). A self-calibrating method for heavy tailed data modelling. application in neuroscience and finance. *arXiv preprint arXiv:1612.03974*.
- Dick, J. & Pillichshammer, F. (2010). *Digital Nets and Sequences: Discrepancy Theory and Quasi-Monte Carlo Integration*. Cambridge University Press.
- Edridge, A. W., Kaczorowska, J., Hoste, A. C., Bakker, M., Klein, M., Loens, K., Jebbink, M. F., Matser, A., Kinsella, C. M., Rueda, P., et al. (2020). Seasonal coronavirus protective immunity is short-lasting. *Nature medicine*, 26(11), 1691–1693.
- Erlangga, D., Suhrcke, M., Ali, S., & Bloor, K. (2019). The impact of public health insurance on health care utilisation, financial protection and health status in low-and middle-income countries: a systematic review. *PloS one*, 14(8), e0219731.
- Eshelman, L. J. & Schaffer, J. D. (1993). Real-coded genetic algorithms and interval-schemata. In *Foundations of genetic algorithms*, volume 2 (pp. 187–202). Elsevier.
- EUROPEEN, G. C. A. (2006). Actuarial reflections on pandemic risk and its consequences.
- Ferdinands, J. M., Thompson, M. G., Blanton, L., Spencer, S., Grant, L., & Fry, A. M. (2021). Does influenza vaccination attenuate the severity of breakthrough infections? a narrative review and recommendations for further research. *Vaccine*, 39(28), 3678–3695.
- Flaxman, S., Mishra, S., Gandy, A., Unwin, H. J. T., Mellan, T. A., Coupland, H., Whittaker, C., Zhu, H., Berah, T., Eaton, J. W., et al. (2020). Estimating the effects of non-pharmaceutical interventions on covid-19 in europe. *Nature*, 584(7820), 257–261.

- Gaglani, M., Pruszyński, J., Murthy, K., Clipper, L., Robertson, A., Reis, M., Chung, J. R., Piedra, P. A., Avadhanula, V., Nowalk, M. P., et al. (2016). Influenza vaccine effectiveness against 2009 pandemic influenza A (H1N1) virus differed by vaccine type during 2013–2014 in the United States. *The Journal of Infectious Diseases*, 213(10), 1546–1556.
- Goldberg, D. E. & Deb, K. (1991). A comparative analysis of selection schemes used in genetic algorithms. In *Foundations of genetic algorithms*, volume 1 (pp. 69–93). Elsevier.
- Hahné, S., Donker, T., Meijer, A., Timen, A., Van Steenbergen, J., Osterhaus, A., Van Der Sande, M., Koopmans, M., Wallinga, J., Coutinho, R., et al. (2009). Epidemiology and control of influenza A (H1N1) v in the Netherlands: the first 115 cases. *Eurosurveillance*, 14(27), 19267.
- Hambuckers, J. & Kneib, T. (2023). Smooth-transition regression models for non-stationary extremes. *Journal of Financial Econometrics*, 21(2), 445–484.
- Hart, W. S., Maini, P. K., & Thompson, R. N. (2021). High infectiousness immediately before COVID-19 symptom onset highlights the importance of continued contact tracing. *Elife*, 10, e65534.
- Holland, J. H. (1992). *Adaptation in natural and artificial systems: an introductory analysis with applications to biology, control, and artificial intelligence*. MIT press.
- Institute for Health Metrics and Evaluation (IHME) (2020). COVID-19 Projections.
- Karlinsky, A. & Kobak, D. (2021a). Tracking excess mortality across countries during the COVID-19 pandemic with the World Mortality Dataset. *eLife*, 10, e69336.
- Karlinsky, A. & Kobak, D. (2021b). Tracking excess mortality across countries during the COVID-19 pandemic with the World Mortality Dataset. *eLife*, 10, e69336.
- Kermack, W. O. & McKendrick, A. G. (1927). A contribution to the mathematical theory of epidemics. *Proceedings of the Royal Society of London. Series A, Containing papers of a mathematical and physical character*, 115(772), 700–721.
- Kobasa, D., Jones, S. M., Shinya, K., Kash, J. C., Copps, J., Ebihara, H., Hatta, Y., Hyun Kim, J., Halfmann, P., Hatta, M., et al. (2007). Aberrant innate immune response in lethal infection of macaques with the 1918 influenza virus. *Nature*, 445(7125), 319–323.
- Kratz, M. (2019). Introduction to extreme value theory: Applications to risk analysis and management. *2017 MATRIX Annals*, (pp. 591–636).
- Levenberg, K. (1944). A method for the solution of certain non-linear problems in least squares. *Quarterly of Applied Mathematics*, 2(2), 164–168.
- Li, L., Yan, Z.-L., Luo, L., Liu, W., Yang, Z., Shi, C., Ming, B.-W., Yang, J., Cao, P., Ou, C.-Q., et al. (2023). Influenza-associated excess mortality by age, sex, and subtype/lineage: Population-based time-series study with a distributed-lag nonlinear model. *JMIR Public Health and Surveillance*, 9(1), e42530.
- Mathieu, E., Ritchie, H., Ortiz-Ospina, E., Roser, M., Hasell, J., Appel, C., Giattino, C., & Rod s-Guirao, L. (2021). A global database of COVID-19 vaccinations. *Nature Human Behaviour*, 5(7), 947–953.
- McKay, M. D., Beckman, R. J., & Conover, W. J. (2000). A comparison of three methods for selecting values of input variables in the analysis of output from a computer code. *Technometrics*, 42(1), 55–61.

- Memoli, M. J., Han, A., Walters, K.-A., Czajkowski, L., Reed, S., Athota, R., Angela Rosas, L., Cervantes-Medina, A., Park, J.-K., Morens, D. M., et al. (2020). Influenza a reinfection in sequential human challenge: implications for protective immunity and “universal” vaccine development. *Clinical Infectious Diseases*, 70(5), 748–753.
- Meyerowitz-Katz, G. & Merone, L. (2020). A systematic review and meta-analysis of published research data on covid-19 infection fatality rates. *International Journal of Infectious Diseases*, 101, 138–148.
- Michalewicz, Z. (1996). *Genetic algorithms+ data structures= evolution programs*. springer science & business media.
- Mousa, A., Winskill, P., Watson, O. J., Ratmann, O., Monod, M., Ajelli, M., Diallo, A., Dodd, P. J., Grijalva, C. G., Kiti, M. C., et al. (2021). Social contact patterns and implications for infectious disease transmission—a systematic review and meta-analysis of contact surveys. *Elife*, 10, e70294.
- Naing, N. N. (2000). Easy way to learn standardization: direct and indirect methods. *The Malaysian journal of medical sciences: MJMS*, 7(1), 10.
- Nishiura, H. (2010). Case fatality ratio of pandemic influenza. *The Lancet infectious diseases*, 10(7), 443–444.
- Organization, W. H. et al. (2017). Who guidance for surveillance during an influenza pandemic.
- Organization, W. H. et al. (2020). *Estimating mortality from COVID-19: Scientific brief, 4 August 2020*. Technical report, World Health Organization.
- O’Driscoll, M., Ribeiro Dos Santos, G., Wang, L., Cummings, D. A., Azman, A. S., Paireau, J., Fontanet, A., Cauchemez, S., & Salje, H. (2021). Age-specific mortality and immunity patterns of sars-cov-2. *Nature*, 590(7844), 140–145.
- Paraskevis, D., Kostaki, E. G., Alygizakis, N., Thomaidis, N. S., Cartalis, C., Tsiodras, S., & Dimopoulos, M. A. (2021). A review of the impact of weather and climate variables to covid-19: In the absence of public health measures high temperatures cannot probably mitigate outbreaks. *Science of the Total Environment*, 768, 144578.
- Paul Morden, G. W. (2013). Pandemic panic. In *Life Conference and Exhibitions 2013*.
- Payne, A.-M. & McDonald, J. (1958). Symposium on the asian influenza epidemic, 1957. *Proceedings of the Royal Society of Medicine*, 51(12), 1009.
- Ramírez-Soto, M. C., Ortega-Cáceres, G., & Arroyo-Hernández, H. (2021). Sex differences in covid-19 fatality rate and risk of death: an analysis in 73 countries, 2020–2021. *Le infezioni in medicina*, 29(3), 402.
- Romaniuk, A. (2011). Global catastrophes and trends: The next fifty years. *Canadian Studies in Population [ARCHIVES]*, 38(1-2), 179–188.
- Rooker, T. (1991). Review of genetic algorithms in search, optimization, and machine learning. *AI Magazine*, 12(1), 102–102.
- Salje, H., Tran Kiem, C., Lefrancq, N., Courtejoie, N., Bosetti, P., Paireau, J., Andronico, A., Hozé, N., Richet, J., Dubost, C.-L., et al. (2020). Estimating the burden of sars-cov-2 in france. *Science*, 369(6500), 208–211.

- Schlattmann, P., A. E. . W. L. (2016). *rriskDistributions: A Package for fitting distributions to given data.*
<https://www.rdocumentation.org/packages/rriskDistributions/versions/2.1.1>.
- Scrucca, L. (2013). GA: A Package for Genetic Algorithms in R. *Journal of Statistical Software*, 53(4), 1–37.
- Sharma, M., Mindermann, S., Rogers-Smith, C., Leech, G., Snodin, B., Ahuja, J., Sandbrink, J. B., Monrad, J. T., Altman, G., Dhaliwal, G., et al. (2021). Understanding the effectiveness of government interventions against the resurgence of covid-19 in europe. *Nature communications*, 12(1), 5820.
- Sheehan, M. M., Reddy, A. J., & Rothberg, M. B. (2021). Reinfection rates among patients who previously tested positive for coronavirus disease 2019: a retrospective cohort study. *Clinical Infectious Diseases*, 73(10), 1882–1886.
- Solvency II Calibration Paper (2010). Solvency ii calibration paper.
<https://register.eiopa.europa.eu/CEIOPS-Archive/Documents/Advices/CEIOPS-Calibration-paper-Solvency-II.pdf>.
- Stern, A. M., Cetron, M. S., & Markel, H. (2010). The 1918–1919 influenza pandemic in the united states: Lessons learned and challenges exposed.
- Swiss, R. (2007). Pandemic influenza: A 21st century model for mortality shocks.
- Taubenberger, J. & Morens, D. (2009). Pandemic influenza—including a risk assessment of h5n1. *Revue scientifique et technique (International Office of Epizootics)*, 28(1), 187.
- Taubenberger, J. K. & Morens, D. M. (2006). 1918 influenza: the mother of all pandemics. *Revista Biomedica*, 17(1), 69–79.
- Tenforde, M. W. (2020). Symptom duration and risk factors for delayed return to usual health among outpatients with covid-19 in a multistate health care systems network—united states, march–june 2020. *MMWR. Morbidity and mortality weekly report*, 69.
- The European Parliament and The Council of the EU (2009). Directive 2009/138/ec of the european parliament and of the council of 25 november 2009 on the taking-up and pursuit of the business of insurance and reinsurance (solvency ii).
<https://eur-lex.europa.eu/legal-content/EN/TXT/?uri=celex%3A32009L0138>.
- Tsang, T. K., Cowling, B. J., Fang, V. J., Chan, K.-H., Ip, D. K., Leung, G. M., Peiris, J. M., & Cauchemez, S. (2015). Influenza a virus shedding and infectivity in households. *The Journal of infectious diseases*, 212(9), 1420–1428.
- Valenciano, M., Kissling, E., Cohen, J.-M., Oroszi, B., Barret, A.-S., Rizzo, C., Nunes, B., Pitigoi, D., Larrauri Camara, A., Mosnier, A., et al. (2011). Estimates of pandemic influenza vaccine effectiveness in europe, 2009–2010: results of influenza monitoring vaccine effectiveness in europe (i-move) multicentre case-control study. *PLoS medicine*, 8(1), e1000388.
- Valleron, A.-J., Cori, A., Valtat, S., Meurisse, S., Carrat, F., & Boëlle, P.-Y. (2010). Transmissibility and geographic spread of the 1889 influenza pandemic. *Proceedings of the National Academy of Sciences*, 107(19), 8778–8781.

- Viboud, C., Simonsen, L., Fuentes, R., Flores, J., Miller, M. A., & Chowell, G. (2016). Global mortality impact of the 1957–1959 influenza pandemic. *The Journal of infectious diseases*, 213(5), 738–745.
- Weisbart, S. (2006). Pandemic: Can the life insurance industry survive the avian flu? *New York Times A*, 10, 1–18.
- Yao, X., Liu, Y., & Lin, G. (1999). Evolutionary programming made faster. *IEEE Transactions on Evolutionary computation*, 3(2), 82–102.
- Zheng, C., Shao, W., Chen, X., Zhang, B., Wang, G., & Zhang, W. (2022). Real-world effectiveness of covid-19 vaccines: a literature review and meta-analysis. *International journal of infectious diseases*, 114, 252–260.
- Zhu, D., Mishra, S. R., Han, X., & Santo, K. (2020). Social distancing in latin america during the covid-19 pandemic: an analysis using the stringency index and google community mobility reports. *Journal of travel medicine*, 27(8), taaa125.